NAVAL POSTGRADUATE SCHOOL

MONTEREY, CALIFORNIA

THESIS

THEORETICAL CHARACTERIZATION OF THE RADIATIVE PROPERTIES OF DUST AEROSOL FOR THE AIR FORCE COMBAT CLIMATOLOGY CENTER POINT ANALYSIS INTELLIGENCE SYSTEM

by

John D. McMillen

March 2007

Thesis Advisor:	P. A. Durkee
Second Reader:	K. E. Nielsen

THIS PAGE INTENTIONALLY LEFT BLANK

REPORT DOCUMENTATION PAGE		Form Approved OMB No. 0704-0188

1. AGENCY USE ONLY *(Leave blank)*	2. REPORT DATE	3. REPORT TYPE AND DATES COVERED
	March 2007	Master's Thesis

4. TITLE AND SUBTITLE Theoretical Characterization of the Radiative Properties of Dust Aerosol for the Air Force Combat Climatology Center Point Analysis Intelligence System	5. FUNDING NUMBERS
6. AUTHOR(S) John D. McMillen	
7. PERFORMING ORGANIZATION NAME(S) AND ADDRESS(ES) Naval Postgraduate School Monterey, CA 93943-5000	8. PERFORMING ORGANIZATION REPORT NUMBER
9. SPONSORING /MONITORING AGENCY NAME(S) AND ADDRESS(ES) N/A	10. SPONSORING/MONITORING AGENCY REPORT NUMBER

11. SUPPLEMENTARY NOTES The views expressed in this thesis are those of the author and do not reflect the official policy or position of the Department of Defense or the U.S. Government.

12a. DISTRIBUTION / AVAILABILITY STATEMENT	12b. DISTRIBUTION CODE
Approved for public release; distribution is unlimited	A

13. ABSTRACT (maximum 200 words)

The Air Force Combat Climatology Center produces an analysis of meteorological conditions in a column over any point on the globe. Currently this analysis does not include aerosol impact on radiative transfer. Instead, the meteorological parameters are used to choose an aerosol representation native to MODTRAN radiative transfer software. This research investigates the impact of dust aerosol on radiative transfer in the 1-5 μm wavelength band. Theoretical radiative transfer properties are calculated for various dust aerosols. The aerosols vary in size distribution and index of refraction. The aerosols also vary in phase functions, extinction coefficients, absorption coefficients, and asymmetry parameters. MODTRAN is used to simulate radiative transfer in the 1-5 μm wavelength band incorporating the various dust aerosols in the bottom 1-2 km of the atmosphere. Radiance values from MODTRAN are converted into brightness temperatures, allowing interpretation of the impact dust aerosol has on remote sensing in this wavelength band. Dust aerosol does impact radiative transfer in the 1-5 μm wavelength band. Brightness temperatures vary by as much as 50 K between no aerosol simulations and certain dust simulations below 3 μm, and can vary by 1 K above 3 μm.

14. SUBJECT TERMS Radiative Transfer, Aerosols, Dust	15. NUMBER OF PAGES 145
	16. PRICE CODE

17. SECURITY CLASSIFICATION OF REPORT	18. SECURITY CLASSIFICATION OF THIS PAGE	19. SECURITY CLASSIFICATION OF ABSTRACT	20. LIMITATION OF ABSTRACT
Unclassified	Unclassified	Unclassified	UL

NSN 7540-01-280-5500 Standard Form 298 (Rev. 2-89)
Prescribed by ANSI Std. 239-18

THIS PAGE INTENTIONALLY LEFT BLANK

Approved for public release; distribution is unlimited

THEORETICAL CHARACTERIZATION OF THE RADIATIVE PROPERTIES OF DUST AEROSOL FOR THE AIR FORCE COMBAT CLIMATOLOGY CENTER POINT ANALYSIS INTELLIGENCE SYSTEM

John D. McMillen
Captain, United States Air Force
B.S., United States Air Force Academy, 2000

Submitted in partial fulfillment of the
requirements for the degree of

MASTER OF SCIENCE IN METEOROLOGY

from the

NAVAL POSTGRADUATE SCHOOL
March 2007

Author: John D. McMillen

Approved by: P. A. Durkee
Thesis Advisor

K. E. Nielsen
Second Reader

P. A. Durkee
Chairman, Department of Meteorology

THIS PAGE INTENTIONALLY LEFT BLANK

ABSTRACT

The Air Force Combat Climatology Center produces an analysis of meteorological conditions in a column over any point on the globe. Currently this analysis does not include aerosol impact on radiative transfer. Instead, the meteorological parameters are used to choose an aerosol representation native to MODTRAN radiative transfer software. This research investigates the impact of dust aerosol on radiative transfer in the 1-5 μm wavelength band. Theoretical radiative transfer properties are calculated for various dust aerosols. The aerosols vary in size distribution and index of refraction. The aerosols also vary in phase functions, extinction coefficients, absorption coefficients, and asymmetry parameters. MODTRAN is used to simulate radiative transfer in the 1-5 μm wavelength band incorporating the various dust aerosols in the bottom 1-2 km of the atmosphere. Radiance values from MODTRAN are converted into brightness temperatures, allowing interpretation of the impact dust aerosol has on remote sensing in this wavelength band. Dust aerosol does impact radiative transfer in the 1-5 μm wavelength band. Brightness temperatures vary by as much as 50 K between no aerosol simulations and certain dust simulations below 3 μm, and can vary by 1 K above 3 μm.

THIS PAGE INTENTIONALLY LEFT BLANK

TABLE OF CONTENTS

THIS PAGE INTENTIONALLY LEFT BLANK

LIST OF FIGURES

THIS PAGE INTENTIONALLY LEFT BLANK

LIST OF TABLES

THIS PAGE INTENTIONALLY LEFT BLANK

ACKNOWLEDGMENTS

I acknowledge the steadfast support provided by my wife Jennifer. She orchestrated, while pregnant, all the little details of an entire household move so I could produce this document. A finer woman, I have never met.

I acknowledge Professor Durkee for his guidance and enthusiasm for this topic and my results.

I also acknowledge Kurt Nielsen for his help in conveying the reason this project exists to several audiences.

THIS PAGE INTENTIONALLY LEFT BLANK

I. INTRODUCTION

The Air Force Combat Climatology Center (AFCCC) Point Analysis Intelligence System (PAIS) produces a comprehensive analysis of weather conditions at any given instant for any point on the globe. In order to produce this analysis, the system combines output from numerical weather prediction models, observed weather data analyzed by numerical weather prediction models, and information from several databases on various atmospheric phenomena. This data is used to determine atmospheric aerosol conditions defined within the MODerate spectral resolution atmospheric TRANsmittance algorithm and computer model (MODTRAN) radiative transfer model version 4 (Berk et al., 1999). Studies of aerosols have provided much more information about the characteristics of aerosol composition and behavior in the years since the aerosol conditions were defined for MODTRAN. Incorporating improvements in aerosol characterization into the Point Analysis Intelligence System will improve the resultant characterization of radiative transfer output by MODTRAN. Of particular interest is the behavior of dust aerosol in the 1-5 μm wavelength band.

The type of aerosol and the range of wavelengths narrow the focus of the study, but also complicate the study. One complication is that dust aerosol is known to absorb radiation in these wavelengths. Therefore, the absorptive properties of the aerosol must be taken into account to determine the radiative transfer characteristics of the aerosol bearing atmosphere. This study first focused on dust aerosol composition and electromagnetic properties to determine the appropriate representation of the dust aerosol in radiative transfer calculations. Once characteristics of dust aerosol were understood, aerosol size distributions were researched to determine the most appropriate theoretical representation of dust aerosol to include in radiative transfer modeling. Several different dust aerosol size distributions were studied. Two distributions already used by the Naval Postgraduate School (NPS) to retrieve aerosol properties were compared to both observational dust aerosol studies and other state-of-the-art approximations of aerosol distributions. Mie theory was used to calculate phase function, asymmetry parameter,

extinction coefficient, and absorption coefficient for each of the various representations of dust aerosol. The electromagnetic properties were then applied to the dust aerosol size distributions to present a range of dust bearing atmospheric conditions.

The wavelength band (1-5 μm) complicates the problem because there are multiple sources of energy interacting with the aerosol. In this case energy emitted by the sun and energy emitted by the Earth's surface both interact with the aerosol as well as energy emitted by the aerosol itself. Due to the complicated radiative nature of the environment, determining the effect of the dust aerosol on radiation propagation is complicated. The study addressed this problem by modeling various radiative transfer situations using MODTRAN and comparing the results. The MODTRAN radiance data output were converted to brightness temperature values by inverting the Planck function. This was done to emphasize the impact of dust aerosol on remote sensing systems that usually convert radiance measurements to brightness temperatures in this wavelength band.

To highlight the variability possible in the radiative transfer solution in the 1- 5 μm wavelength band, several different dust aerosol representations were compared with calculations that included no dust aerosol. In addition there were two sets of dust aerosol representations, each of which had different electromagnetic properties. One set of dust aerosol representations exhibited absorption and the other set represented dust aerosol that was non-absorptive. These sets of aerosol representation were then compared. In addition the atmospheric thermal characteristics were varied. Thermal profiles of a summer day and night in addition to a spring day and night were studied. Finally, the scene viewing angle was varied from a nadir view to a zenith angle of 30°. Varying dust aerosol representations by both size distribution and electromagnetic properties allowed characterization of the impact of dust aerosol on the radiative transfer problem.

The objectives of this thesis are:

- Understand the impact of dust aerosol on radiative transfer in the 1-5 μm wavelength band.
- Quantify a range of remotely sensed brightness temperature values possible in the absence or presence of dust aerosol.
- Compare MODTRAN dust aerosol with various modern dust aerosol representations.
- Compare various dust aerosol representations as input for radiative transfer modeling.

Chapter II describes aerosol composition and size distributions. Chapter III describes radiative transfer in the 1-5 μm wavelength band. Chapter IV discusses research methodology. Chapter V describes the results. Chapter VI presents conclusions from the study.

THIS PAGE INTENTIONALLY LEFT BLANK

II. AEROSOL REPRESENTATION

Several aspects of atmospheric dust aerosol are important to the PAIS operational analysis and to accurate radiative transfer modeling. The most important concerns are determining the presence or lack of aerosol, horizontal aerosol distribution, and vertical aerosol distribution. This problem is highlighted by d'Almeida et al., (1991), "Atmospheric aerosol stems from localized and sparse sources, remains only a few days in the atmosphere, and is therefore subject to a high variability in space and time." The presence or lack of aerosol will have an impact on radiative transfer through the column of atmosphere. Shirkey and Tofsted (2006) point out that "These atmospheric particles, or aerosols, are ubiquitous in nature and frequently are the determining factor in the amount of radiation received at a sensor." The horizontal and vertical distributions of aerosol are an important concern because the path radiation follows from target to sensor is generally narrow and changes in horizontal and vertical distribution impact the amount of aerosol along the path. Furthermore, since the wavelength range examined is between 1 and 5 μm the emission of aerosol, that depends on its temperature and therefore depends on its altitude, becomes important. MODTRAN version 4 approaches this problem by providing a range of climatological representations of likely aerosol. The user is asked to specify a type of aerosol and a meteorological visual range. The aerosol is then applied from 0-2 km altitude with extinction values determined by the meteorological visual range and in some cases the humidity (Berk et al., 1999).

The MODTRAN example above has simplified the aerosol problem for the user by bundling several important aerosol characteristics into groups that match with land use parameters. The important extinction characteristics the MODTRAN models are derived from are: physical aerosol type, aerosol size, aerosol shape, and aerosol size distribution. These parameters are significant in understanding radiative properties through an atmosphere containing aerosol. Physical aerosol type determines the relative density distribution and refractive index properties (Shirkey and Tofsted, 2006). Aerosol size becomes important in radiative transfer when scattering is considered; this will be discussed in the radiative transfer chapter. A range of values of dust aerosol radii

considered in this study stretches from 0.01 to 10 μm. Aerosol shape is important because it can influence scattering and is not accounted for when using Mie theory to calculate the aerosols electromagnetic properties (Longtin et al., 1988). Aerosol size distribution is significant because aerosols are complex and frequently composed of multiple physical aerosol types (Shirkey and Tofsted, 2006). In addition the different amounts of aerosol of certain radius affect the radiative transfer solution. The log-normal distribution was chosen for this study to define the various dust aerosols because it emphasizes individual components in a mixture of particles (D'Almeida et al., 1991). The log-normal distribution does this by simply adding individual mode radius and standard deviation characteristics.

Due to the wavelength range covered by this study, dust aerosol is the most significant aerosol type. Dust aerosol is aerosol composed of mostly mineral particles. Dust aerosol is known to absorb radiation in these wavelengths. Therefore it was important to research the refractive indices of various minerals to find a representative value to apply to the selected distributions. Furthermore, two size distributions examined, m0 and m6, were non-absorptive and it was important to find reasonable refractive indices to produce absorption in these models.

The scattering and absorption of a material are described by the material's refractive index. The real part of the refractive index describes scattering behavior, while the absorption is described by the imaginary part of the index of refraction (Kidder and Vonder Harr, 1995). The real part of the index of refraction was held to 1.4 across all wavelengths and for all different aerosols. This value was used by Brown (1997) and by Ignatov et al. (1995). In addition this value is similar to the real index of refraction described by Jennings et al. (1978). This consistency lends weight to the approximation of static real part of the index of refraction across multiple wavelengths. Absorption is governed by the imaginary value of the index of refraction.

This study compares an aerosol with no absorptive properties (i.e., the imaginary index of refraction is zero) to an aerosol that exhibits absorption. The imaginary index of refraction was chosen from three studies. First an observational study was researched. Fischer (1975) studied the mass absorption index of aerosol particles in the 2-17 μm

wavelength range. This mass absorption index is described as the imaginary index of refraction divided by the density of the aerosol in question. He measured mass absorption index in Israel's Negev Desert over three days at 3, 4, and 5 μm. By multiplying his data by a mean dust density provided in his paper the following maximum values of the imaginary index of refraction were found:

- 3 μm n' = 8.81×10^{-2}
- 4 μm n' = 1.347×10^{-1}
- 5 μm n' = 1.165×10^{-1}

(Fischer, 1975)

These values were used as the absorptive dust imaginary indices of refraction for all dust aerosols. The Jennings et al. (1978) paper included a table of values of complex refractive indices. The 3.8 μm values were similar to the Fischer study (Jennings et al., 1978). Finally, Patterson collected several studies in a chart that plotted imaginary index of refraction as a function of wavelength. This chart also shows general agreement with the previously mentioned studies (Patterson, 1981).

Several existing log-normal distributions were used to represent dust aerosol (see Figure 1). The first are the m0 and m6 distribution created for use in the NPS algorithm. The m0 distribution was initially created to represent the background condition for use in retrieval of aerosol optical depth over water via the NPS retrieval scheme. The m6 distribution is bimodal including the m0 distribution and larger particles representative of ocean produced aerosols (Brown, 1997). It provides a distribution of aerosols that include particles representative of dust aerosol in low concentration. Behavior of this distribution may later be applicable to retrievals of aerosol optical depth due to dust. The previous chapters describing the research into index of refraction both real and imaginary apply primarily to these two representations of dust aerosol. By combining the appropriate indices of refraction with these distributions, they truly represent dust.

The remaining representations discussed have more complicated indices of refraction by design. This study held the indices of refraction constant across the size

distribution for most of the various distributions to allow better comparison with one another. The exception is the Optical properties of Aerosols and Clouds (OPAC) Desert representation (Hess et al., 1998). This representation was discovered late in research and there was not time to apply the general indices of refraction to these distributions. It is included to allow some comparison between this study and work done by Lucyk (2007) regarding vertical dust aerosol distribution.

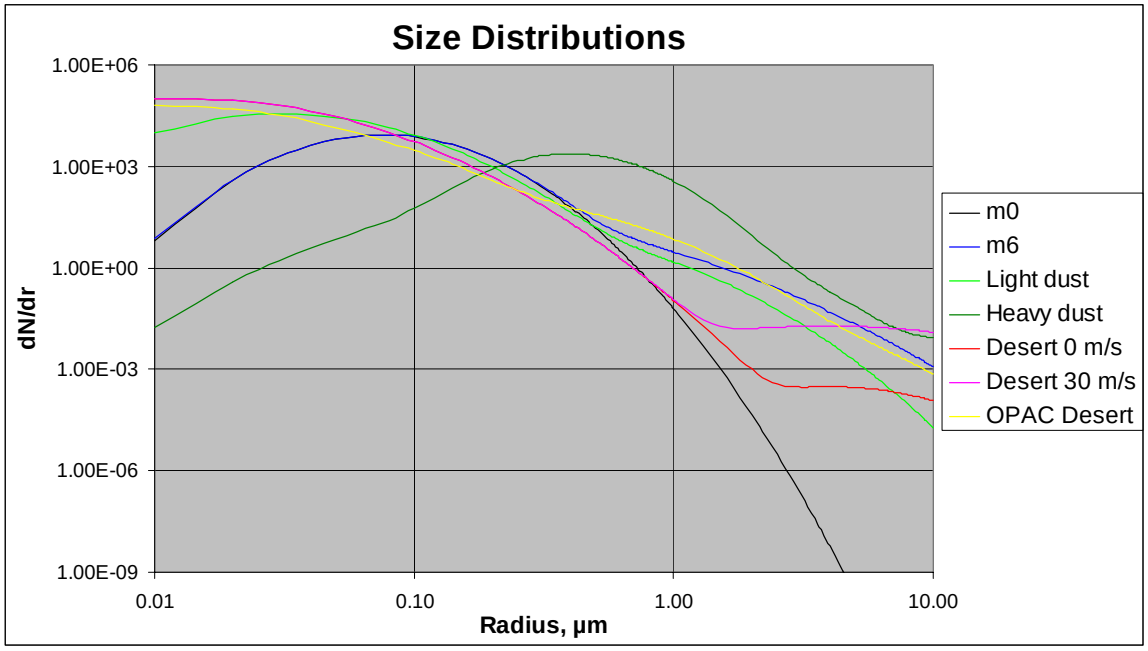

Figure 1. Size distributions of seven dust aerosol representations examined in this study.

The next group of aerosol distributions to consider is from the Army Research Lab *High Resolution Electro-Optical Aerosol Phase Function Database PFNDAT2006.* The database includes several manmade and natural aerosol types, but this study is limited to dust aerosol. The database contains six such aerosols, but only four are considered as representative of high dust loading and light dust loading conditions. The Light dust distribution was created to represent the background desert condition. It is meant to apply globally and in a climatological sense. It is composed of three modes; one representing ammonium sulfate, the second representing quartz and the third representing carbon (see Table 1). Each of these modes has a different index of

refraction. Coupled with the Light dust distribution is the Heavy dust distribution. This distribution is also tri-modal but it represents extreme dust conditions in dust generation areas that are expected to last only a short time. The modes represent Montmorillonite and quartz dust of two different particle radii. Again each mode has a different index of refraction (Shirkey and Tofsted, 2006).

Table 1. Dust aerosol representation size distribution properties.

Aerosol Properties			
Name	Number Density N, cm^-3	Particle Radius r, μm	Standard Deviation
m0 †			
Background	1000.00	0.10	1.70
m6 †			
Background	1000.00	0.10	1.70
Ocean-Produced	15.00	0.30	2.70
Light Dust ‡			
Ammonium Sulfate	1988.00	0.05	2.00
Quartz	3.79	0.50	2.00
Carbon	488.50	0.05	2.00
Heavy Dust ‡			
Montmorillonite	39.62	0.50	2.00
Quartz	0.1128	0.50	1.60
Quartz	1218.60	0.50	1.60
Desert 0 m/s ‡			
Carbonaceous	367.90	0.0118	2.00
Water Soluble	3650.60	0.0285	2.24
Sand	0.002459	6.24	1.89
Desert 30 m/s ‡			
Carbonaceous	367.90	0.0118	2.00
Water Soluble	3650.60	0.0285	2.24
Sand	.31613	10.80	2.74
OPAC Desert ≈			
Water Soluble	2000.00	0.0212	2.24
Mineral Nucleation	269.50	0.07	1.95
Mineral Accumulation	30.50	0.39	2.00
Mineral Coarse	0.142	1.90	2.15
† Brown Thesis ‡PFNDAT 2006 Army Research Lab ≈ OPAC			

PFNDAT2006 also includes a wind-lofted desert aerosol. The Desert 0 m/s wind case and Desert 30 m/s wind case are used in this study. Both are composed of identical carbonaceous and water soluble modes with differing indices of refraction. They each have a third mode representing wind-lofted particles. Wind speed in these distributions lofts sand aerosol of larger size and larger numbers as wind speed increases (see Table 1). This wind driven aerosol representation is the dust aerosol representation used by MODTRAN, except for updated changes to the indices of refraction of the quartz component of the wind-lofted sand (Shirkey and Tofsted, 2006). This study applies index of refraction by wavelength instead of by dust aerosol component, so these changes will not be apparent in the results.

The OPAC Desert aerosol is also considered. This aerosol is used in the NRL Navy Aerosol Analysis and Prediction System (NAAPS) model to represent dust in NAAPS output. NAAPS output may be very valuable to improving the PAIS process and therefore this distribution is presented with the others to test its utility. This distribution has four modes to represent water soluble particles; and nucleation, accumulation, and coarse mineral components (see Table 1). There are two distinct indices of refraction with this representation, one for the water soluble contribution and the second from the mineral contribution (Hess et al., 1998).

III. RADIATIVE TRANSFER

To understand the radiation measured at the top-of-the-atmosphere by a remote sensing satellite pointing at the surface of the earth, one must account for the origin of the radiation reaching the sensor. I have included a schematic to represent the radiation sources present in this wavelength range (see Figure 2). In an atmosphere without a dust aerosol present radiant energy from the sun is transmitted through the atmosphere, reflects off of the Earth's surface and is then transmitted through the atmosphere to space. The Earth is also emitting radiant energy in this wavelength range. This energy is transmitted through the atmosphere towards space. In this study the contributions of solar and terrestrial energy are nearly equal in the 4-5 μm band. Below 4 μm the amount of solar energy is much larger than the terrestrial energy, and above 5 μm terrestrial energy is much larger than the solar contribution.

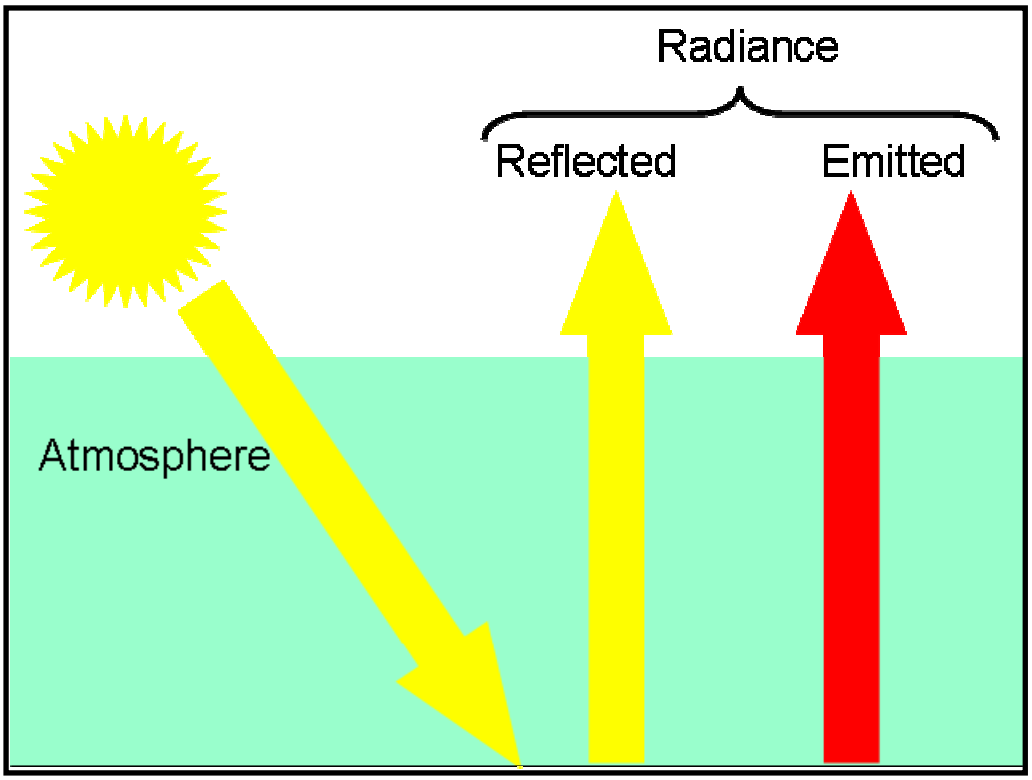

Figure 2. Schematic representing atmospheric radiative transfer without dust interaction.

The previous paragraph described the sources of radiant energy within the wavelength range studied. Further consideration must be paid to the amount of energy that reaches the satellite. Between the surface of the earth and the sensor a finite volume of intervening atmosphere is present. This volume is referred to as the radiation beam. Radiation in the beam is subject to four main interactions that increase radiation reaching the sensor and/or prevent radiation from reaching the sensor. There are two possible radiation sources and two possible radiation sinks. The sources include emitted radiant energy and reflected radiant energy. The solar radiant energy reflected off of the surface is one source, as is the Earth surface emission. When a dust layer is added, scatter by aerosol into the beam and emissions by aerosol within the beam are also possible. The sinks include absorption of energy within the beam and scattering of energy out of the beam. Dust aerosol added to the atmosphere will cause a loss of radiant energy reaching the sensor because of these sinks. The important thing to note here is the relative magnitudes of the sources and sinks. In Figure 3, the source terms and the loss terms are represented. Variation in these values will cause a change in the radiance measured at the top-of-the-atmosphere (see Figure 3).

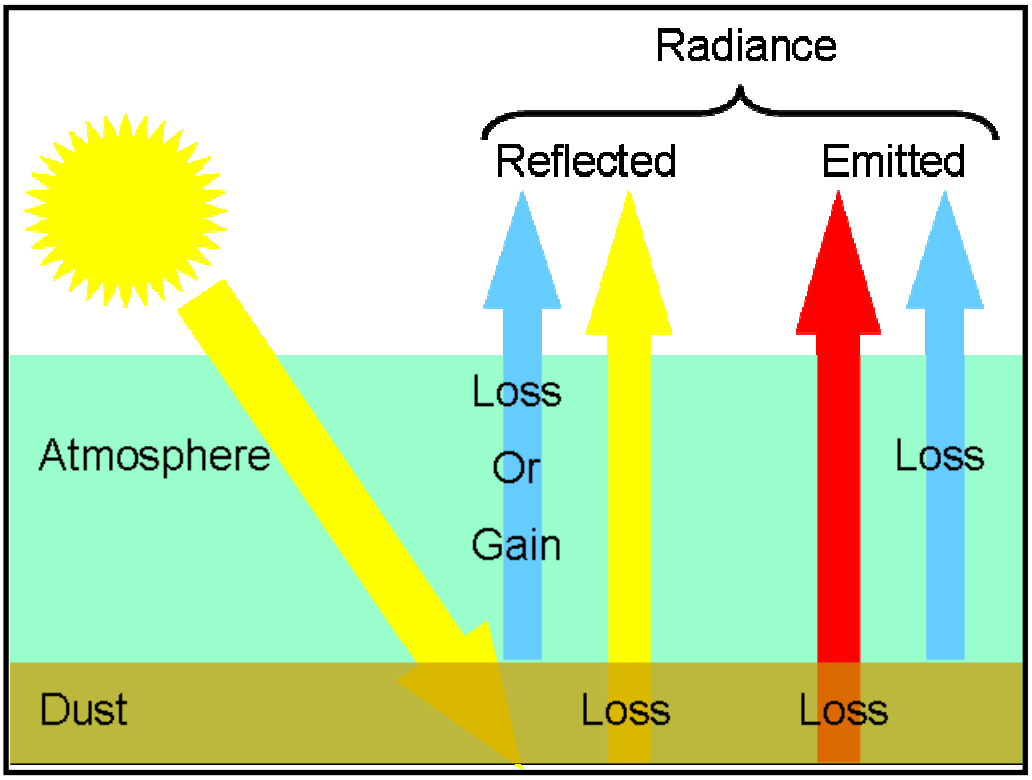

Figure 3. Schematic representing atmospheric radiative transfer with dust aerosol in a layer between the surface and some altitude.

The qualitative discussion above is represented by the radiative transfer equation for non-polarized radiation (Kidder and Vonder Harr, 1995).

$$\frac{dL_\lambda}{ds} = -\sigma_a(\lambda)L_\lambda(\theta,\phi) - \sigma_s(\lambda)L_\lambda(\theta,\phi) + \sigma_a(\lambda)B_\lambda(T) + \frac{\sigma_s(\lambda)}{4\pi}\int_0^{2\pi}\int_0^{\pi} L_\lambda(\theta',\phi')P(\psi_s)\sin(\theta')d\theta' d\phi' \quad (1)$$

The left hand side of the equation represents the rate of change of monochromatic radiance over some path distance. The right hand side of the equation is composed of four terms that represent the four interactions possible between the radiation beam and intervening atmosphere.

The first term represents a loss of radiant energy due to absorption. The radiant energy indicated in this term is reflected solar energy for this study. Absorption is represented by σ_a, the absorption coefficient. In this study σ_a is calculated for the each

dust aerosol and provided as an input to a radiative transport model. There will also be absorption due to the atmospheric gases and background aerosols. Values of σ_a to represent absorption by these particles are handled solely by the radiative transport model. The background aerosols and atmospheric gases will be the same for each set of dust aerosol cases so that when the results are compared the differences can be shown to be a result of changing the dust aerosol only.

The second term is similar to the first in that it represents a loss of radiant energy. In this term, the loss is due to scattering, represented by σ_s. The radiant energy indicated in this term is reflected solar energy. In this study σ_s is calculated for the each dust aerosol and provided as an input to a radiative transport model. There will also be scattering due to the atmospheric gases and background aerosols. Values of σ_s to represent scattering by these particles are handled solely by the radiative transport model. The background aerosols and atmospheric gases will be the same for each set of dust aerosol cases so that when the results are compared the differences can be shown to be a result of changing the dust aerosol only.

The third term represents emission multiplied by σ_a. The dust aerosols studied are not black bodies and the use of absorption efficiency here upholds Kirchoff's law which holds that a material is as good an emitter as it is an absorber (Kidder and Vonder Harr, 1995). Once again the background aerosols and atmosphere will be handled by the radiative transfer model. Emission is represented by the Planck function given by the following formula:

$$L_\lambda = \frac{2hc^2\lambda^{-5}}{e^{\frac{hc}{\lambda kT}} - 1} \qquad (2)$$

It is clear from this equation that emission is dependent on both wavelength and temperature. The temperature of the dust aerosol will be equal to the temperature of atmosphere at the same vertical level which will be specified for each case. If this equation is inverted it takes on this form:

$$T = \left(\frac{hc}{k\lambda}\right)\left(\frac{1}{\ln\left[\frac{(2hc^2\lambda^{-5})}{L_\lambda}+1\right]}\right) \quad (3)$$

This formula produces a temperature value that represents the temperature a blackbody would have in order to produce the radiance value input to the formula. This temperature is referred to as the brightness temperature. This formula will be used to convert the radiance values extracted from our radiative transport model to brightness temperature values.

The fourth and final term represents scatter of radiation into the beam. The scattering efficiency, Q_s, and the phase function, $P(\psi_s)$, are both calculated for the dust aerosols in this study using Mie theory. The radiant energy in this term is any energy outside of the beam that may interact with a particle in the beam and scatter energy along the beam. This term is influenced by dust aerosol size and composition as noted in chapter II, but it is also affected by dust aerosol shape. This study calculates scattering efficiency and phase function using Mie theory. This requires the assumption that all aerosol particles are spherical. Longtin et al. (1988) notes that desert aerosols are not spherical and applying the spherical assumption and Mie theory is a simplification of the problem.

The physical properties of the dust aerosol determine the scattering coefficient, σ_s, absorption coefficient, σ_a, and the phase function, $P(\psi_s)$. In order to calculate values for these parameters, Mie theory was used. From PFNDAT2006 the required assumptions for using Mie theory to calculate these parameters are that scatter events are independent, the particles in question are spherical, the scattering properties of a given distribution can be represented by a weighted integral over the particle size distribution, polarization is ignored, and the size distribution is homogeneous over the volume considered (Shirkey and Tofsted, 2006). Once these conditions are met the physical properties of the aerosol can be calculated and then applied to the radiative transfer models.

THIS PAGE INTENTIONALLY LEFT BLANK

IV. METHODOLOGY

The range of dust aerosol electromagnetic properties and size distributions were discussed in the previous chapter. This chapter focuses on translating these properties and characteristics into viable input for radiative transfer modeling and the process of conducting simulations of radiative transfer for various dust aerosol situations. Since the wavelength range of interest is between 1-5 μm, and research into electromagnetic properties of aerosols did not yield continuous index of refraction values, the 3, 4, and 5 μm wavelengths were chosen as representatives for the range. The 0.55 μm wavelength was characterized as well because it is a required input for user defined aerosols for the MODTRAN program. MODTRAN requires input in the form of extinction coefficient, absorption coefficient and asymmetry parameter to characterize the radiative transfer properties of an aerosol. To determine these values Mie calculation software was used.

Mie calculations for the 0.55, 3, 4, and 5 μm wavelength were carried out in order to determine the appropriate phase function that in turn yielded the asymmetry parameter of the various dust aerosols. Production of the phase function was left to MiePlot, a program written by Phillip Laven (2007, http://www.philiplaven.com/index1.html). In order for MiePlot to produce a set of phase function values, the number of aerosol particles in an aerosol radius range was required as the definition of the aerosol size distribution. In addition the refractive index, both real and imaginary values were required. For each wavelength different imaginary indices of refraction were input in order to gauge the impact of absorption on the phase function solution. This produced a range of values for each size distribution at a given wavelength. The range of imaginary indices of refraction allowed examination of the range of possible phase function values expected for an array of different aerosols. It became clear that the non-absorbing dust aerosol and the dust aerosol with the largest imaginary index of refraction were the outliers of the phase function values (see Figure 4). This did not hold true when comparing the dust aerosol representations with complex indices of refraction to the dust aerosols with a static index of refraction (see Figure 5). The PFNDAT2006 aerosol phase

function values were quite different from the MiePlot produced phase function values. PFNDAT2006 used different indices of refraction for each mode when producing phase function values. The MiePlot phase function values were produced from the same aerosol size distribution, but with a single index of refraction. The different phase function values are a result of this simplification. Despite the simplification, the shape of the phase function values in all cases is similar. The PFNDAT2006 data all exhibited much larger forward scatter response. Representative phase function values produced by MiePlot and input into MODTRAN are shown in Figure 6. These phase functions are from the dust aerosol representations used in the study that had an absorptive imaginary index of refraction.

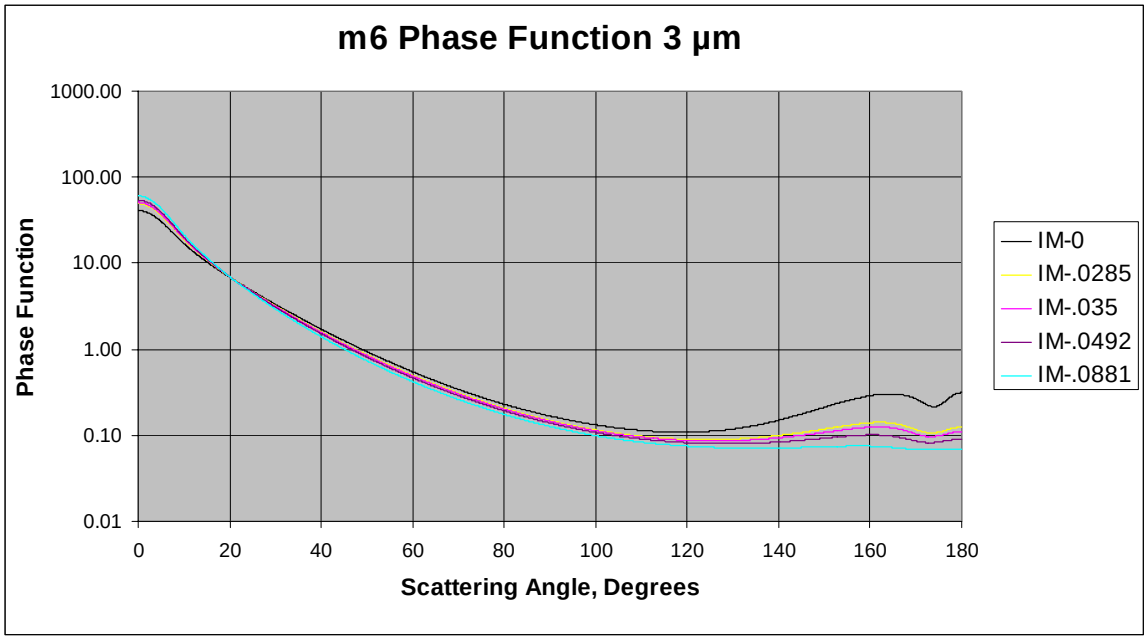

Figure 4. Phase function values from the m6 dust aerosol representation with varying index of refraction.

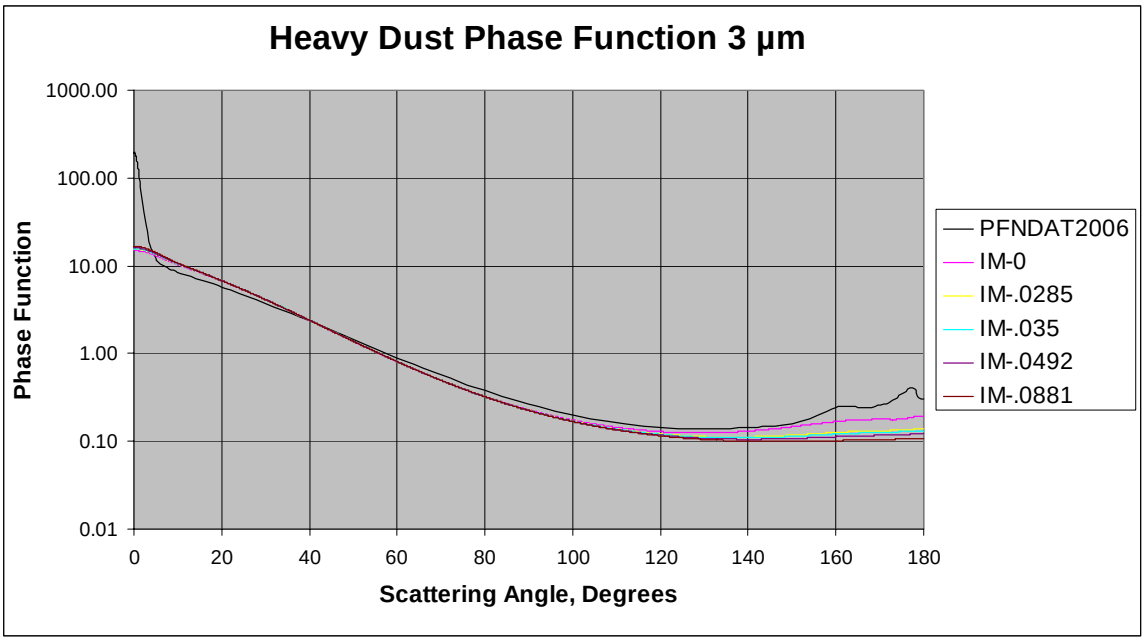

Figure 5. Phase function values from the Heavy dust aerosol representation with varying index of refraction.

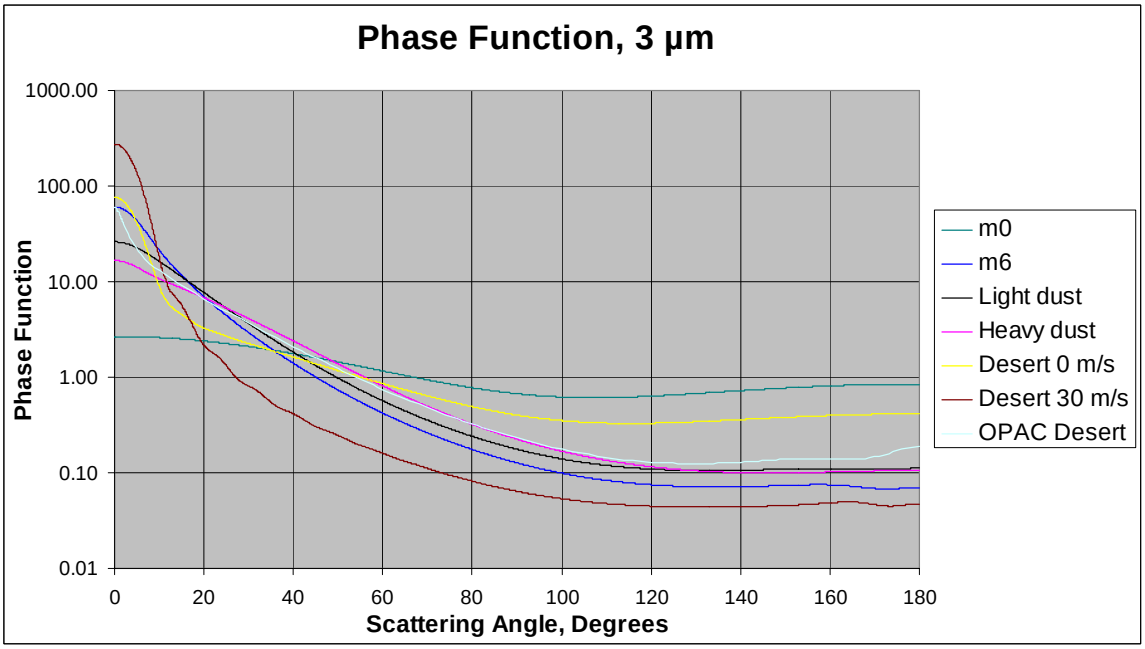

Figure 6. Phase function values from all seven absorptive dust aerosol representations at the 3 µm wavelength.

The asymmetry parameter was required as input for the MODTRAN calculation. Values of the asymmetry parameter were high due to the preference for forward scatter in almost every aerosol case. Phase function values were converted to asymmetry parameter by the following formula.

$$g = \frac{1}{2}\int_0^{\pi} \cos(\theta) P(\theta) \sin(\theta) d\theta \tag{1}$$

Mie calculation was also used to describe the extinction and absorption coefficients of each different dust aerosol. The calculation of extinction and absorption coefficients was carried out by the following formulae.

$$\sigma_e = \int_0^{r_{\max}} \pi r^2 Q_e n(r) dr \tag{2}$$

$$\sigma_a = \int_0^{r_{\max}} \pi r^2 Q_a n(r) dr \tag{3}$$

Notice in these formulas the extinction efficiency, Q_e, and absorption efficiency, Q_a, were required to solve for the extinction coefficient and the absorption coefficient. These values were produced by MiePlot. The extinction efficiency represents the amount of energy that is removed from an incident electromagnetic wave by a particle of a given radius. The value of extinction efficiency is expected to oscillate, and its oscillations should be damped with an increase in absorption (Twomey, 1977). The data produced by MiePlot matches with this qualitative description (see Figures 7 and 8). Figure 7 is a plot of extinction efficiency at the four representative wavelength plotted against the range of particle radii. The oscillation noted by Twomey is present and as far as the 0.55 μm wavelength is concerned, the value approaches 2 with increasing radius as expected. Figure 8 represents the extinctions of the absorptive aerosol. When absorption occurs oscillation is indeed damped as stated in Twomey. The value of extinction efficiency of the 0.55 μm wavelength still approaches 2 as expected.

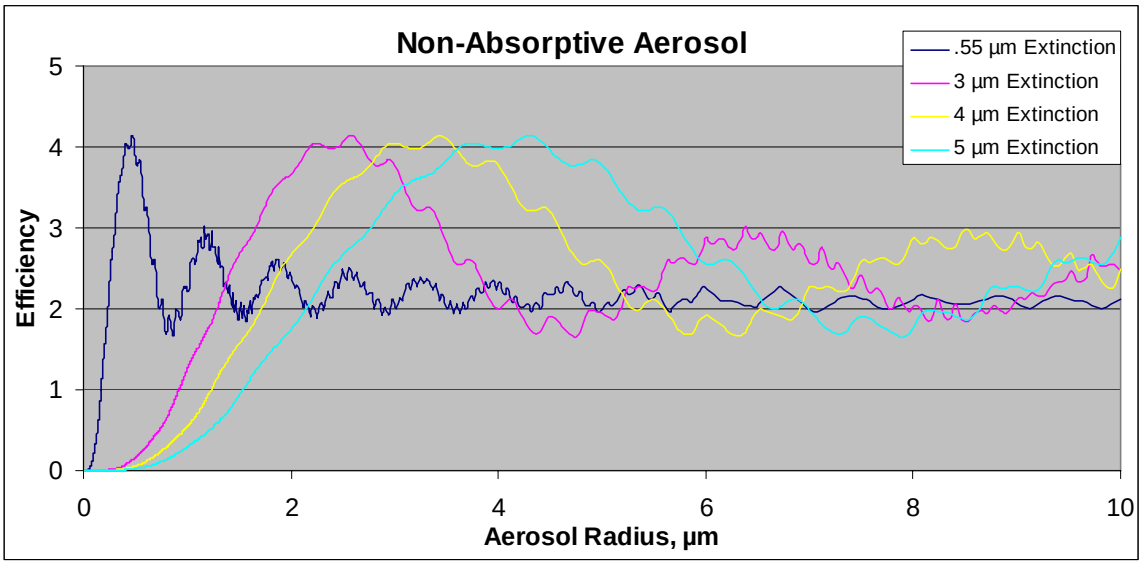

Figure 7. Extinction efficiencies of four wavelengths over the same particle radius range.

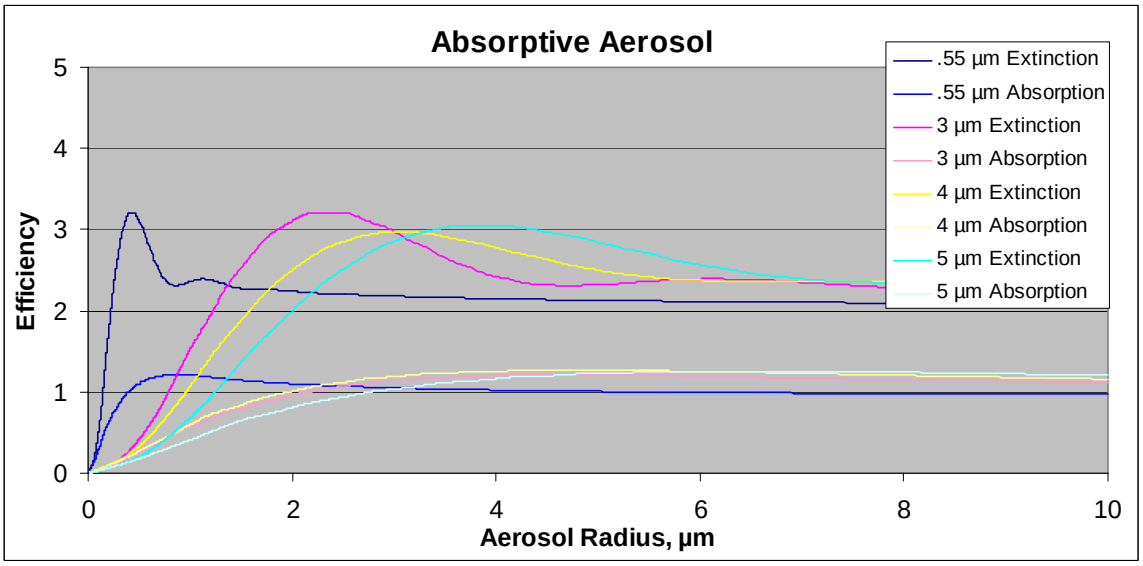

Figure 8. Extinction and absorption efficiencies of four wavelengths over the same particle radius range.

After calculation of the appropriate asymmetry parameters, extinction coefficients, and absorption coefficients these values were coded into cards for MODTRAN to ingest. MODTRAN was run with the following baseline parameters for every dust aerosol representation. The sensor was located over 33 N Lat. 43 E Lon., in the Iraq desert near Bagdad. A nadir view from the sensor was calculated as well as a

30° zenith angle case. The 30° zenith angle cases were run with the same inputs as the nadir views except for geometry. The 30° zenith angle cases applied the zenith angle at 90 degrees east of North. The desert surface reflectance model was selected in MODTRAN. Atmospheric constituents including water vapor were modeled by the 1976 standard atmosphere model. The first case was the no aerosol case and the 0.55, 3, 4, and 5 μm aerosol extinctions were set to 0 for the lowest aerosol layer. The remaining aerosol layers were left as the default values. Then for each aerosol representation, the 0.55, 3, 4, and 5 μm extinctions and phase functions were input to the user defined aerosol in the lowest aerosol level from 0-2 kilometers. The remaining aerosol layers were left as the default values. MODTRAN was run to produce top-of-the-atmosphere radiance values. The DISORT multiple scattering routine with 4 streams was used.

The atmospheric temperature profile was altered to represent both day and night for two different seasons. The summer day simulation was created with the following meteorological parameters. The surface temperature was set to 320 K and the temperature profile was adjusted from the 1976 standard at the mandatory meteorological pressure levels to better match with the surface temperature. The adjusted temperature profile was an average of three randomly chosen soundings from Bagdad, Iraq sampled from the last 20 years in mid July.

The summer night simulation was created with the following meteorological parameters. The surface temperature was set to 302.5 K and the temperature profile was adjusted from the 1976 standard at the mandatory meteorological pressure levels to better match with the surface temperature. The adjusted temperature profile was an average of three randomly chosen soundings from Bagdad, Iraq sampled from the last 20 years in mid July.

The spring day simulation was created with the following meteorological parameters. The surface temperature was set to 307.5 K and the temperature profile was adjusted from the 1976 standard at the mandatory meteorological pressure levels to better

match with the surface temperature. The adjusted temperature profile was an average of three randomly chosen soundings from Bagdad, Iraq sampled from the last 20 years in mid May.

The spring night simulation was created with the following meteorological parameters. The surface temperature was set to 297.3 K and the temperature profile was adjusted from the 1976 standard at the mandatory meteorological pressure levels to better match with the surface temperature. The adjusted temperature profile was an average of three randomly chosen soundings from Bagdad, Iraq sampled from the last 20 years in mid May.

The next step involves solving for the top-of-the-atmosphere radiance by running MODTRAN. Radiance values were produced in a range from 1-5 μm. These radiance values were converted via the inverse Planck function into brightness temperature values. Brightness temperature differences between the solution with no aerosol and the solutions with various aerosol layers were also calculated. This was done to quantify the radiative impact of dust aerosol on a satellite measurement. The brightness temperature differences were also calculated between the absorptive and non-absorptive dust cases. These values are used to represent a range of top-of-the-atmosphere measurements when absorption is considered. These values are presented in the results chapter.

THIS PAGE INTENTIONALLY LEFT BLANK

V. RESULTS

A. SUMMER DAY NADIR

The summer day nadir view case was run with the MODTRAN input parameters described in the methodology section. The no dust aerosol simulation results in radiance values presented in Figure 9. Between 1 and 2.6 µm the magnitude of radiance generally decreases according to the Planck function for solar temperature – modified by gaseous absorption regions. Radiance values decrease from 3.63 x 10^{-3} W•cm^{-2}•ster^{-1}•µm^{-1} to a minimum of 5.00 x 10^{-7} W•cm^{-2}•ster^{-1}•µm^{-1} in the carbon dioxide absorption band between 2 and 3 µm. The radiance increases beyond 3 µm, roughly corresponding to the Planck function associated with the blackbody temperature of the earth. The minimum radiance of 5.00 x 10^{-7} W•cm^{-2}•ster^{-1}•µm^{-1} between 2 and 3 µm increases to a value of 2.61 x 10^{-4} W•cm^{-2}•ster^{-1}•µm^{-1} near the 5 µm wavelength. Above 3 µm atmospheric absorption is represented by bands of reduced radiance values. First water vapor absorption is present at wavelengths just greater than 3 µm. Finally, carbon dioxide and nitrous oxide absorption is present between 4 and 5 µm.

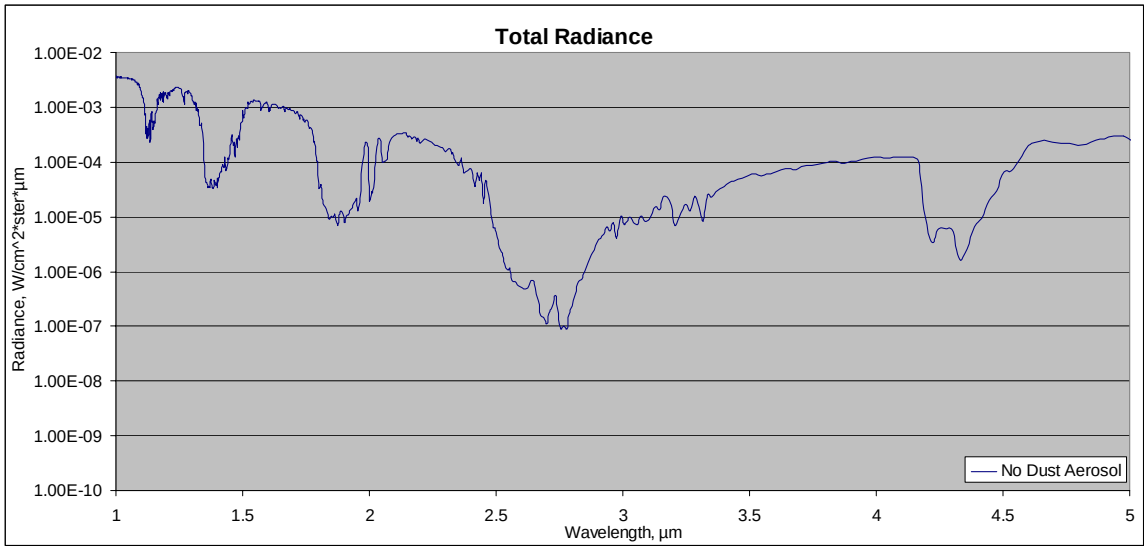

Figure 9. Top-of-the-atmosphere total radiance, no dust aerosol, summer day, nadir.

After conversion to brightness temperature, as described in Chapter IV, the brightness temperatures behave as expected with no dust aerosol present (see Figure 10). Important to note here is the surface temperature of 320 K for this case, as the brightness temperature values calculated should be near this value in the atmospheric windows of the wavelength band outside of solar influence. At 1 μm the brightness temperature is 959.119 K. This value is cut nearly in half at 2.033 μm where the brightness temperature is 501.498 K. At 3.003 μm the brightness temperature value is 305.308 K. This sharp decrease in brightness temperature values is due to the surface reflectance model used in the MODTRAN simulations. In the same wavelength span the reflectance changes from 0.7 to just 0.1, therefore much less solar energy is being reflected off of the surface and towards the top-of-the-atmosphere.

The atmospheric absorption bands noted above are revealed as bands of lower brightness temperature, which is expected. Surface reflection is very low, but the scattering of radiation by the tropospheric, stratospheric and meteoric background aerosol is present in the simulation. Evidence that this type of scattering is occurring is in the profile of brightness temperatures in the absorption bands. The brightness temperatures show little change across the band, in contrast to the sharp decrease in brightness temperature in the neighboring windows that mirror the surface reflectance.

The windows in the band between 3.4 and 5 μm are quite interesting when viewed from the brightness temperature perspective. This band shows the interaction of solar energy and terrestrial energy. The transmission in this band is a maximum near 3.5 μm. With this in mind the brightness temperature is expected to be near the 320 K surface temperature. The simulations reveal that the brightness temperature is greater than expected at 3.5 μm. The brightness temperatures between 3.4 and 4.1 μm decrease from 319 to 307 K. From 4.5 to 5 μm brightness temperatures vary between 297 and 309 K. Since the brightness temperatures in this band are closer to the surface temperature than transmission would allow, the energy in the simulation must be due to contribution from solar scattering.

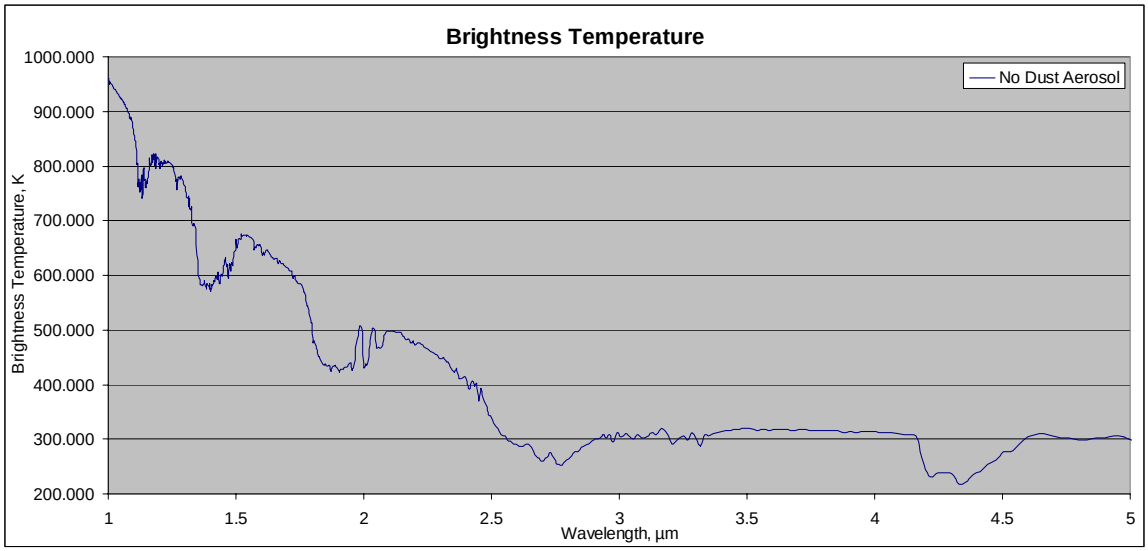

Figure 10. Top-of-the-atmosphere brightness temperature, no dust aerosol, summer day, nadir.

With the previous paragraphs addressing the background atmosphere, the dust aerosol layer simulations must be considered. As mentioned in the methodology chapter dust aerosols that were non-absorptive were considered as well as absorptive dust aerosols. The difference between the brightness temperatures of the absorptive dust and the non-absorptive dust was significant in all of the atmospheric windows (see Table 2). The differences were larger at shorter wavelengths than at longer wavelengths. This probably relates to the amount of energy involved in these bands, although the wavelength dependence of emitted radiation is also a factor. In addition, the differences were larger for the representations with higher 0.55 µm optical depth (m6 and Desert 30 m/s) than the representations with lower 0.55 µm optical depth (m0 and Desert 0 m/s). The higher 0.55 µm optical depth values result from representations with a larger number of dust aerosol particles per cubic centimeter. Larger dust aerosol particle loading suggests larger extinction by these aerosols. Larger extinction due to dust aerosol causes larger changes to top-of-the-atmosphere brightness temperature. This is why the Desert 30 m/s dust representation exhibits a larger average brightness temperature difference from the no aerosol simulation than the m6 representation. Since the brightness temperature values from both the non-absorptive and absorptive

Desert 30 m/s dust representations are larger than the brightness temperature values from both m6 representations, the difference between the non-absorptive and absorptive Desert 30 m/s dust aerosols are correspondingly larger than the difference between the m6 representations. The exception here is the Heavy dust and Light dust representations. The non-absorptive aerosols minus the absorptive aerosol brightness temperature differences were similar in both the Light dust and Heavy dust aerosol representation despite having different 0.55 μm optical depths. The 0.55 μm optical depths were similar to the other representations with Heavy dust having the higher 0.55 μm optical depth. Brightness temperature differences in this table reveal the importance of accounting for absorption by dust aerosol when calculating radiative transfer between 1 and 5 μm. With that in mind the following examination of brightness temperatures among the different dust representations will focus on the absorptive dust aerosol only.

Table 2. Average brightness temperature difference between non-absorptive and absorptive dust aerosol, summer day nadir.

	Average Brightness Temperature Difference, K					
Wavelength Band	Non Absorptive - Absorptive Dust Aerosol Representation					
μm	m0	m6	Light dust	Heavy dust	Desert 0 m/s	Desert 30 m/s
1.0-1.1	2.864	8.411	4.255	3.661	-1.786	11.900
1.188-1.315	2.535	9.213	4.802	4.203	-1.043	12.817
1.502-1.797	2.258	10.493	5.855	5.215	0.640	14.134
2.096-2.407	1.841	11.736	7.030	6.302	2.824	15.299
3.401-3.992	0.218	2.820	1.914	1.725	1.701	3.412
4.63-4.975	0.044	0.067	0.056	0.126	0.056	0.219

Brightness temperatures resultant from the addition of dust aerosol across the entire 1 through 5 μm band are presented in Figure 11. Since the brightness temperatures range from near 1000 K to below 300 K it is difficult to visually quantify the difference between the no aerosol simulation and the various dust aerosol simulations. Some spread among the plots between 1 and 3 μm is apparent, but as wavelength increases, the difference between the no aerosol case and the various aerosol simulations decrease. One visible difference between the no aerosol case and the dust aerosol cases is in the absorption bands between 1 and 3 μm. The brightness temperature differences in these bands are nearly 50 K, with the no aerosol simulation having the highest brightness

temperature. Extinction due to dust aerosol is responsible for this difference in brightness temperature. To better understand the effect of the various dust aerosols on brightness temperature closer examination of narrower wavelength bands is required.

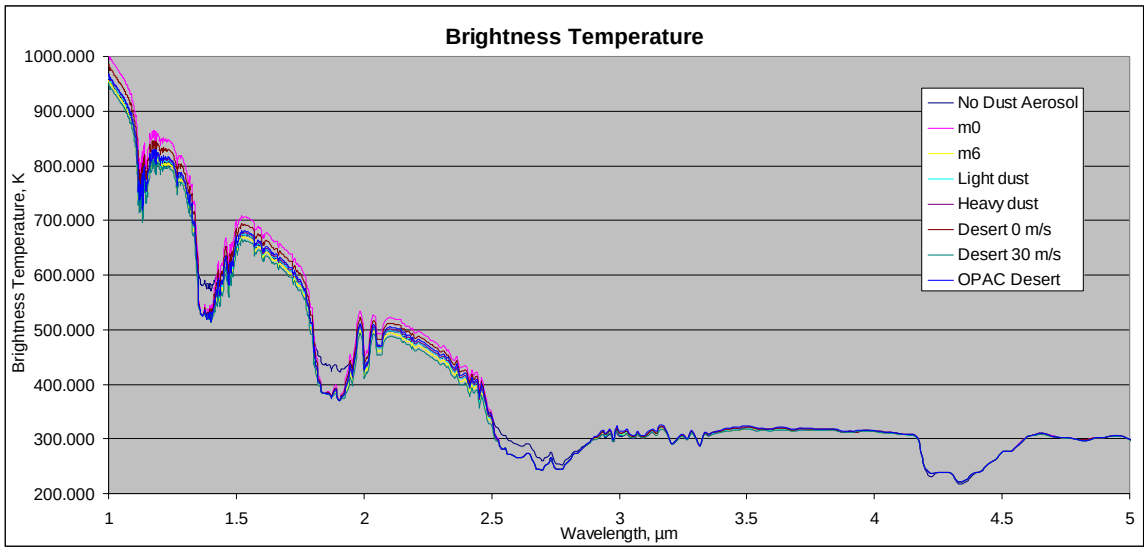

Figure 11. Top-of-the-atmosphere brightness temperature, all cases, summer day, nadir.

Wavelength bands were chosen arbitrarily to match up with radiative windows, based on examination of the wavelength range and the variability of the aerosol in the window band. Brightness temperature plots in the first wavelength band between 1 and 1.1 µm are shown in Figure 12. Brightness temperatures decrease for all simulations similar to the no aerosol simulation. The range of brightness temperature values from every simulation is nearly 50 K. The largest brightness temperature values come from the m0 absorptive representation. The smallest brightness temperature values result from the Desert 30 m/s dust aerosol representation. The brightness temperature values for each simulation do not cross, and retain the same difference from the no aerosol simulation throughout this window.

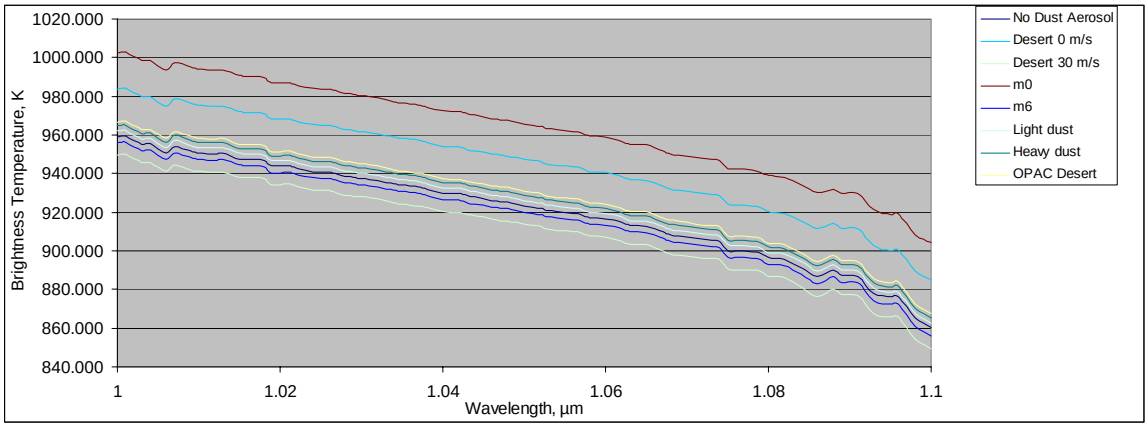

Figure 12. Top-of-the-atmosphere brightness temperature, all cases, summer day, nadir.

Brightness temperatures in the wavelength band between 1.19 and 1.31 µm are similar to brightness temperatures in the first band examined (see Figure 13). Brightness temperatures decrease for all simulations similarly to the no aerosol simulation. The range of brightness temperature values from every simulation remains nearly 50 K. The largest brightness temperature values come from the m0 absorptive representation. The smallest brightness temperature values result from the Desert 30 m/s dust aerosol representation. The brightness temperature values for each simulation do not cross, and retain roughly the same difference from the no aerosol simulation throughout this window.

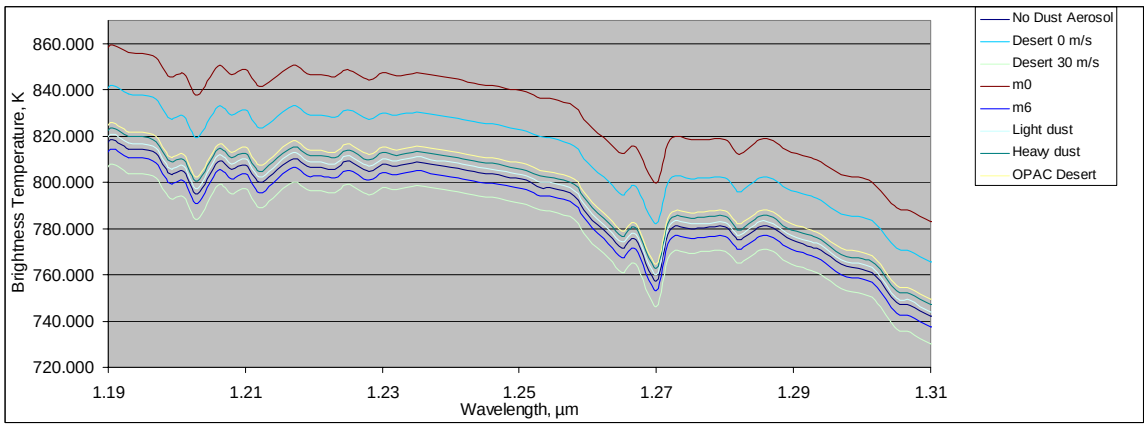

Figure 13. Top-of-the-atmosphere brightness temperature, all cases, summer day, nadir.

Brightness temperatures in the wavelength band between 1.505 and 1.797 µm follow a similar pattern to brightness temperatures in the previous shorter wavelength windows (see Figure 14). Brightness temperatures decrease for all simulations similarly to the no aerosol simulation. The range of brightness temperature values from every simulation is over 40 K. The largest brightness temperature values come from the m0 absorptive representation. The smallest brightness temperature values result from the Desert 30 m/s dust aerosol representation. The brightness temperature values for each simulation do not cross, and retain roughly the same difference from the no aerosol simulation through most of this window. As the wavelength surpasses 1.755 µm the brightness temperatures of all simulations converge.

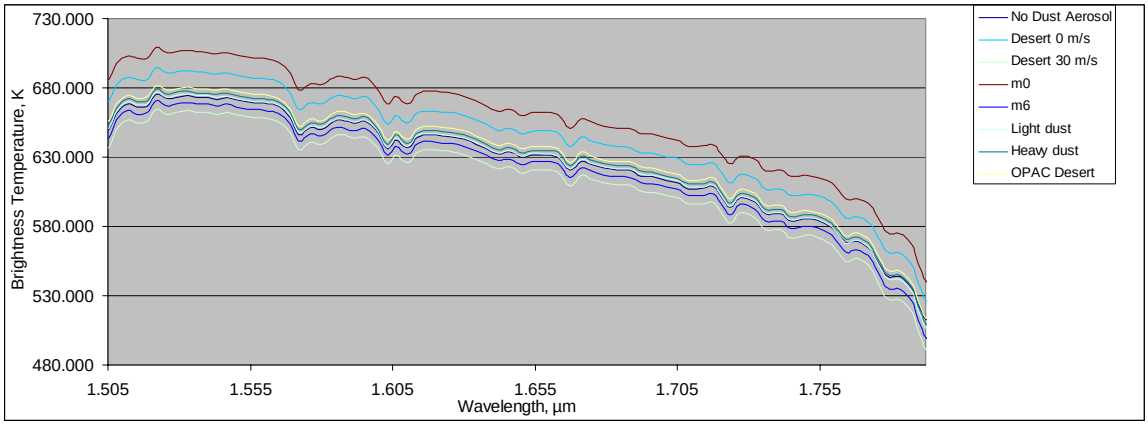

Figure 14. Top-of-the-atmosphere brightness temperature, all cases, summer day, nadir.

Brightness temperatures in the wavelength band between 2.1 and 2.4 µm follow a similar pattern to brightness temperatures in the previous shorter wavelength windows (see Figure 15). Brightness temperatures decrease for all simulations similarly to the no aerosol simulation. The range of brightness temperature values from every simulation has decreased to near 30 K. The largest brightness temperature values come from the m0 absorptive representation. The smallest brightness temperature values result from the Desert 30 m/s dust aerosol representation. The brightness temperature values for each simulation do not cross, and retain roughly the same difference from the no aerosol simulation through most of this window.

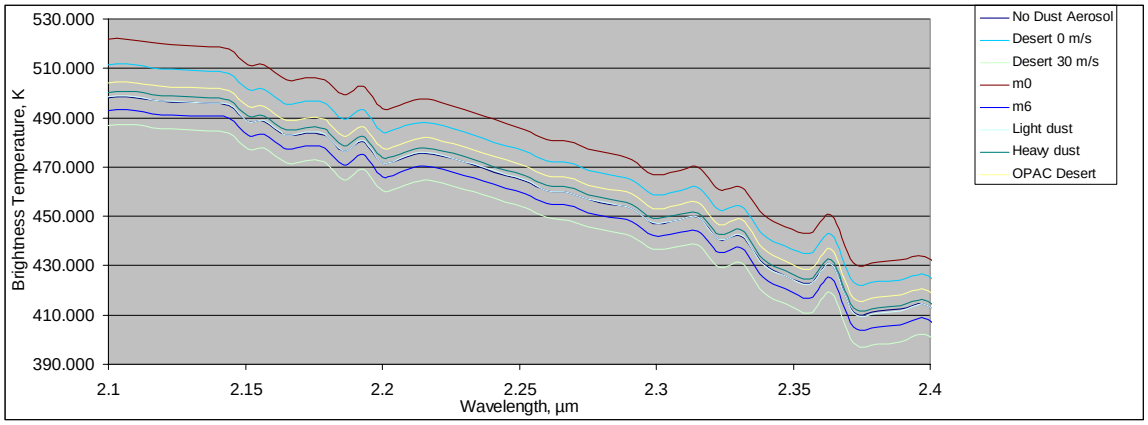

Figure 15. Top-of-the-atmosphere brightness temperature, all cases, summer day, nadir.

Brightness temperatures in the wavelength band between 3.401 and 3.992 µm are fairly flat with a slight decrease in brightness temperature as wavelength increases (see Figure 16). Brightness temperature values for all simulations are similar to the no aerosol simulation. The range of brightness temperature values from every simulation is roughly 5 K at wavelengths below 3.8 µm and only 2 K above 3.8 µm. The largest brightness temperature values come from the OPAC Desert representation. The smallest brightness temperature values result from the Desert 30 m/s dust aerosol representation. The brightness temperature values for each simulation do not cross. The average brightness temperature difference between no aerosol and dust aerosol across this range are small for all simulations.

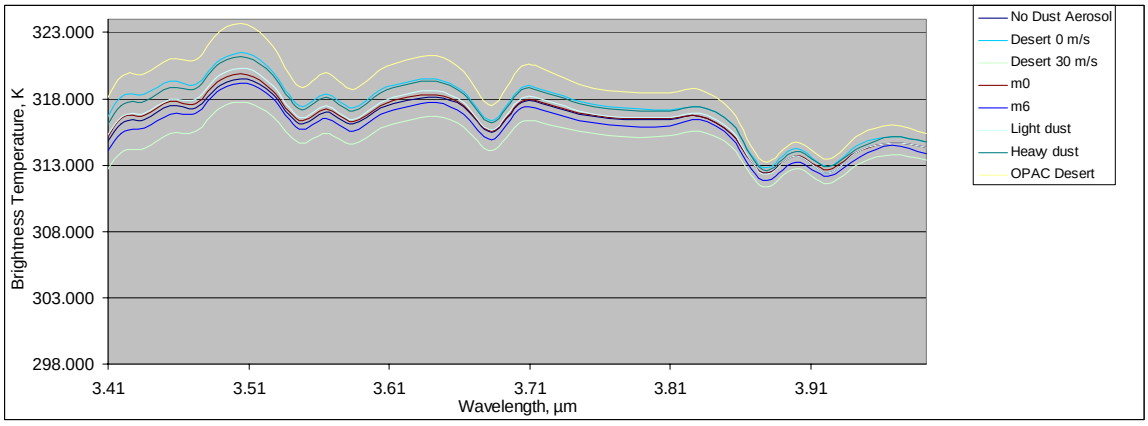

Figure 16. Top-of-the-atmosphere brightness temperature, all cases, summer day, nadir.

Brightness temperatures in the wavelength band between 4.63 and 4.975 µm are variable, with decreasing brightness temperature values through 4.8 µm and increasing values from the 4.8 µm wavelength and higher (see Figure 17). Brightness temperature values for all simulations are very similar to the no aerosol simulation. The range of brightness temperature values from every simulation is roughly 1 K. The largest brightness temperature values come from the no aerosol simulation. The smallest brightness temperature values result from the Desert 30 m/s dust aerosol representation. The brightness temperature values for each simulation do not cross. The average brightness temperature difference between no aerosol and dust aerosol across this range are less than 1 K for all simulations. The Desert 30 m/s dust aerosol results in an average brightness temperature difference from the no aerosol simulation of 0.814 K.

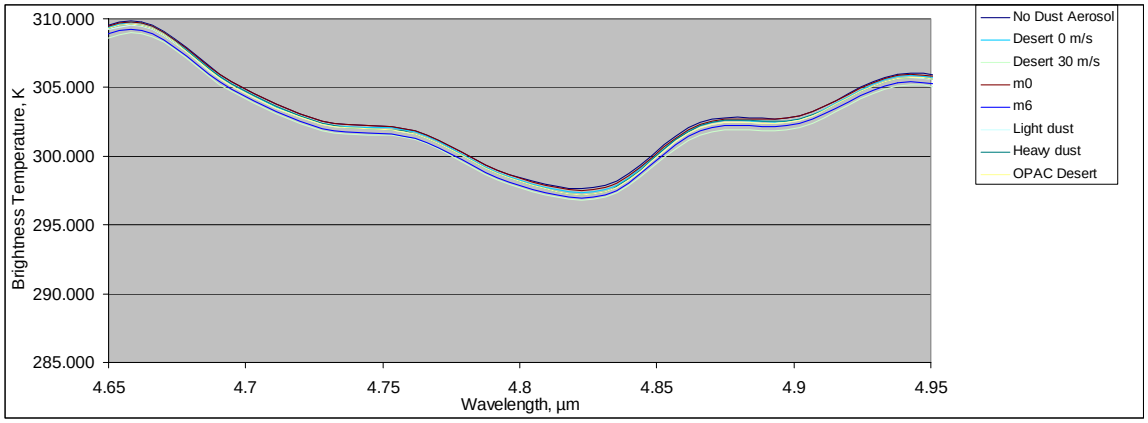

Figure 17. Top-of-the-atmosphere brightness temperature, all cases, summer day, nadir.

The average difference between the no aerosol simulation brightness temperature and the brightness temperatures of various dust aerosols are presented in Figures 18, 19, and Table 3. Of note in this table are the large brightness temperature differences. As wavelength increases, the brightness temperature difference between the no aerosol simulation and any dust aerosol simulation decrease. Another interesting observation is the change in magnitude of the brightness temperature difference with respect to wavelength when comparing the low 0.55 µm optical depth simulations to their high 0.55 µm optical depth counterpart. The m0 simulation produced much higher brightness

temperatures than the no aerosol case below 2.4 µm. The magnitude of the difference is greater than 20 K. At wavelengths longer than 2.4 µm the difference between the m0 simulation brightness temperature and the no aerosol simulation were at most 0.167 K. Contrast this with the m6 simulation - in wavelengths below 2.4 µm, the magnitude of the brightness temperature difference from no aerosol was as much as 5 K. At wavelengths longer the 2.4 µm, the m6 simulation brightness temperature was different from the no aerosol simulation by 0.456 to 0.617 K. The m6 representation is essentially the m0 representation with the addition of a lower concentration, but larger radius mode of dust aerosol. The large disparity between the m0 and m6 representations in terms of average brightness temperature difference when compared with the no aerosol atmosphere must be due to the larger particles. Therefore, the addition of particles of larger radius has a significant impact on top-of-the-atmosphere brightness temperature.

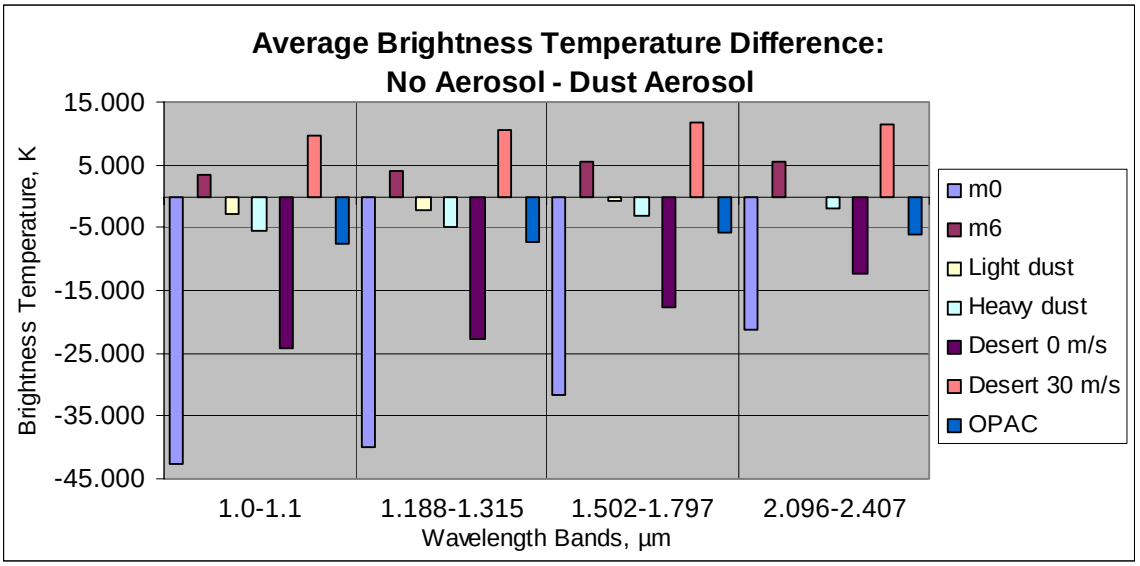

Figure 18. Average brightness temperature difference between no aerosol and dust aerosol, summer day, nadir.

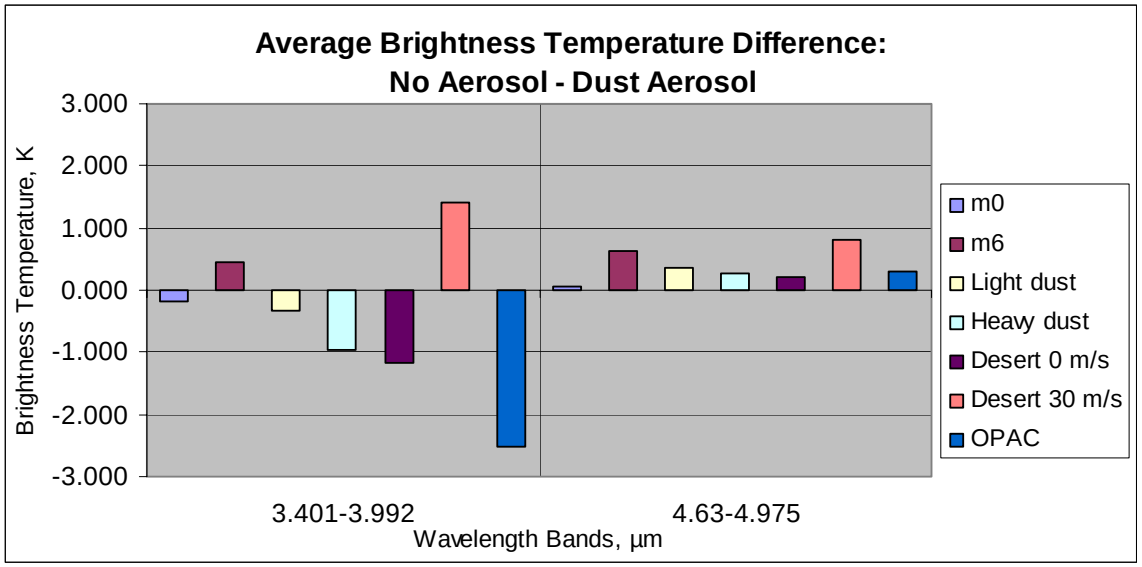

Figure 19. Average brightness temperature difference between no aerosol and dust aerosol, summer day, nadir.

Table 3. Average brightness temperature difference between no aerosol and dust aerosol, summer day, nadir.

	Average Brightness Temperature Difference, K						
Wavelength Band	No Aerosol - Dust Aerosol Representation						
µm	m0	m6	Light dust	Heavy dust	Desert 0 m/s	Desert 30 m/s	OPAC
1.0-1.1	-42.672	3.399	-2.749	-5.429	-24.200	9.727	-7.575
1.188-1.315	-39.813	4.105	-2.220	-4.840	-22.582	10.558	-7.211
1.502-1.797	-31.611	5.430	-0.688	-2.994	-17.608	11.662	-5.893
2.096-2.407	-21.384	5.452	-0.081	-2.079	-12.416	11.374	-6.061
3.401-3.992	-0.167	0.456	-0.340	-0.961	-1.173	1.421	-2.515
4.63-4.975	0.067	0.617	0.347	0.266	0.196	0.814	0.314

B. SUMMER DAY 30° ZENITH ANGLE

The summer day 30° zenith angle case was run with the MODTRAN input parameters described in the methodology section. The no dust aerosol simulation results in radiance values presented in Figure 20. By visual inspection, this off-axis simulation does not appear different from the nadir simulation for radiative transfer with no aerosol. Between 1 and 2.6 µm the magnitude of radiance generally decreases according to the Planck function for solar temperature – modified by gaseous absorption regions. The values decrease from 3.76×10^{-3} $W \cdot cm^{-2} \cdot ster^{-1} \cdot \mu m^{-1}$ to a minimum of 9.6×10^{-8} $W \cdot cm^{-2} \cdot ster^{-1} \cdot \mu m^{-1}$ in the carbon dioxide absorption band between 2 and 3 µm.

Radiance increases beyond 3 µm, roughly corresponding to the Planck function associated with the blackbody temperature of the earth. The minimum radiance of 9.6 x 10^{-8} W•cm^{-2}•$ster^{-1}$•μm^{-1} between 2 and 3 µm increases to a value of 2.89 x 10^{-4} W•cm^{-2}•$ster^{-1}$•μm^{-1} near 5 µm. Above 3 µm, atmospheric absorption is represented in the data. First water vapor absorption is present at wavelengths just greater than 3 µm. Carbon dioxide and nitrous oxide absorption is present between 4 and 5 µm.

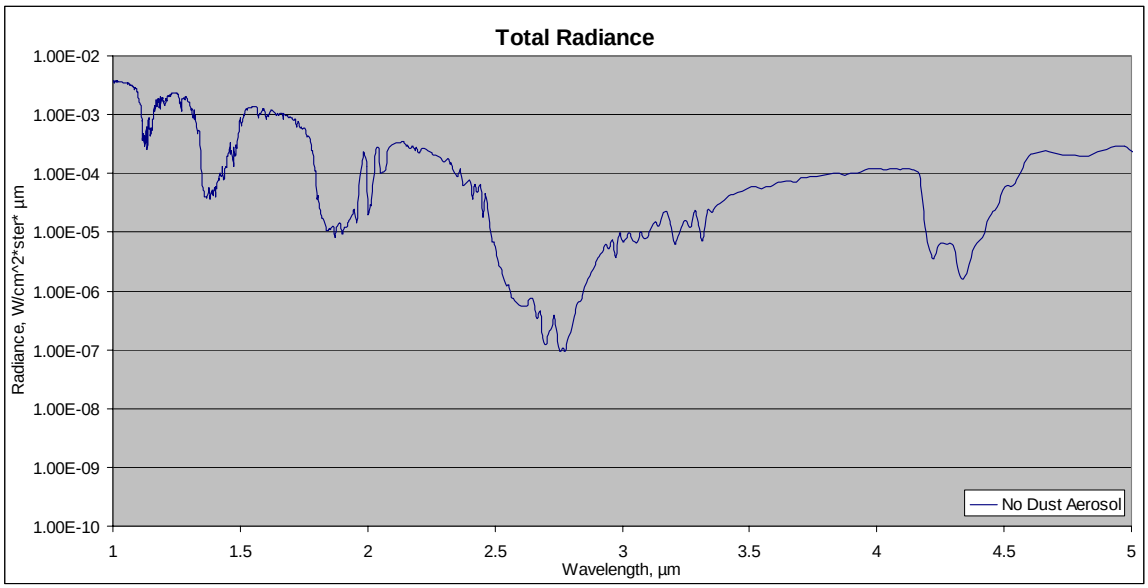

Figure 20. Top-of-the-atmosphere total radiance, no dust aerosol, summer day, 30° zenith angle.

The off-axis, no aerosol simulation brightness temperature values are very similar to the nadir case (see Figure 21). Important to note here is the surface temperature of 320 K for this case, as the brightness temperature values calculated should be near this value in the atmospheric windows of the wavelength band outside of solar influence. At 1 µm the brightness temperature is 961.197 K. This value is slightly higher than the nadir case. At 2.033 µm the brightness temperature is 502.052 K, again slightly higher than the nadir case. At 3.003 µm the brightness temperature value is 304.012 K, which is slightly lower than the nadir case. The decrease in brightness temperature values is similar to the nadir case and is again due to the surface reflectance model used in the MODTRAN simulations.

The atmospheric absorption bands again show lower brightness temperature values than the neighboring windows, as expected. The flat profile of brightness temperature in the absorption bands again provides evidence that surface reflection is negligible when compared to scattering of radiation by the tropospheric, stratospheric and meteoric background aerosol present in the simulation.

The windows in the band between 3.4 and 5 μm are quite interesting when viewed from the brightness temperature perspective. This band shows the interaction of solar energy and terrestrial energy. The transmission in this band is a maximum near 3.5 μm. With this in mind the brightness temperature is expected to be near the 320 K surface temperature. The simulations reveal that the brightness temperature is greater than expected at 3.5 μm. The brightness temperatures between 3.4 and 4.1 μm decrease from 319 to 307 K. From 4.5 to 5 μm brightness temperatures vary between 296 and 309 K. Since the brightness temperatures in this band are closer to the surface temperature than transmission would allow, the energy in the simulation must be due to contribution from solar scattering.

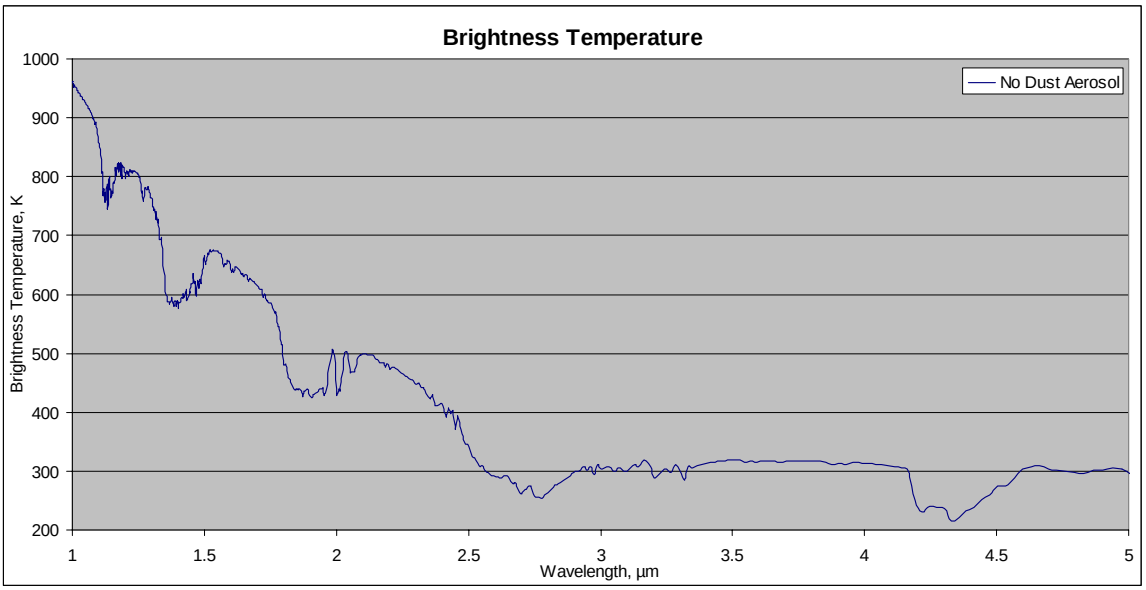

Figure 21. Top-of-the-atmosphere brightness temperature, no dust aerosol, summer day, 30° zenith angle.

As mentioned in the methodology chapter dust aerosols that were non-absorptive were considered as well as absorptive dust aerosols. The difference between the brightness temperatures of the absorptive dust and the non-absorptive dust was significant in all of the atmospheric windows (see Table 4). The differences were larger at shorter wavelengths than at longer wavelengths. This probably relates to the amount of energy involved in these bands, although the wavelength dependence of emitted radiation is also a factor. In addition, the differences were larger for the representations with higher 0.55 μm optical depth (m6 and Desert 30 m/s) than the representations with lower 0.55 μm optical depth (m0 and Desert 0 m/s). The higher 0.55 μm optical depth values result from representations with a larger number of dust aerosol particles per cubic centimeter. Larger dust aerosol particle loading suggests larger extinction by these aerosols. Larger extinction due to dust aerosol causes larger changes to top-of-the-atmosphere brightness temperature. This is why the Desert 30 m/s dust representation exhibits a larger average brightness temperature difference from the no aerosol simulation than the m6 representation. Since the brightness temperature values from both the non-absorptive and absorptive Desert 30 m/s dust representations are larger than the brightness temperature values from both m6 representations, the difference between the non-absorptive and absorptive Desert 30 m/s dust aerosols are correspondingly larger than the difference between the m6 representations. The exception here is the Heavy dust and Light dust representations. The non-absorptive aerosols minus the absorptive aerosol brightness temperature differences were similar in both the Light dust and Heavy dust aerosol representation despite having different 0.55 μm optical depths. The 0.55 μm optical depths were similar to the other representations with Heavy dust having the higher 0.55 μm optical depth. Brightness temperature differences in this table reveal the importance of accounting for absorption by dust aerosol when calculating radiative transfer between 1 and 5 μm. With that in mind the following examination of brightness temperatures among the different dust representations will focus on the absorptive dust aerosol only.

Table 4. Average brightness temperature difference between non-absorptive and absorptive dust aerosol, summer day, 30° zenith angle.

	Average Brightness Temperature Difference, K					
Wavelength Band	Non Absorptive - Absorptive Dust Aerosol Representation					
μm	m0	m6	Light dust	Heavy dust	Desert 0 m/s	Desert 30 m/s
1.0-1.1	2.755	11.820	6.822	5.756	-2.496	12.074
1.188-1.315	2.435	12.638	7.383	6.240	-1.688	13.016
1.502-1.797	2.200	13.518	8.071	6.991	0.144	14.193
2.096-2.407	1.820	14.370	8.931	7.722	2.597	15.065
3.401-3.992	0.240	3.609	2.344	1.895	1.961	4.046
4.63-4.975	0.059	0.121	0.083	0.118	0.119	0.284

Brightness temperatures calculated from the various dust aerosols across the 1 through 5 μm band are presented in Figure 22. Since the brightness temperatures range from near 1000 K to below 300 K it is difficult to quantify the difference between the no aerosol simulation and the various dust aerosol simulations. Some spread among the plots between 1 and 3 μm is apparent, but as wavelength increases, the difference between the no aerosol case and the various aerosol simulations decrease. One visible difference is between the no aerosol case and the dust aerosol cases in the absorption bands between 1 and 3 μm. These differences are near 50 K, with the no aerosol simulation having the highest brightness temperature. This is caused by extinction due to dust aerosol. To better understand the effect of the various dust aerosols on brightness temperature closer examination of narrower wavelength bands is required.

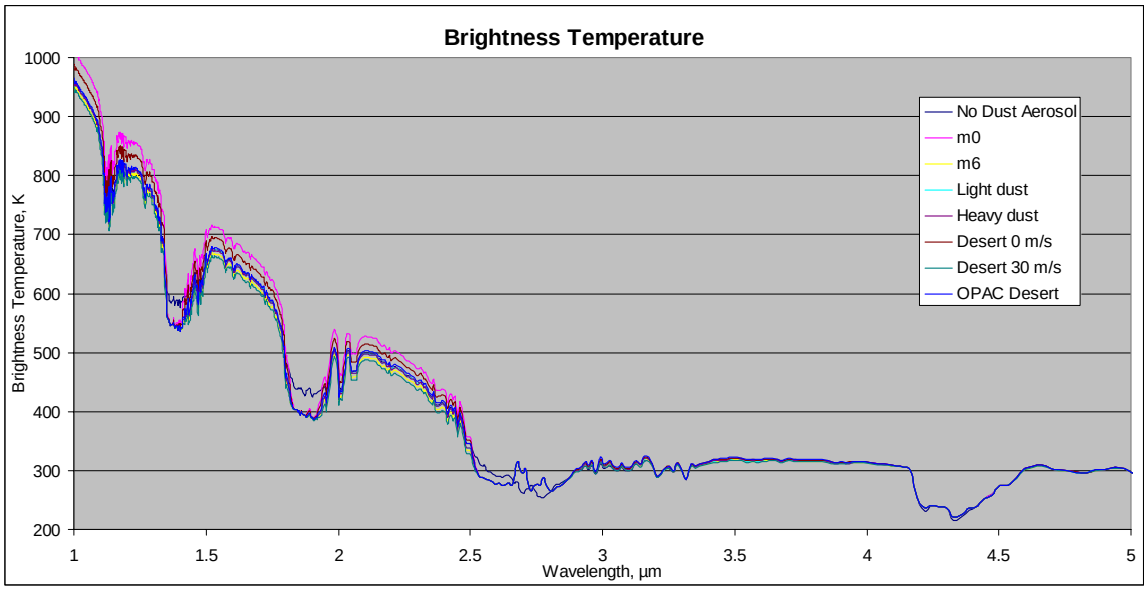

Figure 22. Top-of-the-atmosphere brightness temperature, all cases, summer day, 30° zenith angle.

Wavelength bands were chosen arbitrarily to match up with radiative windows, based on examination of the wavelength range and the variability of the aerosol in the window band. Brightness temperatures in the first wavelength band between 1 and 1.1 µm are plotted in Figure 23. Brightness temperatures decrease for all simulations similarly to the no aerosol simulation. The range of brightness temperature values from every simulation is over 60 K. The largest brightness temperature values come from the m0 dust aerosol representation. The smallest brightness temperature values result from the Desert 30 m/s dust aerosol representation. The brightness temperature values for each simulation do not cross, and retain the same difference from the no aerosol simulation throughout this window.

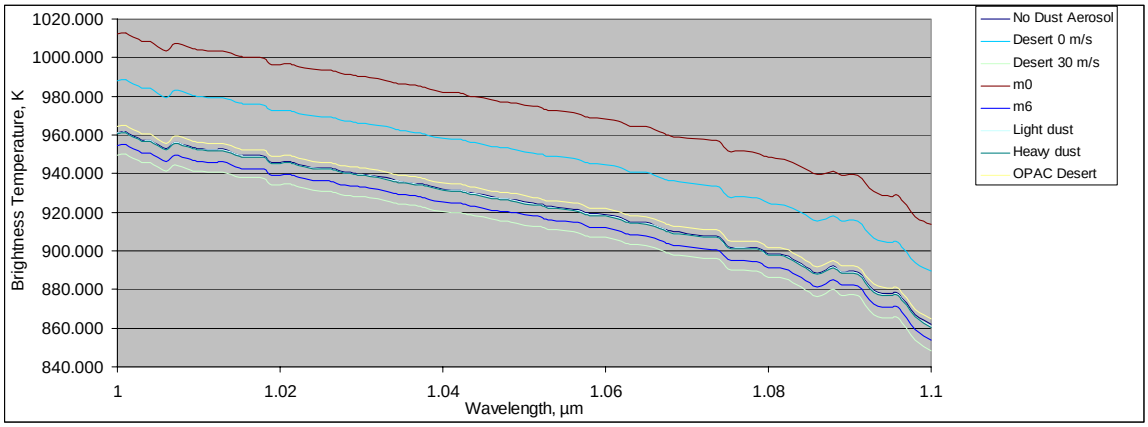

Figure 23. Top-of-the-atmosphere brightness temperature, all cases, summer day, 30° zenith angle.

Brightness temperatures in the wavelength band between 1.19 and 1.31 µm are similar to brightness temperatures in the first band examined (see Figure 24). Brightness temperatures decrease for all simulations similarly to the no aerosol simulation. The range of brightness temperature values from every simulation remains nearly 60 K. The largest brightness temperature values come from the m0 dust aerosol representation. The smallest brightness temperature values result from the Desert 30 m/s dust aerosol representation. The brightness temperature values for each simulation do not cross, and retain roughly the same difference from the no aerosol simulation throughout this window.

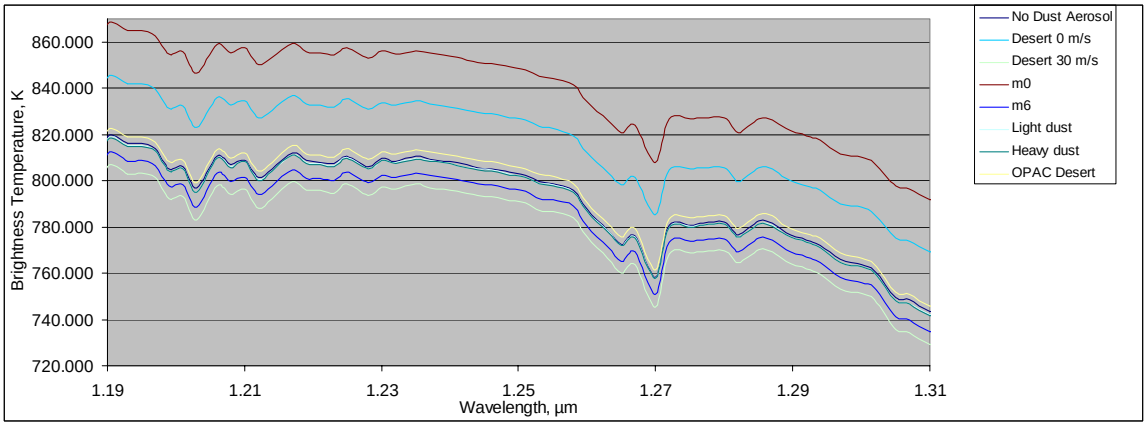

Figure 24. Top-of-the-atmosphere brightness temperature, all cases, summer day, 30° zenith angle.

Brightness temperatures in the wavelength band between 1.505 and 1.797 µm follow a similar pattern as in the previous shorter wavelength windows (see Figure 25). Brightness temperatures decrease for all simulations similarly to the no aerosol simulation. The range of brightness temperature values from every simulation is over 50 K. The largest brightness temperature values come from the m0 dust aerosol representation. The smallest brightness temperature values result from the Desert 30 m/s dust aerosol representation. The brightness temperature values for each simulation do not cross, and retain roughly the same difference from the no aerosol simulation through most of this window. As the wavelength surpasses 1.755 µm the brightness temperatures of all simulations converge.

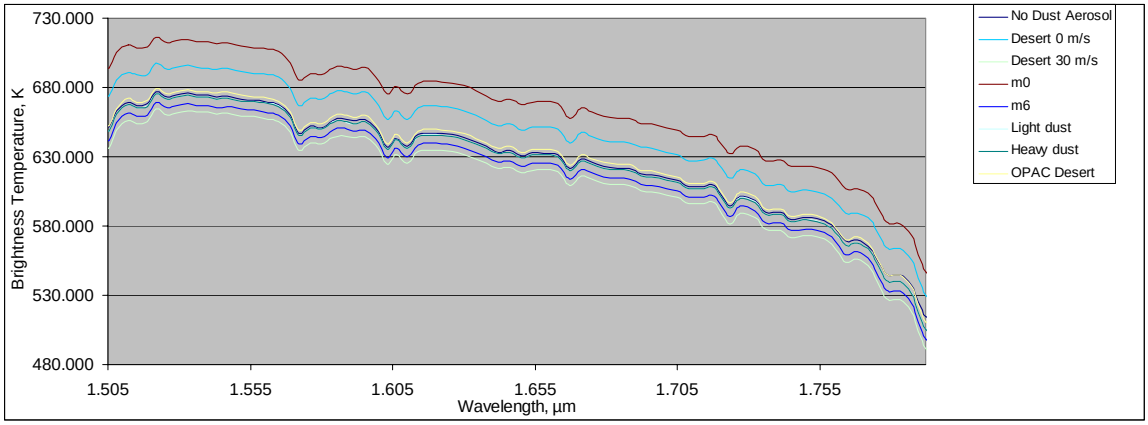

Figure 25. Top-of-the-atmosphere brightness temperature, all cases, summer day, 30° zenith angle.

Brightness temperatures in the wavelength band between 2.1 and 2.4 µm follow a similar pattern as in the previous shorter wavelength windows (see Figure 26). Brightness temperatures decrease for all simulations similarly to the no aerosol simulation. The range of brightness temperature values from every simulation has decreased to over 30 K. The largest brightness temperature values come from the m0 dust aerosol representation. The smallest brightness temperature values result from the Desert 30 m/s dust aerosol representation. The brightness temperature values for each simulation do not cross, and retain roughly the same difference from the no aerosol simulation through most of this window.

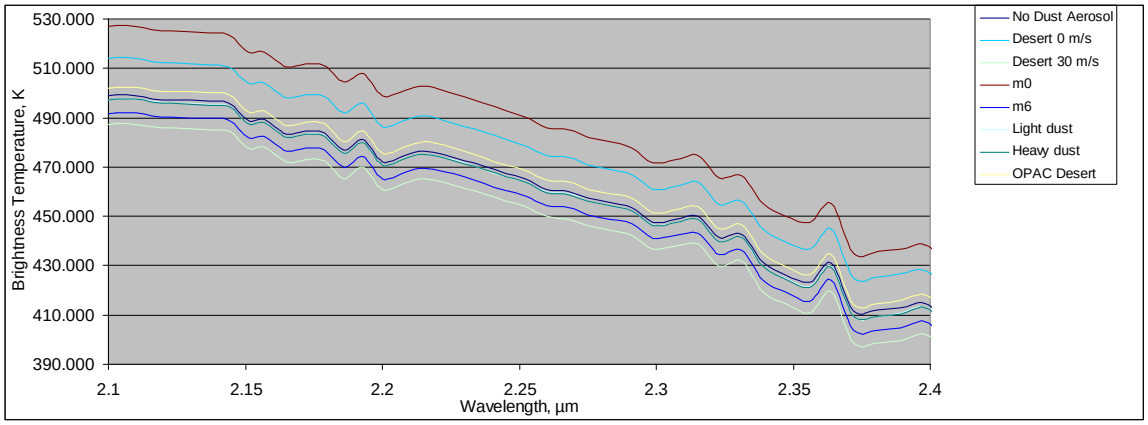

Figure 26. Top-of-the-atmosphere brightness temperature, all cases, summer day, 30° zenith angle.

Brightness temperatures in the wavelength band between 3.401 and 3.992 µm are fairly flat with a slight decrease in brightness temperature as wavelength increases (see Figure 27). Brightness temperature values for all simulations are similar to the no aerosol simulation. The range of brightness temperature values from every simulation is roughly 5 K at wavelengths below 3.8 µm and only 2 K above 3.8 µm. The largest brightness temperature values come from the OPAC Desert representation. The smallest brightness temperature values result from the Desert 30 m/s dust aerosol representation. The brightness temperature values for each simulation do not cross. The average brightness temperature difference between no aerosol and dust aerosol across this range are small for all simulations.

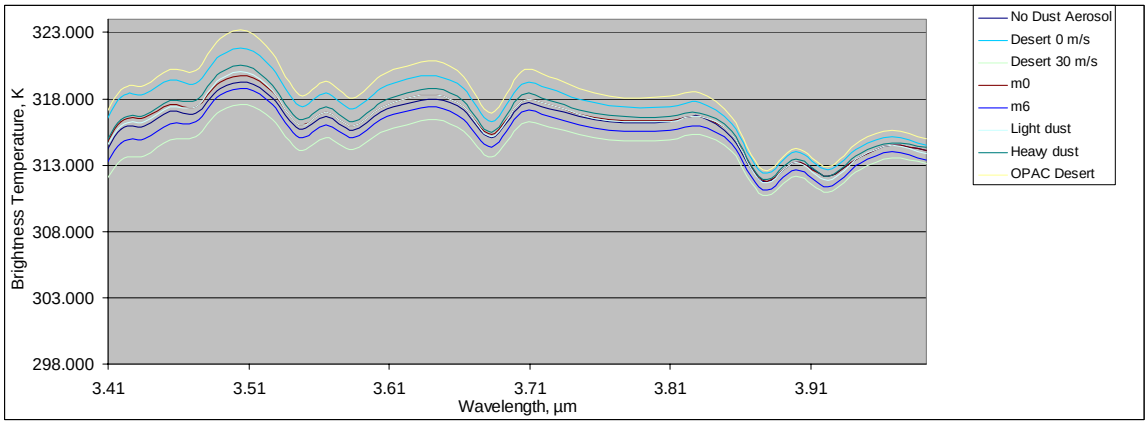

Figure 27. Top-of-the-atmosphere brightness temperature, all cases, summer day, 30° zenith angle.

Brightness temperatures in the wavelength band between 4.63 and 4.975 µm are variable, first brightness temperature values decrease through 4.8 µm and then increase from 4.8 µm wavelength and higher (see Figure 28). Brightness temperature values for all simulations are very similar to the no aerosol simulation. The range of brightness temperature values from every simulation is roughly 1 K. The largest brightness temperature values come from the no aerosol simulation. The smallest brightness temperature values result from the Desert 30 m/s dust aerosol representation. The brightness temperature values for each simulation do not cross. The average brightness temperature difference between no aerosol and dust aerosol across this range are less than 1 K for all simulations. The Desert 30 m/s dust aerosol results in an average brightness temperature difference from the no aerosol simulation of 0.947 K.

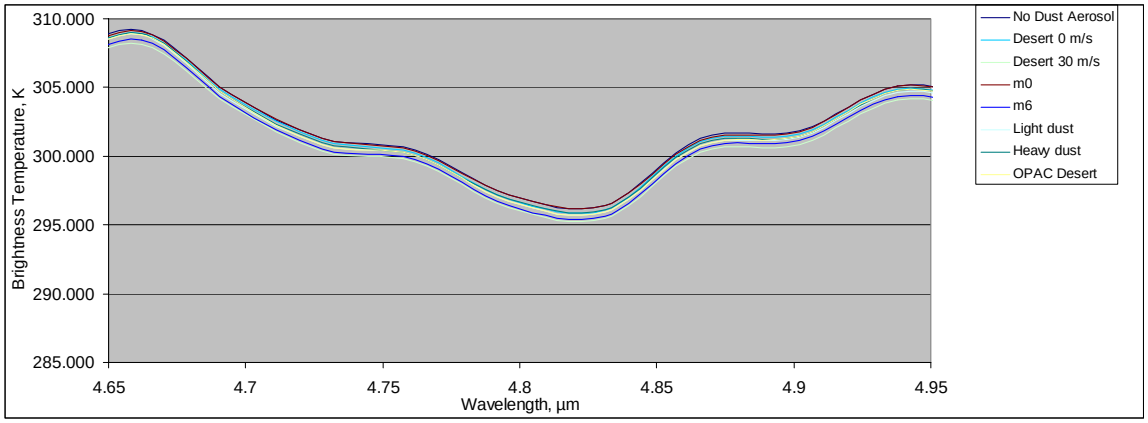

Figure 28. Top-of-the-atmosphere brightness temperature, all cases, summer day, 30° zenith angle.

The average difference between the no aerosol simulation brightness temperature and the brightness temperatures of various dust aerosols are presented in Figures 29, 30, and Table 5. Of note in this table are the large brightness temperature differences. As wavelength increases, the brightness temperature difference between the no aerosol simulation and any dust aerosol simulation decrease.

Another interesting observation is the change in magnitude of the brightness temperature difference with respect to wavelength when comparing the low 0.55 µm

optical depth simulations to their high 0.55 μm optical depth counterpart. The m0 simulation produced much higher brightness temperatures than the no aerosol case below 2.4 μm. The magnitude of the difference is greater than 25 K. At wavelengths longer than 2.4 μm the difference between the m0 simulation brightness temperature and the no aerosol simulation is at most 0.275 K. Contrast this with the m6 simulation - in wavelengths below 2.4 μm, the magnitude of the brightness temperature difference from no aerosol was as much as 8 K. At wavelengths longer the 2.4 μm, the m6 simulation brightness temperature was different from the no aerosol simulation by 0.641 to 0.756 K. The m6 representation is essentially the m0 representation with the addition of a lower concentration, but larger radius mode of dust aerosol. The large disparity between the m0 and m6 representations in terms of average brightness temperature difference when compared with the no aerosol atmosphere must be due to the larger particles. Therefore, the addition of particles of larger radius has a significant impact on top-of-the-atmosphere brightness temperature.

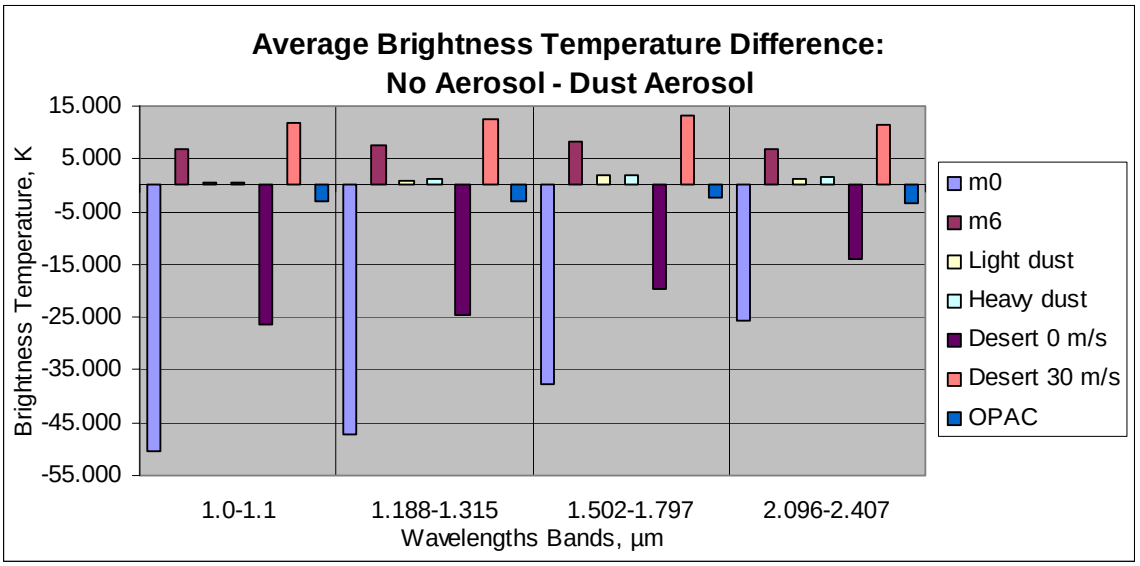

Figure 29. Average brightness temperature difference between no aerosol and dust aerosol, summer day, 30° zenith angle.

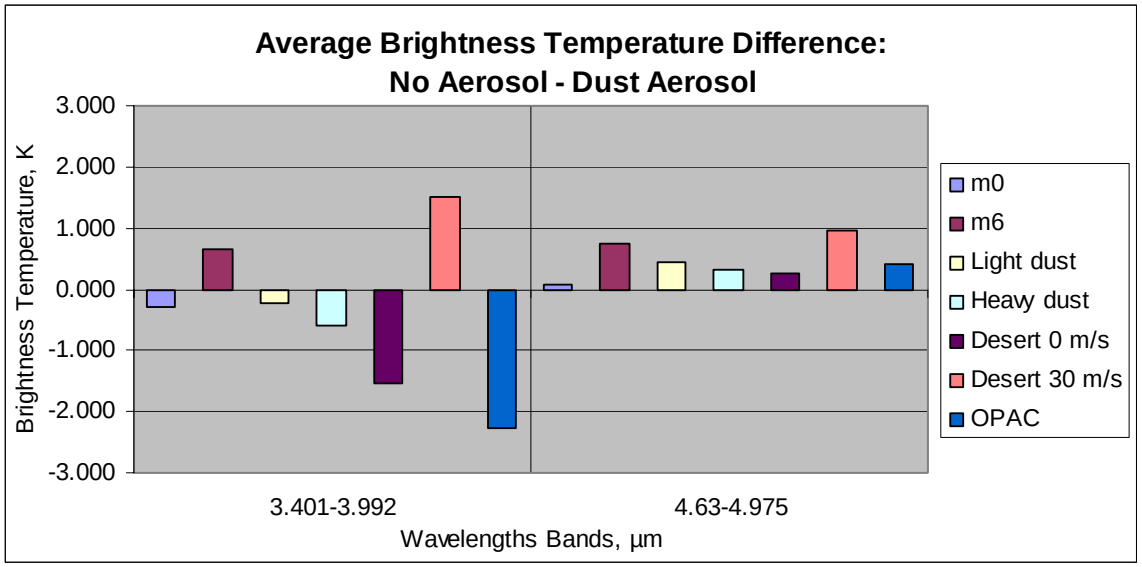

Figure 30. Average brightness temperature difference between no aerosol and dust aerosol, summer day, 30° zenith angle.

Table 5. Average brightness temperature difference between no aerosol and dust aerosol, summer day, 30° zenith angle.

	Average Brightness Temperature Difference, K						
Wavelength Band	No Aerosol - Dust Aerosol Representation						
µm	m0	m6	Light dust	Heavy dust	Desert 0 m/s	Desert 30 m/s	OPAC
1.0-1.1	-50.373	6.774	0.456	0.681	-26.440	11.819	-3.152
1.188-1.315	-47.051	7.437	0.915	1.086	-24.768	12.636	-2.896
1.502-1.797	-37.635	8.124	1.810	1.955	-19.516	13.127	-2.250
2.096-2.407	-25.750	6.950	1.355	1.489	-14.081	11.569	-3.518
3.401-3.992	-0.275	0.641	-0.219	-0.597	-1.535	1.494	-2.283
4.63-4.975	0.069	0.756	0.455	0.334	0.250	0.947	0.409

The average brightness temperature difference across the window wavelengths bands is where the nadir view cases and the off-axis cases differ significantly. The average differences increase in all wavelengths when the following dust aerosol representations are added to the simulation: m0, m6, Desert 0 m/s, and Desert 30 m/s. The Light dust aerosol changed differently for nearly every wavelength band. The magnitude of the difference in the 1 and 1.188 µm band decreases from close to 2 K in the nadir case to less than 1 K in the off-axis case. The magnitude of the difference in the 1.502 and 2.096 µm band increases from close to 0.5 K in the nadir case to more than 1 K in the off-axis case. The magnitude of the difference in the 3.401 µm band decreases from 0.340 K in the nadir case to 0.219 K in the off-axis case. The magnitude of the difference in the 4.63 µm band increases from close to 0.3 K in the nadir case to close to

0.5 K in the off-axis case. The Heavy dust aerosol also changed differently in each wavelength band. The magnitude of the difference in the 1, 1.188, 1.502, 2.096 and 3.401 μm band decrease from a range of nearly 1 to 5 K in the nadir case to a range of 0.5 to 1.9 K in the off-axis case. The magnitude of the difference in the 4.63 μm band increases from 0.2 K in the nadir case to 0.3 K in the off-axis case. The OPAC Desert aerosol behaves similarly to the Heavy dust aerosol. The magnitude of the difference in the 1, 1.188, 1.502, 2.096 and 3.401 μm band decrease from a range of nearly 2 to 7 K in the nadir case to a range of 2 to 3 K in the off-axis case. The magnitude of the difference in the 4.63 μm band increases from 0.3 K in the nadir case to 0.5 K in the off-axis case.

C. SUMMER NIGHT NADIR

The summer night nadir view case was run with the MODTRAN input parameters described in the methodology section. The no dust aerosol simulation results in radiance values presented in Figure 31. Between 1 and 2.6 μm the magnitude of radiance is small. This energy is solar energy reflected off of the moon and into the scene in the MODTRAN simulation. Radiance increases above 3 μm, roughly corresponding to the Planck function associated with the blackbody temperature of the earth. The minimum radiance of 1.55×10^{-10} $W \bullet cm^{-2} \bullet ster^{-1} \bullet \mu m^{-1}$ occurs at 1.316 μm, in the absorption band below 1.5 μm. Terrestrial emission is evident at wavelengths beyond 1 μm with a minimum value of 4.04×10^{-10} $W \bullet cm^{-2} \bullet ster^{-1} \bullet \mu m^{-1}$. From this minimum, radiance increases to a value of roughly 2.08×10^{-4} $W \bullet cm^{-2} \bullet ster^{-1} \bullet \mu m^{-1}$ near 5 μm. Atmospheric absorption is represented by reduced radiance values in the data between 3 and 5 μm. First, water vapor absorption is present at wavelengths just greater than 3 μm. Carbon dioxide and nitrous oxide absorption bands are present between 4 and 5 μm.

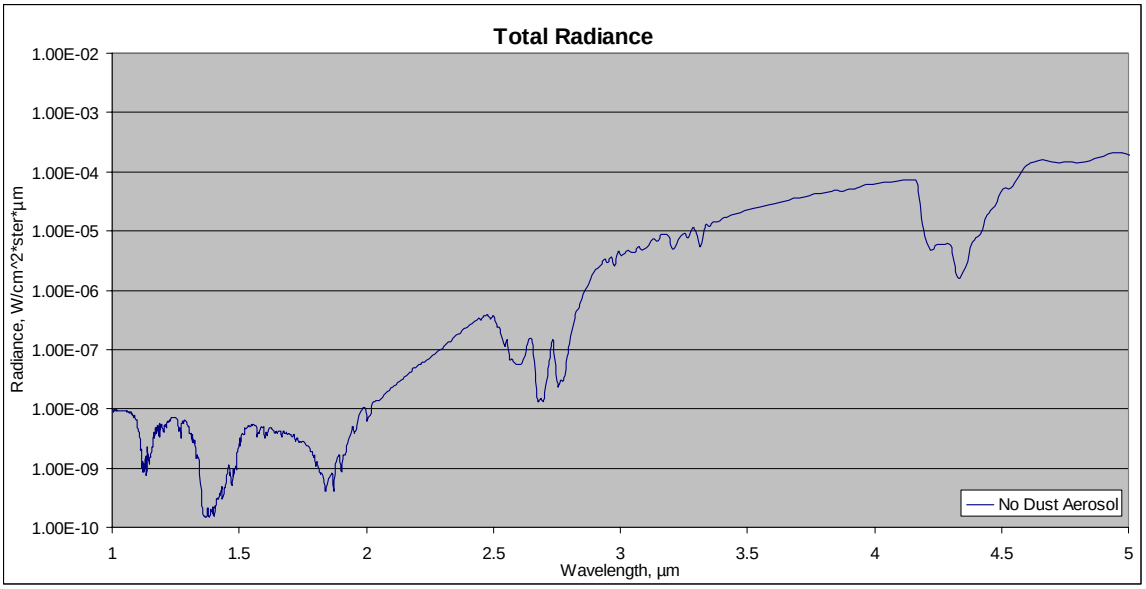

Figure 31. Top-of-the-atmosphere total radiance, no dust aerosol, summer night, nadir.

Brightness temperatures reveal the presence of the lunar energy in the 1 through 3 µm wavelength band (see Figure 32). Important to note here is the surface temperature of 302.5 K for this case, as the brightness temperature values calculated should be near this value in the atmospheric windows of the wavelengths outside of lunar influence. At 1 µm the brightness temperature is 516.578 K this is slightly more than half of the daytime simulation. At 2.014 µm the brightness temperature value decreases to 290.702 K. At 3.003 µm the brightness temperature value is 293.184 K. This decrease in brightness temperature values is due to the surface reflectance model used in the MODTRAN simulations. In the same wavelength span the reflectance changes from 0.7 to just 0.1, therefore much less lunar energy is being reflected off of the surface and towards the top-of-the-atmosphere.

Also interesting to note is the similarity of the 2 and 3 µm brightness temperatures. Since the lunar source inputs much less energy into the calculation, the entire lunar brightness temperature curve shifts further down the chart, and it intersects the terrestrial emission curve at shorter wavelengths as a result. In the daytime

simulation it seemed that solar energy was influencing the brightness temperature up to 5 μm. This night time simulation reveals the terrestrial energy influencing brightness temperatures at wavelengths as small as 2 μm.

The atmospheric absorption bands below 2 μm are revealed as bands of lower brightness temperature, as expected. Also expected is the fact that the reduction of brightness temperature is smaller in this simulation due to the lower amounts of radiant energy. Surface reflection is very low, but the scattering of radiation by the tropospheric, stratospheric and meteoric background aerosol is present in the simulation. Evidence that this type of scattering is occurring is in the profile of brightness temperatures in the absorption bands. The brightness temperatures show little change across the absorption band, in contrast to the sharp decrease in brightness temperature in the neighboring windows which mirror the surface reflectance. The absorption bands at wavelengths greater than 2.4 μm are similar to the absorption bands of the daytime simulation in that they represent a decrease from the neighboring atmospheric window of similar magnitude. This points to the relative influence of terrestrial versus solar radiance once again. In this simulation it is clear that terrestrial radiance dominates the brightness temperature to wavelengths as low as 1.9 μm, because outside of the absorption bands the brightness temperature is similar to the surface temperature.

Despite the dominance of terrestrial energy at short wavelengths, the windows in the band between 3.4 and 5 μm are still influenced somewhat by the lunar source. The transmission in this band is a maximum near 3.5 μm. With this in mind the brightness temperature is expected to be near the 302.5 K surface temperature. The simulations reveal that the brightness temperature is greater than expected at 3.5 μm. The brightness temperatures between 3.4 and 4.1 μm decrease from 297 to 295 K. From 4.5 to 5 μm brightness temperatures vary between 284 and 296 K. Since the brightness temperatures in this band are closer to the surface temperature than transmission would allow, the energy in the simulation must be due to contribution from lunar scattering.

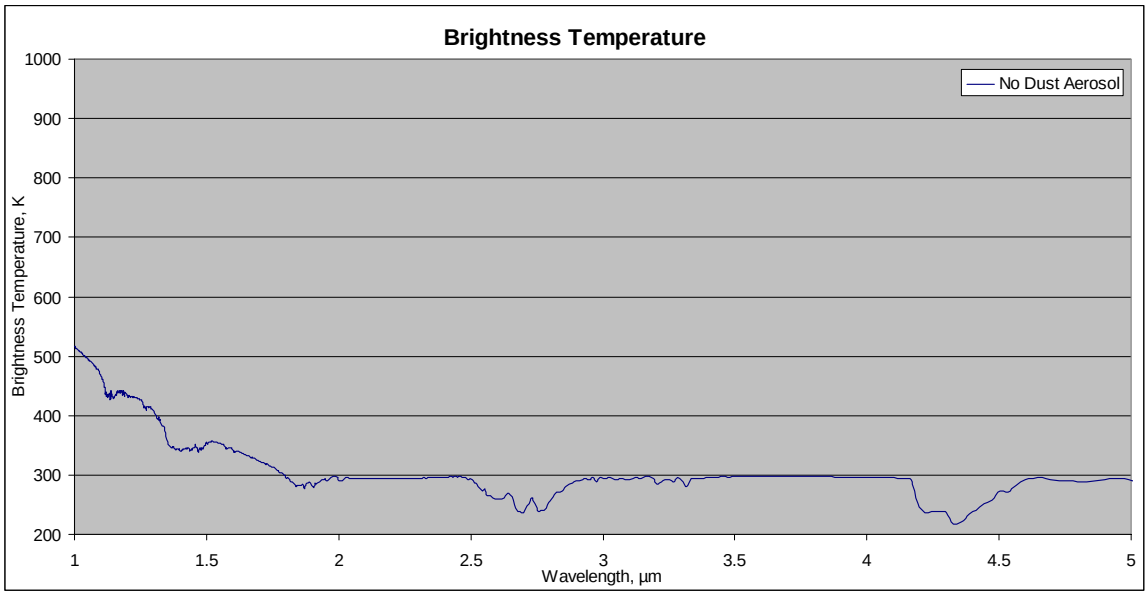

Figure 32. Top-of-the-atmosphere brightness temperature, no dust aerosol, summer night, nadir.

As mentioned in the methodology chapter dust aerosols that were non-absorptive were considered as well as absorptive dust aerosols. The difference between the brightness temperatures of the absorptive dust and the non-absorptive dust was significant in all of the atmospheric windows (see Table 6). The differences were larger at shorter wavelengths than at longer wavelengths. This probably relates to the amount of energy involved in these bands, although the wavelength dependence of emitted radiation is also a factor. In addition, the differences were larger for the representations with higher 0.55 µm optical depth (m6 and Desert 30 m/s) than the representations with lower 0.55 µm optical depth (m0 and Desert 0 m/s). The higher 0.55 µm optical depth values result from representations with a larger number of dust aerosol particles per cubic centimeter. Larger dust aerosol particle loading suggests larger extinction by these aerosols. Larger extinction due to dust aerosol causes larger changes to top-of-the-atmosphere brightness temperature. This is why the Desert 30 m/s dust representation exhibits a larger average brightness temperature difference from the no aerosol simulation than the m6 representation. Since the brightness temperature values from both the non-absorptive and absorptive Desert 30 m/s dust representations are larger than the

brightness temperature values from both m6 representations, the difference between the non-absorptive and absorptive Desert 30 m/s dust aerosols are correspondingly larger than the difference between the m6 representations. The exception here is the Heavy dust and Light dust representations. The non-absorptive aerosols minus the absorptive aerosol brightness temperature differences were similar in both the Light dust and Heavy dust aerosol representation despite having different 0.55 μm optical depths. The 0.55 μm optical depths were similar to the other representations with Heavy dust having the higher 0.55 μm optical depth. Brightness temperature differences in this table reveal the importance of accounting for absorption by dust aerosol when calculating radiative transfer between 1 and 5 μm. With that in mind the following examination of brightness temperatures among the different dust representations will focus on the absorptive dust aerosol only.

Table 6. Average brightness temperature difference between non-absorptive and absorptive dust aerosol, summer night, nadir.

	Average Brightness Temperature Difference, K					
Wavelength Band	Non Absorptive - Absorptive Dust Aerosol Representation					
μm	m0	m6	Light dust	Heavy dust	Desert 0 m/s	Desert 30 m/s
1.0-1.1	0.860	2.819	1.351	1.135	-0.527	4.315
1.188-1.315	0.761	3.105	1.544	1.305	-0.306	4.726
1.502-1.797	0.647	3.098	1.683	1.473	0.187	4.473
2.096-2.407	-0.187	-0.856	-0.590	-0.559	-0.432	-1.027
3.401-3.992	-0.079	-0.661	-0.428	-0.391	-0.295	-0.823
4.63-4.975	-0.017	-0.178	-0.114	-0.115	-0.133	-0.276

Brightness temperatures resultant from the addition of several dust aerosols across the entire 1 through 5 μm band are plotted in Figure 33. Since the brightness temperatures range from near 520 K to below 300 K it is difficult to quantify the difference between the no aerosol simulation and the various dust aerosol simulations by examining the plot of the entire wavelength range. Some spread among the plots between 1 and 2 μm is apparent, but as wavelength increases, the difference between the no aerosol case and the various aerosol simulations decrease. One visible difference is between the no aerosol case and the dust aerosol cases in the absorption band at 1.4 μm. The brightness temperature difference here is roughly 30 K, with the no aerosol

simulation having the highest brightness temperature. This is caused by extinction due to dust aerosol. To better understand the effect of the various dust aerosols on brightness temperature closer examination of narrower wavelength bands is required.

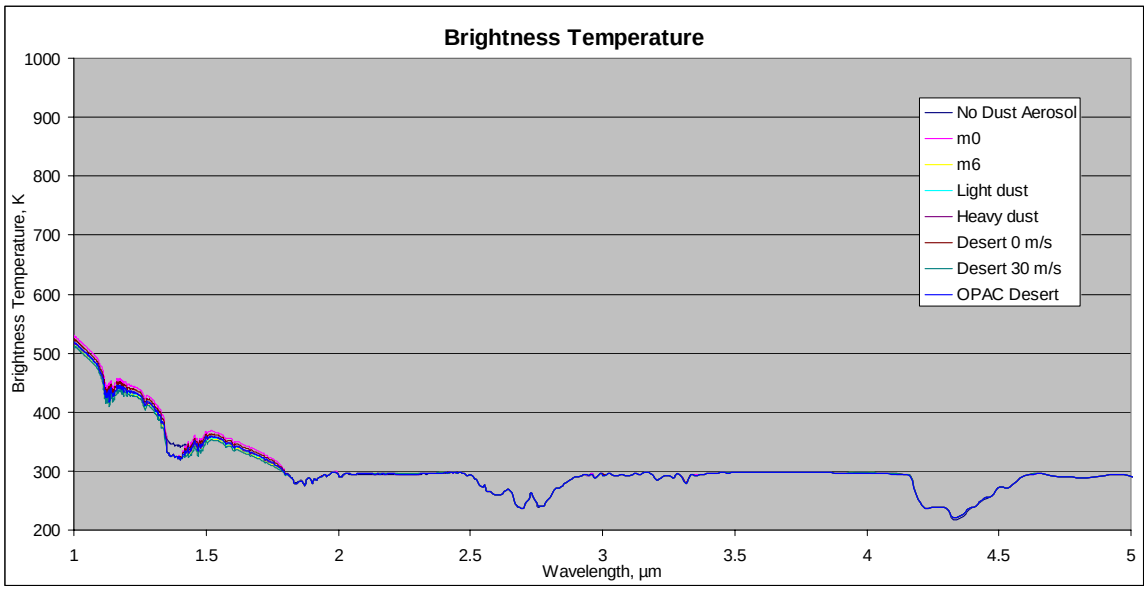

Figure 33. Top-of-the-atmosphere brightness temperature, all cases, summer night, nadir.

Window bands were chosen arbitrarily based on examination of the wavelength range and the variability of the aerosol in the window band. Brightness temperatures in the first band between 1 and 1.1 µm are presented in Figure 34. Brightness temperatures decrease for all simulations similarly to the no aerosol simulation. The range of brightness temperature values from every simulation is smaller than in the daytime simulation roughly 15 K. The largest brightness temperature values come from the m0 dust aerosol representation. The smallest brightness temperature values result from the Desert 30 m/s dust aerosol representation. The brightness temperature values for each simulation do not cross, and retain the same difference from the no aerosol simulation throughout this window.

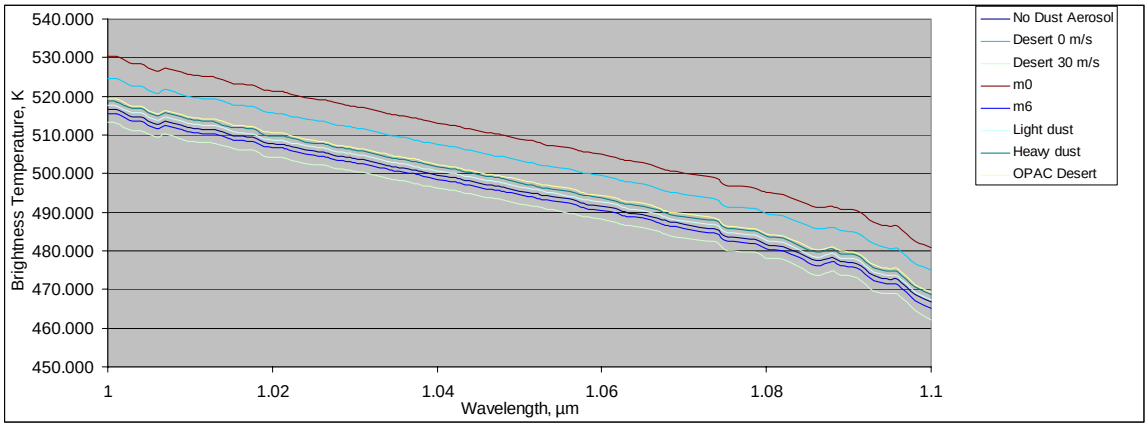

Figure 34. Top-of-the-atmosphere brightness temperature, all cases, summer night, nadir.

Brightness temperatures in the next window band between 1.19 and 1.31 µm are presented in Figure 35. Brightness temperatures decrease for all simulations similarly to the no aerosol simulation. The range of brightness temperature values from every simulation is larger than in the previously examined band with a range of nearly 20 K. The largest brightness temperature values come from the m0 absorptive representation. The smallest brightness temperature values result from the Desert 30 m/s dust aerosol representation. The brightness temperature values for each simulation do not cross, and retain roughly the same difference from the no aerosol simulation throughout this window.

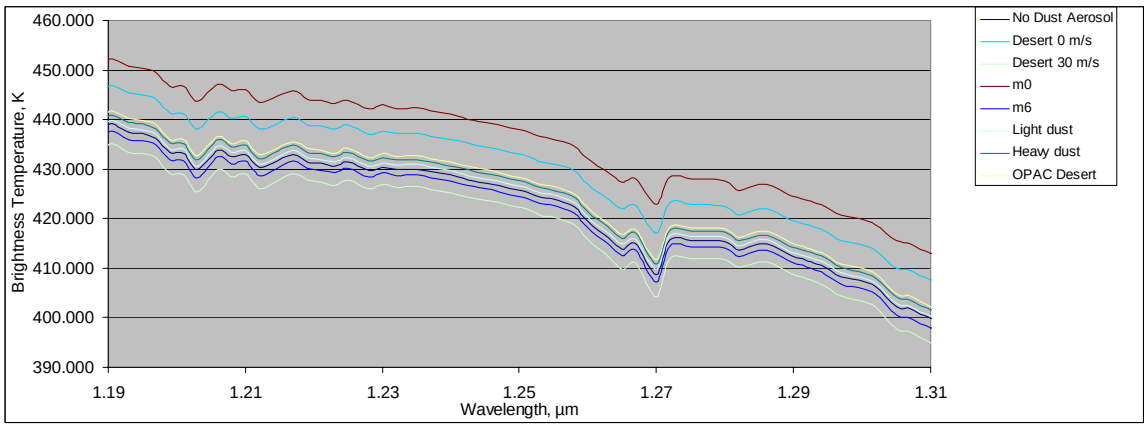

Figure 35. Top-of-the-atmosphere brightness temperature, all cases, summer night, nadir.

Brightness temperatures in the band between 1.505 and 1.797 µm follow a similar pattern as in the previous shorter wavelength windows (see Figure 36). Brightness temperatures decrease for all simulations similarly to the no aerosol simulation. The range of brightness temperature values from every simulation is smaller than the previously examined window with values near 15 K. The largest brightness temperature values come from the m0 absorptive representation. The smallest brightness temperature values result from the Desert 30 m/s dust aerosol representation. The brightness temperature values for each simulation do not cross, and retain roughly the same difference from the no aerosol simulation through most of this window. As the wavelength surpasses 1.755 µm the brightness temperatures of all simulations approach a common value.

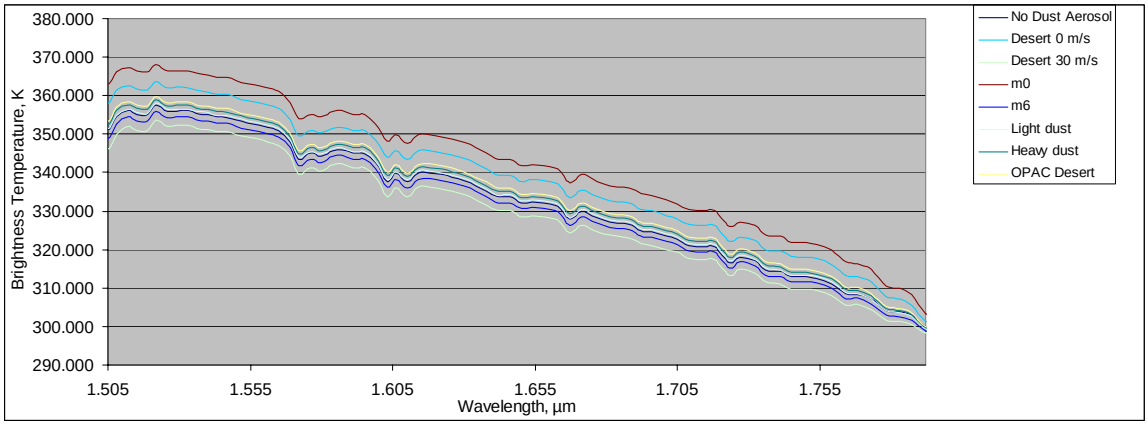

Figure 36. Top-of-the-atmosphere brightness temperature, all cases, summer night, nadir.

Brightness temperatures in the wavelength range between 2.1 and 2.4 µm are quite different from brightness temperatures in the shorter wavelength windows (see Figure 37). Brightness temperatures are steady for all simulations up to 2.3 µm similarly to the no aerosol simulation. At wavelengths higher than 2.3 µm brightness temperatures from all simulations begin to increase and approach a common value. The range of brightness temperature values from every simulation is much smaller than in the shorter wavelength windows, roughly 2 K. The largest brightness temperature values come from

the Desert 30 m/s dust aerosol representation. The smallest brightness temperature values result from the no aerosol simulation. The brightness temperature values for each simulation do not cross, and retain roughly the same difference from the no aerosol simulation through most of this window. A final note on this simulation is the grouping of the dust aerosol models at wavelengths shorter than 2.3 µm. The no aerosol simulation is separated from the remaining aerosol simulations by roughly 0.75 K Each dust aerosol simulation is grouped roughly within 0.5 K of each other.

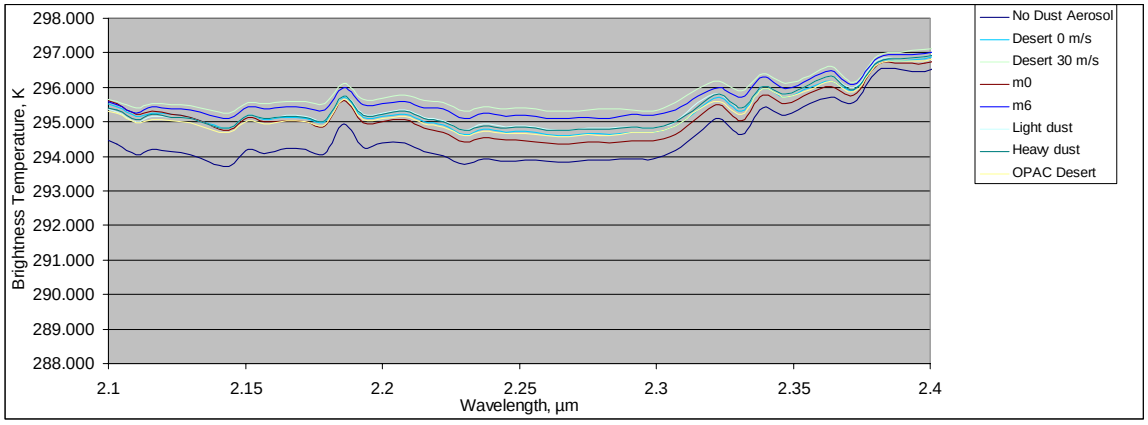

Figure 37. Top-of-the-atmosphere brightness temperature, all cases, summer night, nadir.

Brightness temperature values in the wavelength range between 3.401 and 3.992 µm are somewhat complex (see Figure 38). Below 3.51 µm, all simulations diverge from a common value and increase 2 K. Between 3.51 and 3.81 µm all simulations are steady and range in brightness temperature value by less than 1 K. Above 3.81 µm brightness temperatures converge, drop sharply and then stabilize. The largest brightness temperature values come from the Desert 30 m/s representation. The smallest brightness temperature values result from the no aerosol simulation except for both MODTRAN Desert aerosol representations and the OPAC Desert representation which are nearly equal to the no aerosol simulation. The brightness temperature values for each simulation begin to cross. The average brightness temperature difference between no aerosol and dust aerosol across this range are less than 1 K.

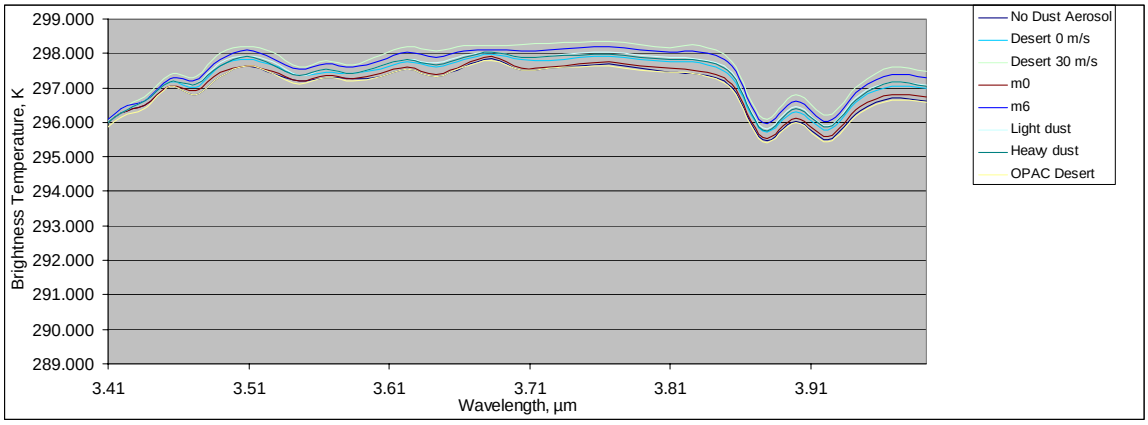

Figure 38. Top-of-the-atmosphere brightness temperature, all cases, summer night, nadir.

Brightness temperatures in the wavelength range between 4.63 and 4.975 µm are variable, with decreasing brightness temperature values through 4.8 µm and increasing values from the 4.8 µm wavelength and higher (see Figure 39). Brightness temperature values for all simulations are very similar to the no aerosol simulation. The range of brightness temperature values from every simulation is less than 0.5 K.

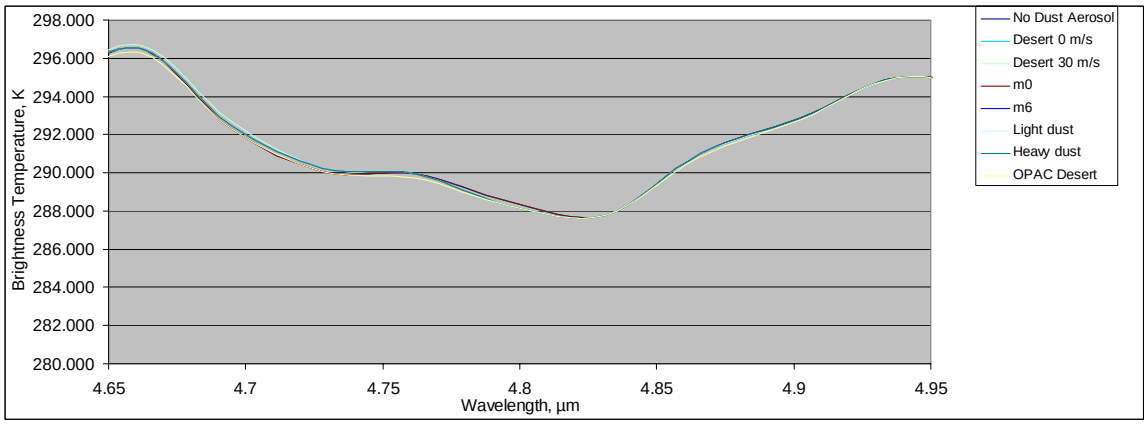

Figure 39. Top-of-the-atmosphere brightness temperature, all cases, summer night nadir.

The average difference between the no aerosol simulation brightness temperature and the brightness temperatures of various dust aerosols are presented in Figures 40, 41,

and Table 7. The magnitudes of values in the table are smaller than exhibited during the daytime case, but there are similarities in behavior. Of note in this table are the relatively large brightness temperature differences. As wavelength increases, the brightness temperature difference between the no aerosol simulation and any dust aerosol simulation decrease. Another interesting observation is the change in magnitude of the brightness temperature difference with respect to wavelength when comparing the low 0.55 μm optical depth simulations to their high 0.55 μm optical depth counterpart. The m0 simulation produced much higher brightness temperatures than the no aerosol case below 1.5 μm. The magnitude of the difference is greater than 9 K. At wavelengths longer than 1.5 μm the difference between the m0 simulation brightness temperature and the no aerosol simulation were at most -0.639 K. Contrast this with the m6 simulation - in wavelengths below 1.5 μm, the magnitude of the brightness temperature difference from no aerosol was as much as 1 K. At wavelengths longer the 1.5 μm, the m6 simulation brightness temperature was different from the no aerosol simulation by -0.008 to -1.092 K. The m6 representation is essentially the m0 representation with the addition of a lower concentration, but larger radius mode of dust aerosol. The large disparity between the m0 and m6 representations in terms of average brightness temperature difference when compared with the no aerosol atmosphere must be due to the larger particles. Therefore, the addition of particles of larger radius has a significant impact on top-of-the-atmosphere brightness temperature.

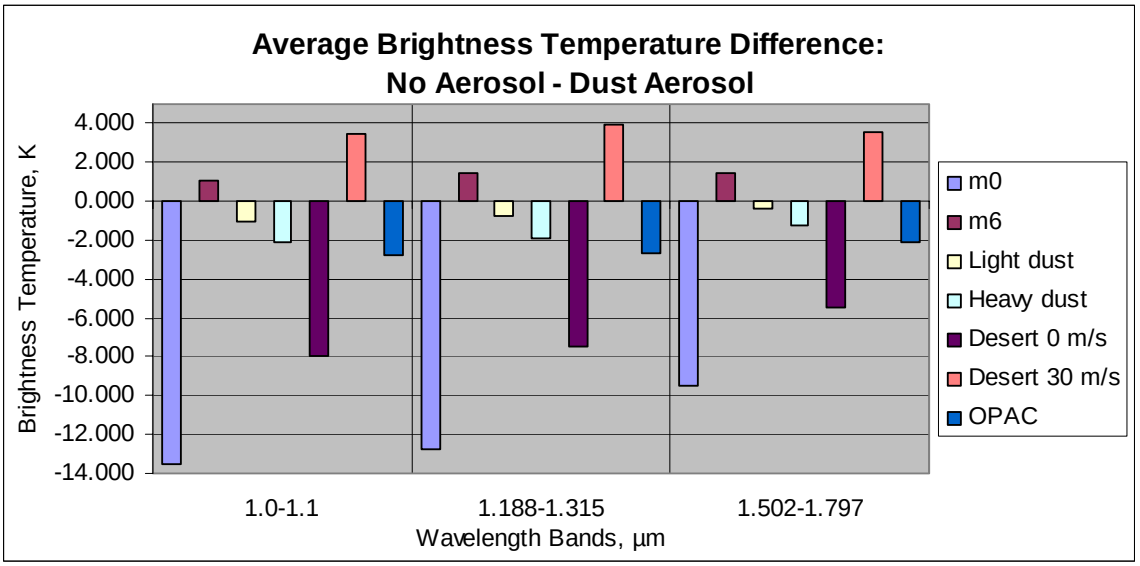

Figure 40. Average brightness temperature difference between no aerosol and dust aerosol, summer night, nadir.

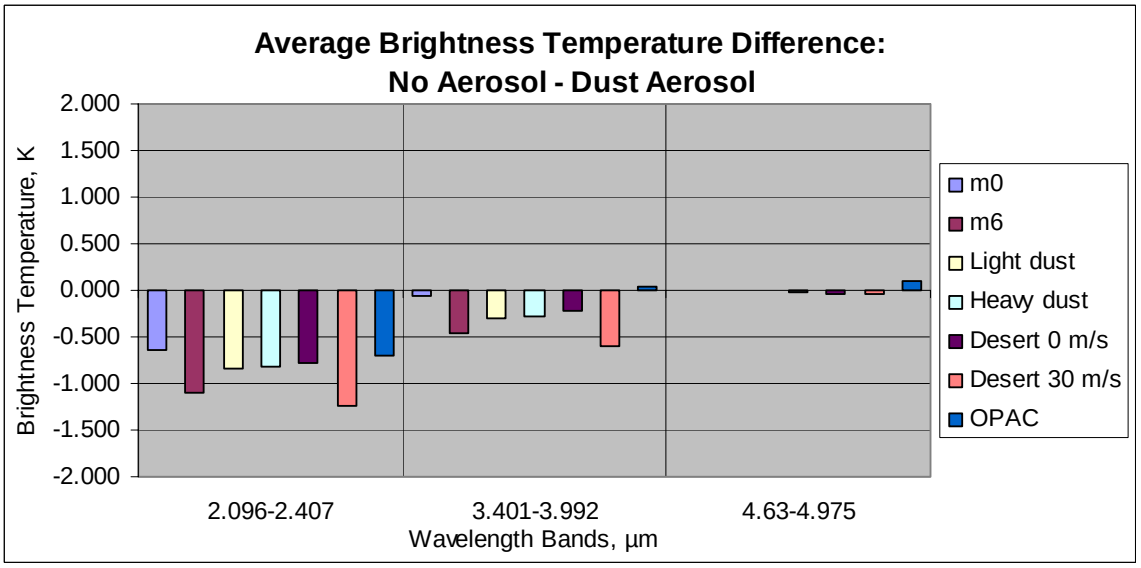

Figure 41. Average brightness temperature difference between no aerosol and dust aerosol, summer night, nadir.

Table 7. Average brightness temperature difference between no aerosol and dust aerosol, summer night, nadir.

	Average Brightness Temperature Difference, K						
Wavelength Band	No Aerosol - Dust Aerosol Representation						
µm	m0	m6	Light dust	Heavy dust	Desert 0 m/s	Desert 30 m/s	OPAC
1.0-1.1	-13.509	1.112	-0.997	-2.109	-7.949	3.484	-2.771
1.188-1.315	-12.754	1.411	-0.791	-1.899	-7.501	3.915	-2.658
1.502-1.797	-9.533	1.464	-0.406	-1.276	-5.501	3.540	-2.107
2.096-2.407	-0.639	-1.092	-0.839	-0.828	-0.775	-1.243	-0.699
3.401-3.992	-0.062	-0.454	-0.310	-0.281	-0.225	-0.594	0.037
4.63-4.975	0.000	-0.008	-0.008	-0.022	-0.039	-0.041	0.094

D. SUMMER NIGHT 30° ZENITH ANGLE

The summer night 30° zenith angle case was run with the MODTRAN input parameters described in the methodology section. The no dust aerosol simulation results in radiance values presented in Figure 42. By visual inspection, this off-axis simulation does not appear different from the nadir simulation for radiative transfer with no aerosol. The magnitude of radiance values at wavelengths below 3 µm is very small. When examined on a logarithmic scale it is evident that the off-axis case is similar to the nadir summer night case. Radiance increases beyond 2 µm, roughly corresponding to the Planck function associated with the blackbody temperature of the earth. Radiance increases from a minimum value of 3.74 x 10^{-10} W•cm^{-2}•ster^{-1}•µm^{-1} between 1 and 2 µm, to a value of 2.05 x 10^{-4} W•cm^{-2}•ster^{-1}•µm^{-1} near 5 µm. Atmospheric absorption is represented by several absorption bands at wavelengths greater than 3 µm. First, water vapor absorption is present at wavelengths just greater than 3 µm. Carbon dioxide and nitrous oxide absorption bands are present between 4 and 5 µm.

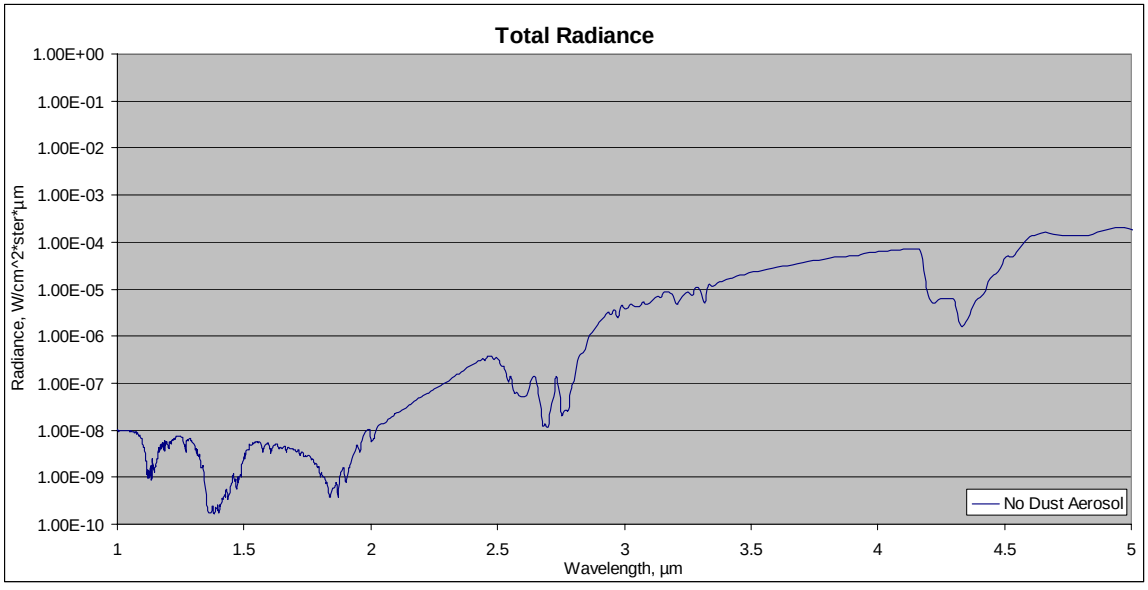

Figure 42. Top-of-the-atmosphere total radiance, no dust aerosol, summer night, 30° zenith angle.

The off-axis no aerosol simulation brightness temperature values are similar to the nadir case (see Figure 43). Important to note here is the surface temperature of 302.5 K for this case, as the brightness temperature values calculated should be near this value in the atmospheric windows of the wavelength band outside of solar influence. At 1 μm the brightness temperature is 517.322 K. This value is slightly higher than the nadir case. At 2.008 μm the brightness temperature is 289.828 K, slightly lower than the nadir case. At 3 μm the brightness temperature value is 292.576 K, which is slightly lower than the nadir case. This decrease in brightness temperature values is due to the surface reflectance model used in the MODTRAN simulations. In the same wavelength span the reflectance changes from 0.7 to just 0.1, therefore much less lunar energy is being reflected off of the surface and towards the top-of-the-atmosphere. The influence of terrestrial emission in shorter wavelengths discussed in the summer night nadir case remains evident in the off-axis case.

The atmospheric absorption bands below 2 μm are revealed as bands of lower brightness temperature, as expected. Also expected is the fact that the reduction of brightness temperature is smaller in this simulation due to the lower amounts of radiant energy. Surface reflection is very low, but the scattering of radiation by the tropospheric, stratospheric and meteoric background aerosol is present in the simulation. Evidence that this type of scattering is occurring is in the profile of brightness temperatures in the absorption bands. The brightness temperatures show little change across the absorption band, in contrast to the sharp decrease in brightness temperature in the neighboring windows that mirror the surface reflectance.

The absorption bands at wavelengths greater than 2.4 μm are similar to the absorption bands of the daytime simulation in that they represent a decrease from the neighboring atmospheric window of similar magnitude. This points to the relative influence of terrestrial versus solar radiance once again. In this simulation it is clear that terrestrial radiance dominates the brightness temperature to wavelengths as low as 1.9 μm. This is revealed outside of the short wavelength absorption bands where the brightness temperature is similar to the surface temperature.

Despite the dominance of terrestrial energy at short wavelengths, the windows in the band between 3.4 and 5 µm are still influenced somewhat by the lunar source. The transmission in this band is a maximum near 3.5 µm. With this in mind the brightness temperature is expected to be near the 302.5 K surface temperature. The simulations reveal that the brightness temperature is greater than expected at 3.5 µm. The brightness temperatures between 3.4 and 4.1 µm decrease from 297 to 294 K. From 4.5 to 5 µm brightness temperatures vary between 286 and 296 K. Since the brightness temperatures in this band are closer to the surface temperature than transmission would allow, the energy in the simulation must be due to contribution from lunar scattering.

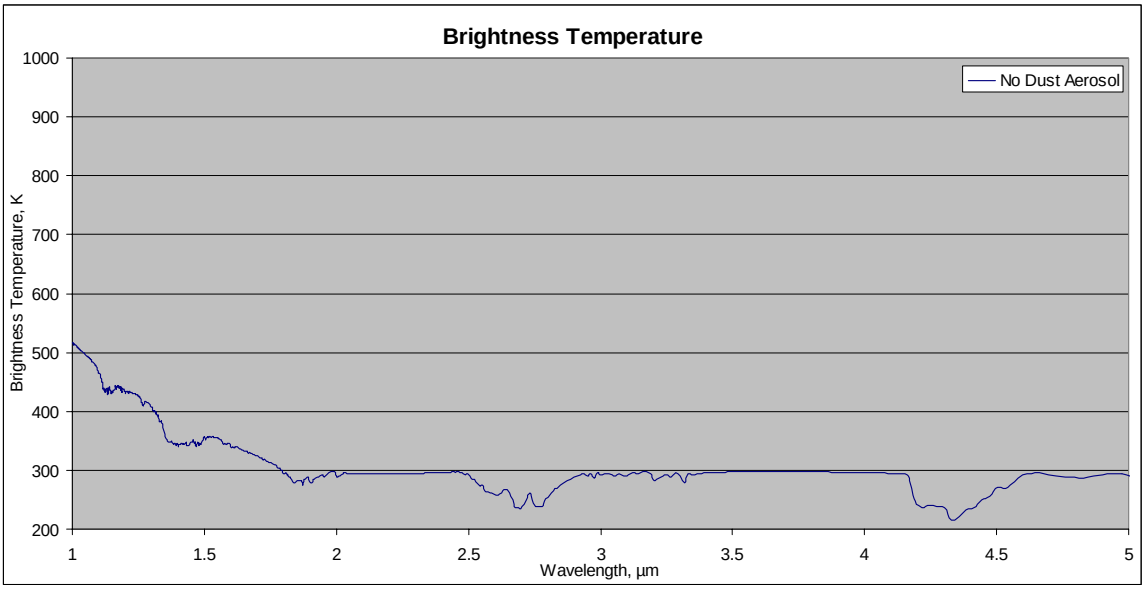

Figure 43. Top-of-the-atmosphere brightness temperature, no dust aerosol, summer night, 30° zenith angle.

As mentioned in the methodology chapter dust aerosols that were non-absorptive were considered as well as absorptive dust aerosols. The difference between the brightness temperatures of the absorptive dust and the non-absorptive dust was significant in all of the atmospheric windows (see Table 8). The differences were larger at shorter wavelengths than at longer wavelengths. This probably relates to the amount of energy involved in these bands, although the wavelength dependence of emitted

radiation is also a factor. In addition, the differences were larger for the representations with higher 0.55 μm optical depth (m6 and Desert 30 m/s) than the representations with lower 0.55 μm optical depth (m0 and Desert 0 m/s). The higher 0.55 μm optical depth values result from representations with a larger number of dust aerosol particles per cubic centimeter. Larger dust aerosol particle loading suggests larger extinction by these aerosols. Larger extinction due to dust aerosol causes larger changes to top-of-the-atmosphere brightness temperature. This is why the Desert 30 m/s dust representation exhibits a larger average brightness temperature difference from the no aerosol simulation than the m6 representation. Since the brightness temperature values from both the non-absorptive and absorptive Desert 30 m/s dust representations are larger than the brightness temperature values from both m6 representations, the difference between the non-absorptive and absorptive Desert 30 m/s dust aerosols are correspondingly larger than the difference between the m6 representations. The exception here is the Heavy dust and Light dust representations. The non-absorptive aerosols minus the absorptive aerosol brightness temperature differences were similar in both the Light dust and Heavy dust aerosol representation despite having different 0.55 μm optical depths. The 0.55 μm optical depths were similar to the other representations with Heavy dust having the higher 0.55 μm optical depth. Brightness temperature differences in this table reveal the importance of accounting for absorption by dust aerosol when calculating radiative transfer between 1 and 5 μm. With that in mind the following examination of brightness temperatures among the different dust representations will focus on the absorptive dust aerosol only.

Table 8. Average difference between non-absorptive and absorptive dust aerosol, summer night, 30° zenith angle.

	Average Brightness Temperature Difference, K					
Wavelength Band	Non Absorptive - Absorptive Dust Aerosol Representation					
μm	m0	m6	Light dust	Heavy dust	Desert 0 m/s	Desert 30 m/s
1.0-1.1	1.042	3.832	1.593	0.849	0.158	8.565
1.188-1.315	0.926	4.085	1.807	1.061	0.366	8.896
1.502-1.797	0.796	4.053	2.029	1.401	0.773	7.953
2.096-2.407	-0.154	-0.807	-0.570	-0.539	-0.385	-0.934
3.401-3.992	-0.092	-0.736	-0.476	-0.419	-0.325	-0.912
4.63-4.975	0.000	-0.215	-0.148	-0.096	-0.065	-0.315

Brightness temperatures calculated from the various dust aerosols across the 1 through 5 µm band are presented in Figure 44. Since the brightness temperatures range from near 500 K to below 300 K it is difficult to quantify the difference between the no aerosol simulation and the various dust aerosol simulations. Some spread among the plots between 1 and 3 µm is apparent, but as wavelength increases, the difference between the no aerosol case and the various aerosol simulations decrease. One visible difference is between the no aerosol case and the dust aerosol cases in the absorption bands between 1 and 3 µm. These differences are near 20 K, with the no aerosol simulation having the highest brightness temperature. This is caused by a reduction in the already small surface reflectance in the absorption bands. To better understand the effect of the various dust aerosols on brightness temperature closer examination of narrower wavelength bands is required.

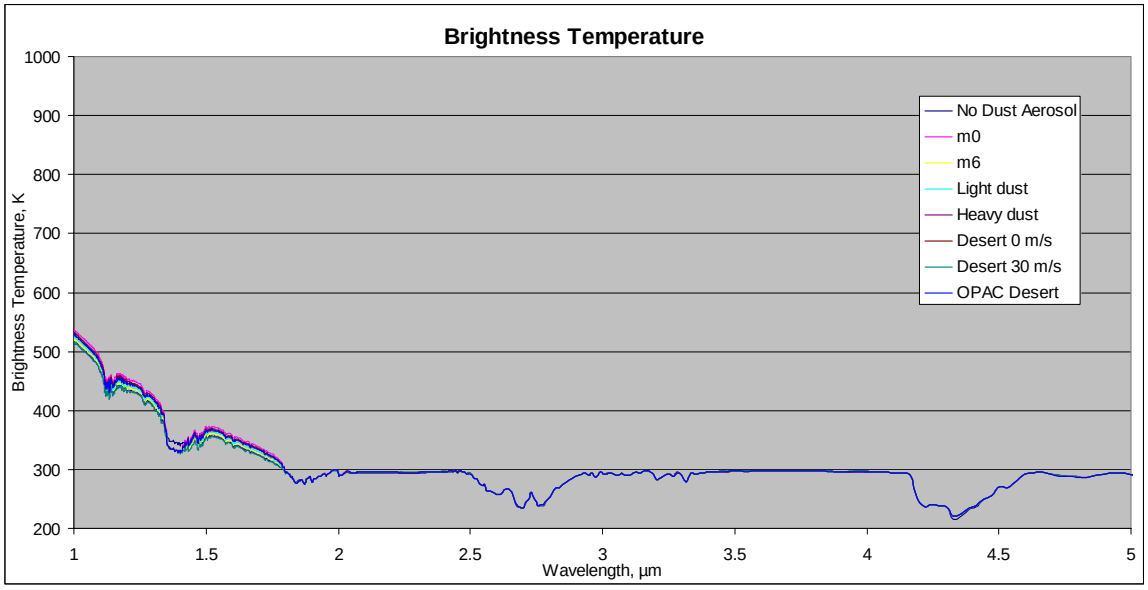

Figure 44. Top-of-the-atmosphere brightness temperature, all cases, summer night, 30° zenith angle.

Wavelength bands were chosen arbitrarily to match up with radiative windows, based on examination of the wavelength range and the variability of the aerosol in the window band. Brightness temperatures in the first wavelength band between

1 and 1.1 µm are presented in Figure 45. Brightness temperatures decrease for all simulations similarly to the no aerosol simulation. The range of brightness temperature values from every simulation is similar to the nadir case, roughly 20 K. The largest brightness temperature values come from the m0 dust aerosol representation. The smallest brightness temperature values result from the no dust aerosol simulation. The brightness temperature values for each simulation do not cross, and retain the same difference from the no aerosol simulation throughout this window.

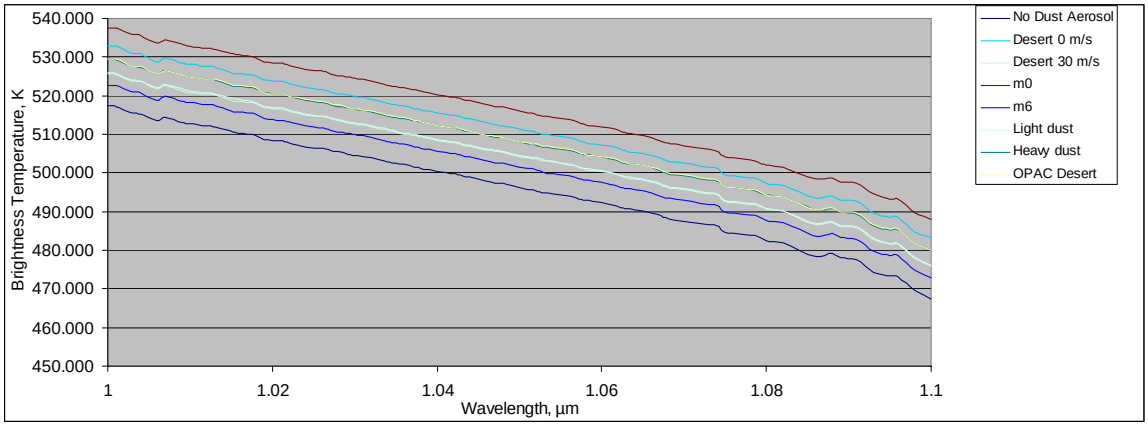

Figure 45. Top-of-the-atmosphere brightness temperature, all cases, summer night, 30° zenith angle.

Brightness temperature values in the wavelength band between 1.19 and 1.31 µm are similar to brightness temperature values in the first band examined (see Figure 46). Brightness temperatures decrease for all simulations similarly to the no aerosol simulation. The range of brightness temperature values from every simulation is near 20 K as in the shorter wavelength window. The largest brightness temperature values come from the m0 dust aerosol representation. The smallest brightness temperature values result from the MODTRAN Desert 30 m/s dust aerosol representation. The brightness temperature values for each simulation do not cross, and retain roughly the same difference from the no aerosol simulation throughout this window.

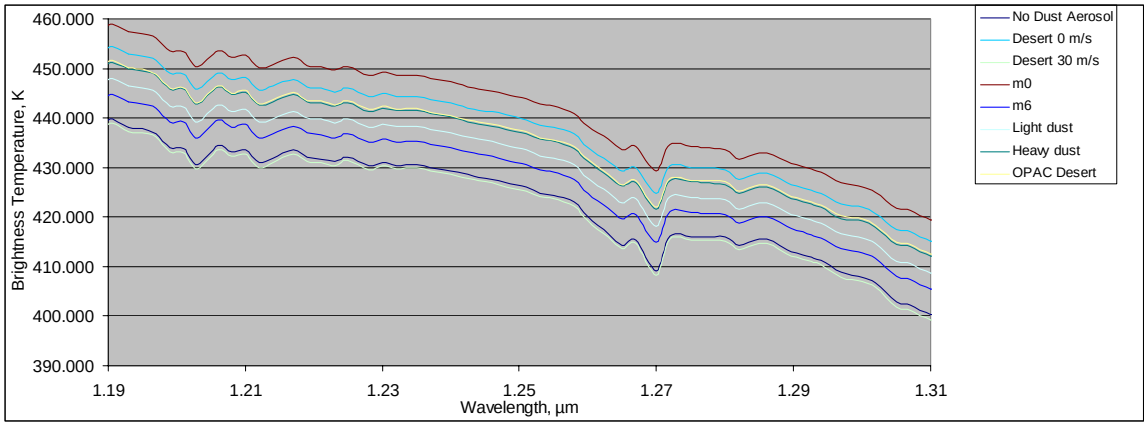

Figure 46. Top-of-the-atmosphere brightness temperature, all cases, summer night, 30° zenith angle.

Brightness temperatures in the wavelength band between 1.505 and 1.797 µm follow a similar pattern as in the previous shorter wavelength windows (see Figure 47). Brightness temperatures decrease for all simulations similarly to the no aerosol simulation. The range of brightness temperature values from every simulation is narrower at 15 K. The largest brightness temperature values come from the m0 dust aerosol representation. The smallest brightness temperature values result from the MODTRAN Desert 30 m/s dust aerosol representation. The brightness temperature values for each simulation do not cross, and retain roughly the same difference from the no aerosol simulation through most of this window. As the wavelength surpasses 1.755 µm the brightness temperatures of all simulations converge.

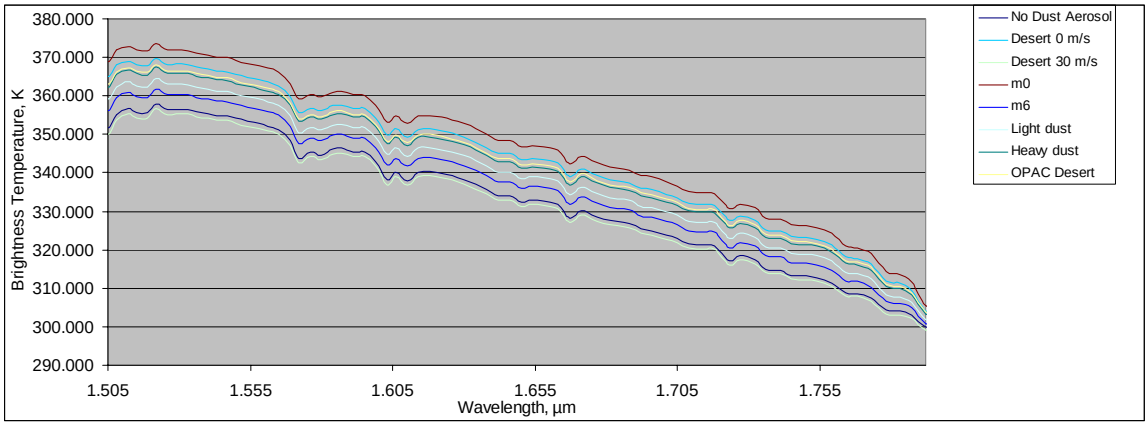

Figure 47. Top-of-the-atmosphere brightness temperature, all cases, summer night, 30° zenith angle.

Brightness the temperature values in the wavelength range between 2.1 and 2.4 µm are quite different from the brightness temperature values in the shorter wavelength windows (see Figure 48). Brightness temperatures are steady for all simulations up to 2.3 µm similarly to the no aerosol simulation. At wavelengths higher than 2.3 µm brightness temperatures from all simulations begin to increase and approach a common value. The range of brightness temperature values from every simulation is much smaller than in the shorter wavelength windows, roughly 2 K. The largest brightness temperature values come from the Desert 30 m/s dust aerosol representation. The smallest brightness temperature values result from the no aerosol simulation. The brightness temperature values for each simulation do not cross, and retain roughly the same difference from the no aerosol simulation through most of this window. A final note on this simulation is the grouping of the dust aerosol models at wavelengths shorter than 2.3 µm. The no aerosol simulation is separated from the other simulations by roughly 0.75 K. The remaining dust aerosol simulations are grouped roughly within 0.5 K of each other.

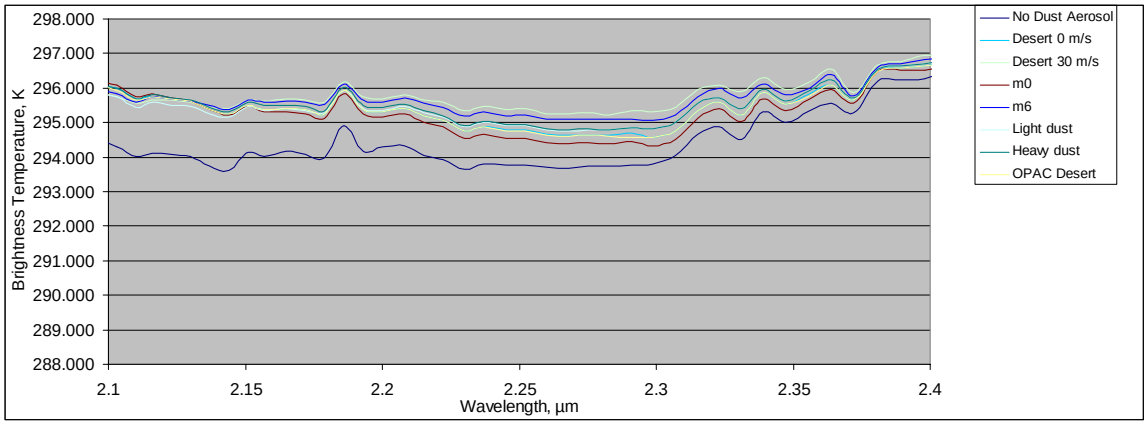

Figure 48. Top-of-the-atmosphere brightness temperature, all cases, summer night, 30° zenith angle.

Brightness temperature values in the wavelength range between 3.401 and 3.992 µm are somewhat complex (see Figure 49). Below 3.51 µm, all simulations diverge from a common value and increase 2.5 K. Between 3.51 and 3.81 µm all simulations are steady and range in brightness temperature value by less than 1 K. Above 3.81 µm brightness temperatures converge, drop sharply and then stabilize. The largest brightness temperature values come from the Desert 30 m/s representation. The smallest brightness temperature values result from the OPAC Desert aerosol representation. The brightness temperature values for each simulation begin to cross. The average brightness temperature difference between no aerosol and dust aerosol across this range are less than 1 K.

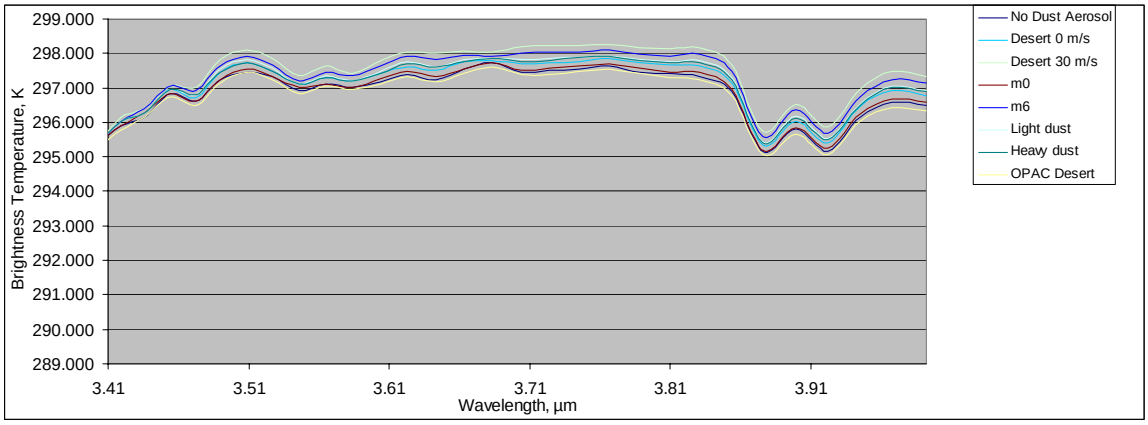

Figure 49. Top-of-the-atmosphere brightness temperature, all cases, summer night, 30° zenith angle.

Brightness temperatures in the wavelength band between 4.63 and 4.975 µm are variable, first brightness temperature values decrease through 4.8 µm and then increase from the 4.8 µm wavelength and higher (see Figure 50). Brightness temperature values for all simulations are very similar to the no aerosol simulation. The range of brightness temperature values from every simulation is less than 1 K. The largest brightness temperature values come from the Desert 30 m/s dust aerosol simulation. The smallest brightness temperature values result from the OPAC Desert dust aerosol representation. The brightness temperature values for each simulation do not cross.

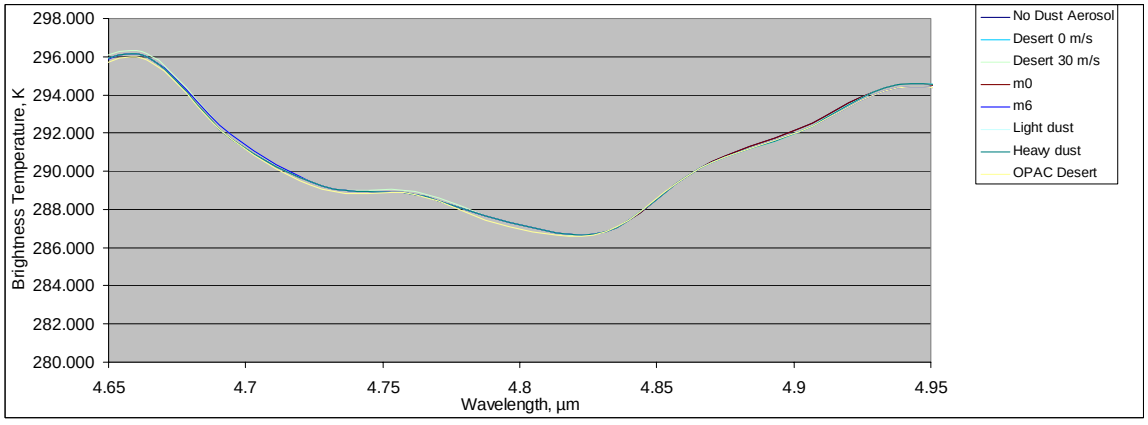

Figure 50. Top-of-the-atmosphere brightness temperature, all cases, summer night, 30° zenith angle.

The average difference between the no aerosol simulation brightness temperature and the brightness temperatures of various dust aerosols are presented in Figures 51, 52, and Table 9. The magnitudes of values in the table are smaller than exhibited during the daytime case, but there are similarities in behavior. Of note in this table are the relatively large brightness temperature differences. As wavelength increases, the brightness temperature difference between the no aerosol simulation and any dust aerosol simulation decrease. Another interesting observation is the change in magnitude of the brightness temperature difference with respect to wavelength when comparing the low 0.55 μm optical depth simulations to their high 0.55 μm optical depth counterpart. The m0 simulation produced much higher brightness temperatures than the no aerosol case below 1.5 μm. The magnitude of the difference is greater than 14 K. At wavelengths longer than 1.5 μm the difference between the m0 simulation brightness temperature and the no aerosol simulation were smaller than 1 K. Contrast this with the m6 simulation - in wavelengths below 1.5 μm, the magnitude of the brightness temperature difference from no aerosol was as much as 5 K. At wavelengths longer the 1.5 μm, the m6 simulation brightness temperature was different from the no aerosol simulation by 0.023 to -1.258 K. The m6 representation is essentially the m0 representation with the addition of a lower concentration, but larger radius mode of dust aerosol. The large disparity between the m0 and m6 representations in terms of average brightness temperature difference when compared with the no aerosol atmosphere must be due to the larger particles. Therefore, the addition of particles of larger radius has a significant impact on top-of-the-atmosphere brightness temperature.

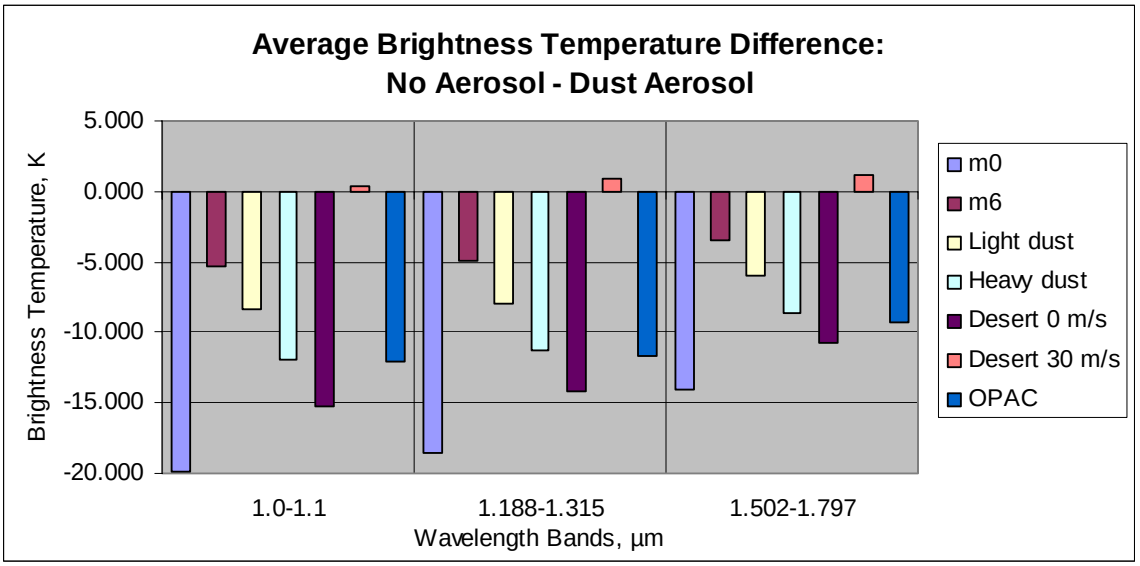

Figure 51. Average brightness temperature difference between no aerosol and dust aerosol, summer night, 30° zenith angle.

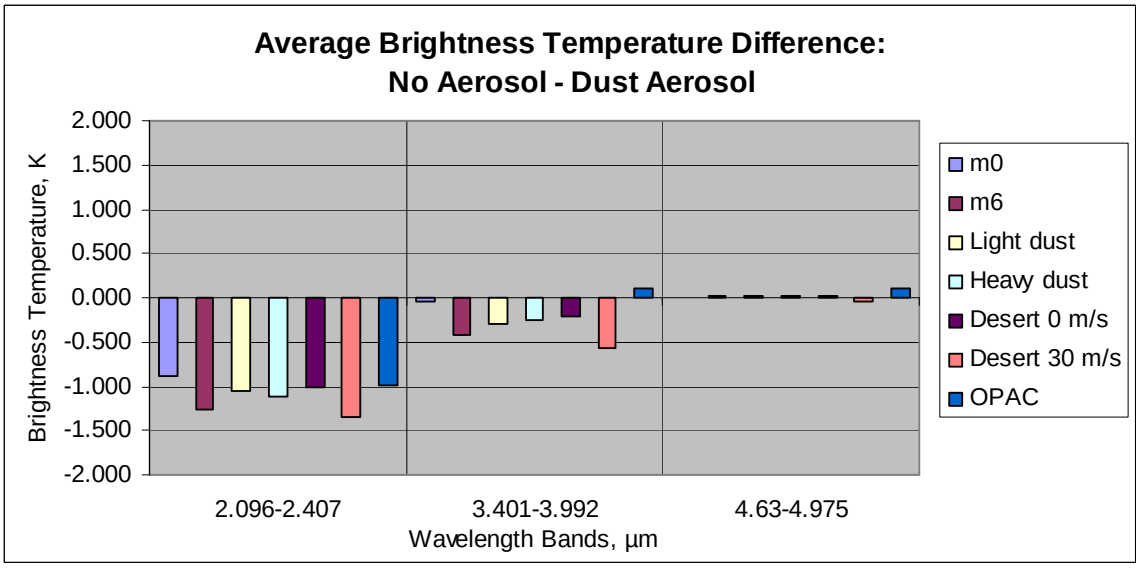

Figure 52. Average brightness temperature difference between no aerosol and dust aerosol, summer night, 30° zenith angle.

Table 9. Average brightness temperature difference between no aerosol and dust aerosol, summer night, 30° zenith angle.

	Average Brightness Temperature Difference, K						
Wavelength Band	No Aerosol - Dust Aerosol Representation						
µm	m0	m6	Light dust	Heavy dust	Desert 0 m/s	Desert 30 m/s	OPAC
1.0-1.1	-19.888	-5.323	-8.425	-11.925	-15.180	0.378	-12.096
1.188-1.315	-18.514	-4.879	-7.917	-11.252	-14.193	0.856	-11.607
1.502-1.797	-14.006	-3.500	-5.981	-8.624	-10.707	1.131	-9.337
2.096-2.407	-0.881	-1.258	-1.046	-1.117	-1.007	-1.351	-0.994
3.401-3.992	-0.052	-0.427	-0.290	-0.252	-0.206	-0.579	0.098
4.63-4.975	0.000	0.023	0.014	0.014	0.014	-0.041	0.111

The average brightness temperature difference across the window wavelength bands is where the nadir view cases and the off-axis cases differ significantly see Table 9. The magnitudes of values in the table are smaller than exhibited during the daytime case, but larger than in the summer night nadir case. Every aerosol representation undergoes large changes between these two cases.

E. SPRING DAY NADIR

The spring day nadir view case was run with the MODTRAN input parameters described in the methodology section. The no dust aerosol simulation results in radiance values (see Figure 53). Between 1 and 2.6 μm the magnitude of radiance generally decreases according to the Planck function for solar temperature – modified by gaseous absorption regions. The values decrease from 3.23 x 10^{-3} W•cm^{-2}•ster^{-1}•μm^{-1} to a minimum of 7.25 x 10^{-8} W•cm^{-2}•ster^{-1}•μm^{-1} in the carbon dioxide absorption band between 2 and 3 μm. The radiance then increases, roughly corresponding to the Planck function associated with the blackbody temperature of the earth. The minimum radiance of 7.25 x 10^{-8} W•cm^{-2}•ster^{-1}•μm^{-1} between 2 and 3 μm increases to a value of 2.13 x 10^{-4} W•cm^{-2}•ster^{-1}•μm^{-1} near 5 μm. Above 3 μm atmospheric absorption is represented by several bands of reduced radiance. First, the water vapor absorption band is visible at wavelengths just greater than 3 μm. Carbon dioxide and nitrous oxide absorption is present between 4 and 5 μm. As expected the spring day case radiance values are less than the summer day case radiance values due to both reductions in solar energy and the reduced surface and atmospheric column temperatures.

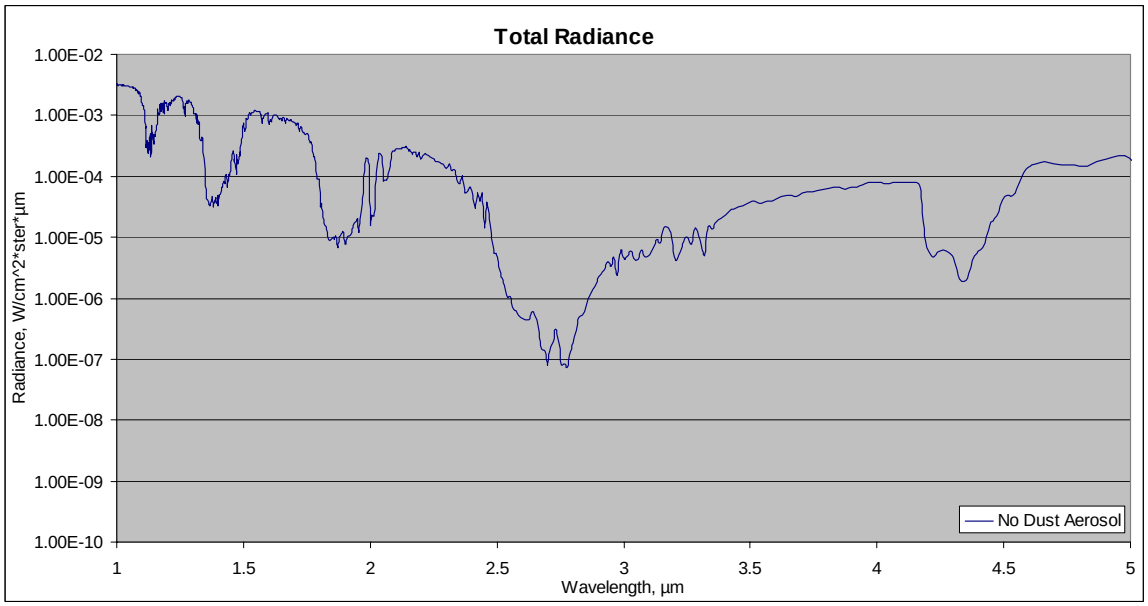

Figure 53. Top-of-the-atmosphere total radiance, no dust aerosol, spring day, nadir.

After conversion to brightness temperature as described in the chapter on methodology, the brightness temperatures behave as expected with no dust aerosol present (see Figure 54). Important to note here is the surface temperature of 307.5 K for this case, as the brightness temperature values calculated should be near this value in the atmospheric windows of the wavelength band outside of solar influence. Furthermore it is important to note that the surface temperature is 12.5 K less than in the summer day simulation. At 1 µm the brightness temperature is 951.539 K. This is roughly 7.5 K less than the summer day case. This value is cut nearly in half at 2.033 µm where the brightness temperature is 497.552 K. At 3.003 µm the brightness temperature value is 295.323 K. Once again the sharp decrease in brightness temperature is due to the surface reflectance model used in the MODTRAN simulations. In the same wavelength span the reflectance changes from 0.7 to just 0.1, therefore much less solar energy is being reflected off of the surface and towards the top-of-the-atmosphere.

The atmospheric absorption bands noted above are revealed as bands of lower brightness temperature, as expected. Surface reflection is very low, but the scattering of radiation by the tropospheric, stratospheric and meteoric background aerosol is present in the simulation. Evidence that this type of scattering is occurring is in the profile of

brightness temperatures in the absorption bands. The brightness temperatures show little change across the band, in contrast to the sharp decrease in brightness temperature in the neighboring windows which mirror the surface reflectance.

The windows in the band between 3.4 and 5 µm are quite interesting when viewed from the brightness temperature perspective. This band shows the interaction of solar energy and terrestrial energy. The transmission in this band peaks at roughly 3.5 µm. With this in mind the brightness temperature is expected to be near the 307.5 K surface temperature. The simulations reveal that the brightness temperature is greater than expected at 3.5 µm. The brightness temperatures between 3.4 and 4.1 µm decrease from 308 to 297 K. From 4.5 to 5 µm brightness temperatures vary between 288 and 298 K. Since the brightness temperatures in this band are closer to the surface temperature than transmission would allow, the energy in the simulation must be due to contribution from solar scattering.

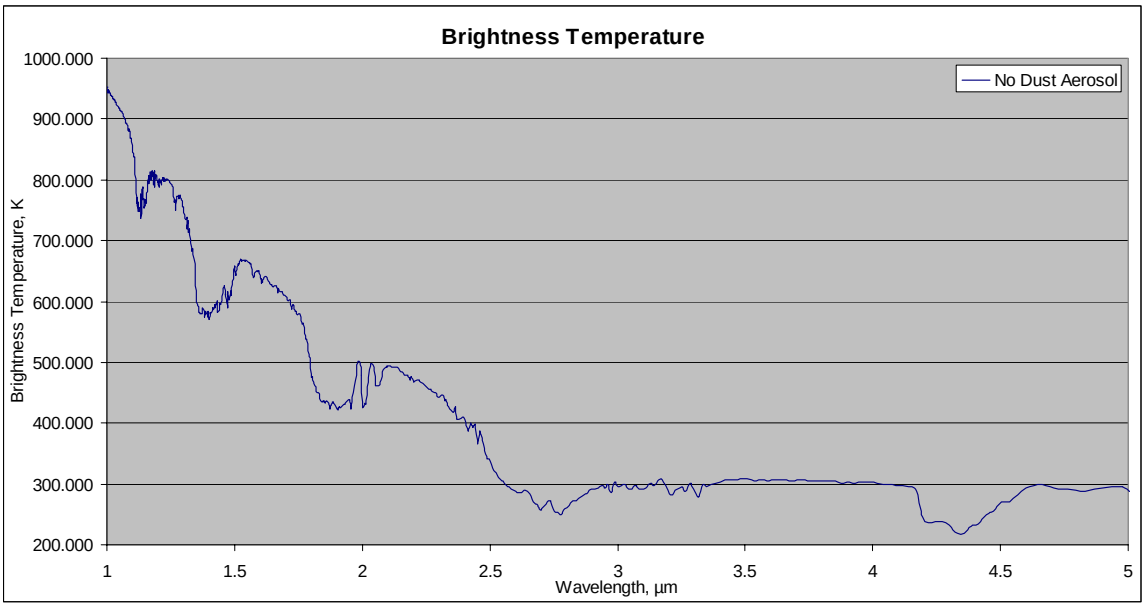

Figure 54. Top-of-the-atmosphere brightness temperature, no dust aerosol, spring day, nadir.

As mentioned in the methodology chapter dust aerosols that were non-absorptive were considered as well as absorptive dust aerosols. The difference between the

brightness temperatures of the absorptive dust and the non-absorptive dust was significant in all of the atmospheric windows (see Table 10). The differences were larger at shorter wavelengths than at longer wavelengths. This probably relates to the amount of energy involved in these bands, although the wavelength dependence of emitted radiation is also a factor. In addition, the differences were larger for the representations with higher 0.55 μm optical depth (m6 and Desert 30 m/s) than the representations with lower 0.55 μm optical depth (m0 and Desert 0 m/s). The higher 0.55 μm optical depth values result from representations with a larger number of dust aerosol particles per cubic centimeter. Larger dust aerosol particle loading suggests larger extinction by these aerosols. Larger extinction due to dust aerosol causes larger changes to top-of-the-atmosphere brightness temperature. This is why the Desert 30 m/s dust representation exhibits a larger average brightness temperature difference from the no aerosol simulation than the m6 representation. Since the brightness temperature values from both the non-absorptive and absorptive Desert 30 m/s dust representations are larger than the brightness temperature values from both m6 representations, the difference between the non-absorptive and absorptive Desert 30 m/s dust aerosols are correspondingly larger than the difference between the m6 representations. The exception here is the Heavy dust and Light dust representations. The non-absorptive aerosols minus the absorptive aerosol brightness temperature differences were similar in both the Light dust and Heavy dust aerosol representation despite having different 0.55 μm optical depths. The 0.55 μm optical depths were similar to the other representations with Heavy dust having the higher 0.55 μm optical depth. Brightness temperature differences in this table reveal the importance of accounting for absorption by dust aerosol when calculating radiative transfer between 1 and 5 μm. With that in mind the following examination of brightness temperatures among the different dust representations will focus on the absorptive dust aerosol only.

Table 10. Average brightness temperature between non-absorptive and absorptive dust aerosol, spring day, nadir.

	Average Brightness Temperature Difference, K					
Wavelength Band	Non Absorptive - Absorptive Dust Aerosol Representation					
μm	m0	m6	Light dust	Heavy dust	Desert 0 m/s	Desert 30 m/s
1.0-1.1	2.923	8.763	4.354	3.694	-1.807	12.735
1.188-1.315	2.589	9.612	4.974	4.278	-1.057	13.803
1.502-1.797	2.333	10.973	6.087	5.367	0.665	15.210
2.096-2.407	1.903	12.308	7.320	6.527	2.954	16.483
3.401-3.992	0.282	3.711	2.519	2.276	2.274	4.555
4.63-4.975	0.029	0.120	0.078	0.123	0.078	0.260

Brightness temperatures resulting from the addition of dust aerosols to the simulation across the entire 1 through 5 μm band are found in Figure 55. Since the brightness temperatures range from near 1000 K to below 300 K it is difficult to quantify the difference between the no aerosol simulation and the various dust aerosol simulations. Some spread among the plots between 1 and 3 μm is apparent, but as wavelength increases, the difference between the no aerosol case and the various aerosol simulations decrease. One visible difference is between the no aerosol case and the dust aerosol cases in the absorption bands between 1 and 3 μm. These differences are near 50 K, with the no aerosol simulation having the highest brightness temperature. This is caused by extinction due to dust aerosol. To better understand the effect of the various dust aerosols on brightness temperature closer examination of narrower wavelength bands is required.

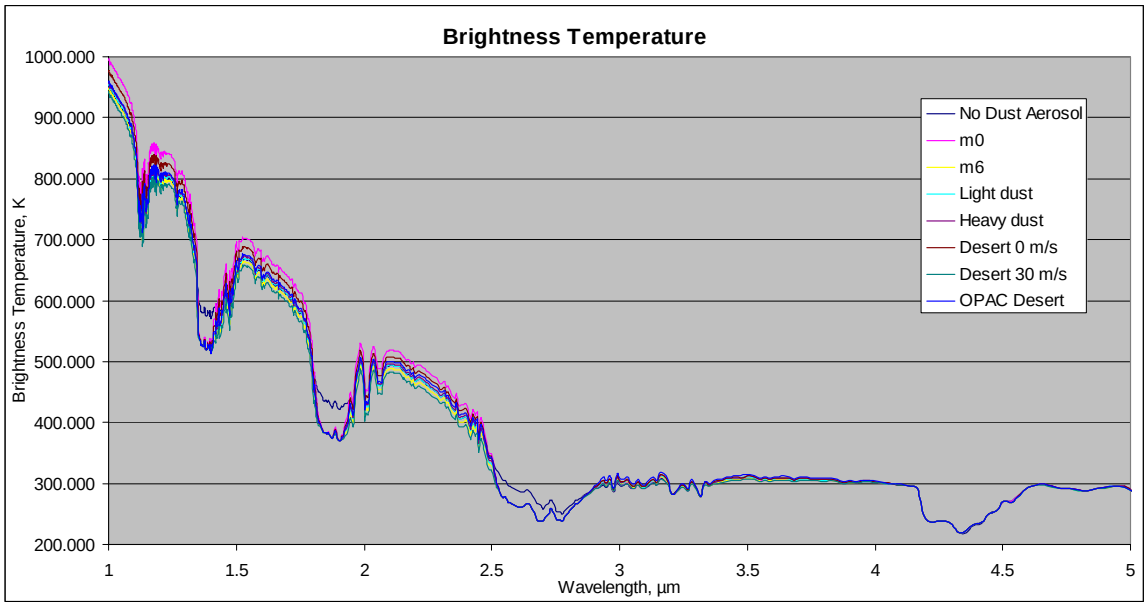

Figure 55. Top-of-the-atmosphere brightness temperature, all cases, spring day, nadir.

Wavelength bands were chosen arbitrarily to match up with radiative windows, based on examination of the wavelength range and the variability of the aerosol in the window band. Brightness temperatures are presented in the first wavelength band between 1 and 1.1 µm (see Figure 56). Brightness temperatures decrease for all simulations similarly to the no aerosol simulation. The range of brightness temperature values from every simulation is over 50 K. The largest brightness temperature values come from the m0 absorptive representation. The smallest brightness temperature values result from the Desert 30 m/s dust aerosol representation. The brightness temperature values for each simulation do not cross, and retain the same difference from the no aerosol simulation throughout this window.

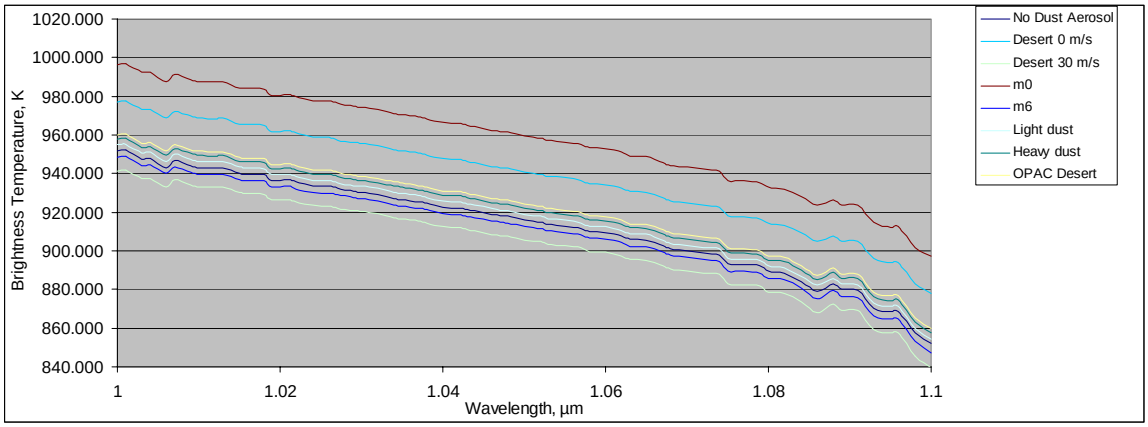

Figure 56. Top-of-the-atmosphere brightness temperature, all cases, spring day, nadir.

Brightness temperature values in the wavelength band between 1.19 and 1.31 µm are similar to brightness temperature values in the first band examined (see Figure 57). Brightness temperatures decrease for all simulations similarly to the no aerosol simulation. The range of brightness temperature values from every simulation remains nearly 50 K. The largest brightness temperature values come from the m0 absorptive representation. The smallest brightness temperature values result from the Desert 30 m/s dust aerosol representation. The brightness temperature values for each simulation do not cross, and retain roughly the same difference from the no aerosol simulation throughout this window.

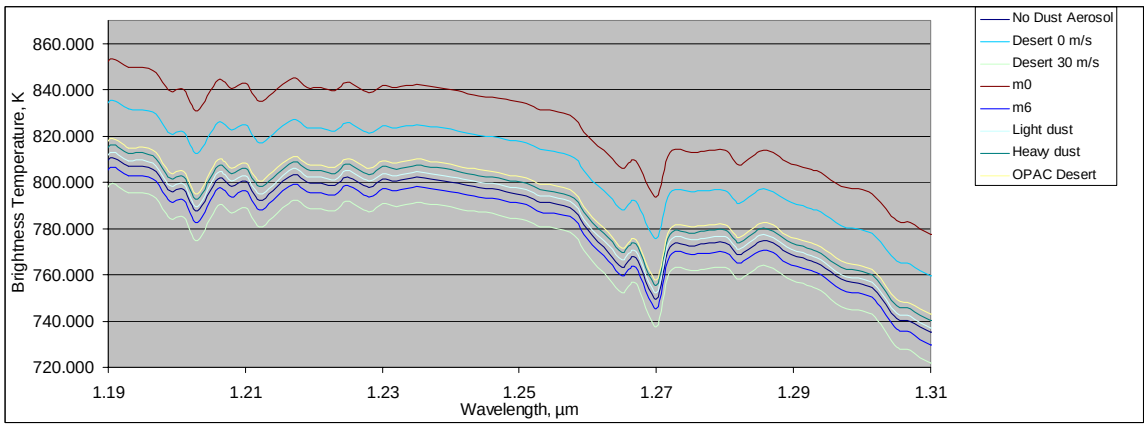

Figure 57. Top-of-the-atmosphere brightness temperature, all cases, spring day, nadir.

Brightness temperature values in the wavelength band between 1.505 and 1.797 µm follow a similar pattern as in the previous shorter wavelength windows (see Figure 58). Brightness temperatures decrease for all simulations similarly to the no aerosol simulation. The range of brightness temperature values from every simulation is over 40 K. The largest brightness temperature values come from the m0 absorptive representation. The smallest brightness temperature values result from the Desert 30 m/s dust aerosol representation. The brightness temperature values for each simulation do not cross, and retain roughly the same difference from the no aerosol simulation through most of this window. As the wavelength surpasses 1.755 µm the brightness temperatures of all simulations converge.

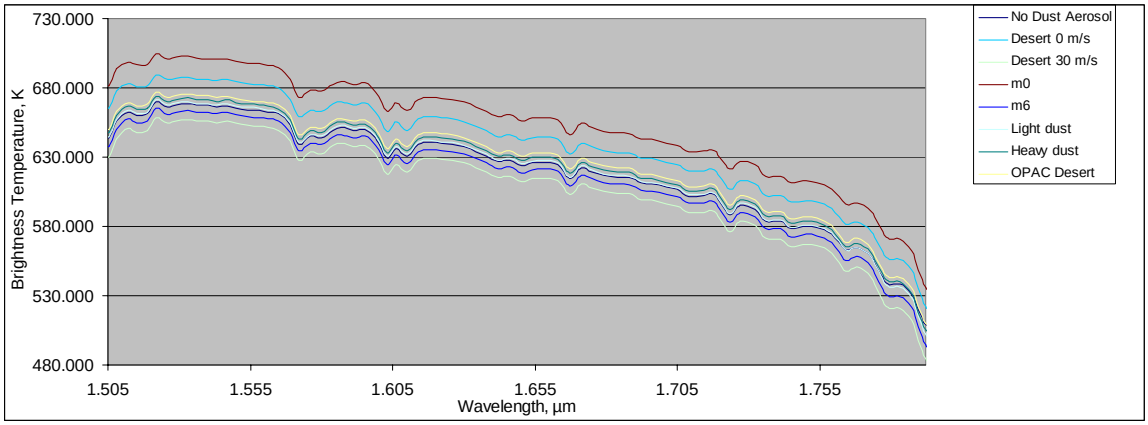

Figure 58. Top-of-the-atmosphere brightness temperature, all cases, spring day, nadir.

Brightness temperatures in the wavelength band between 2.1 and 2.4 µm follow a similar pattern as in the previous shorter wavelength windows (see Figure 59). Brightness temperatures decrease for all simulations similarly to the no aerosol simulation. The range of brightness temperature values from every simulation has decreased to near 40 K. The largest brightness temperature values come from the m0 absorptive representation. The smallest brightness temperature values result from the Desert 30 m/s dust aerosol representation. The brightness temperature values for each simulation do not cross, and retain roughly the same difference from the no aerosol simulation through most of this window.

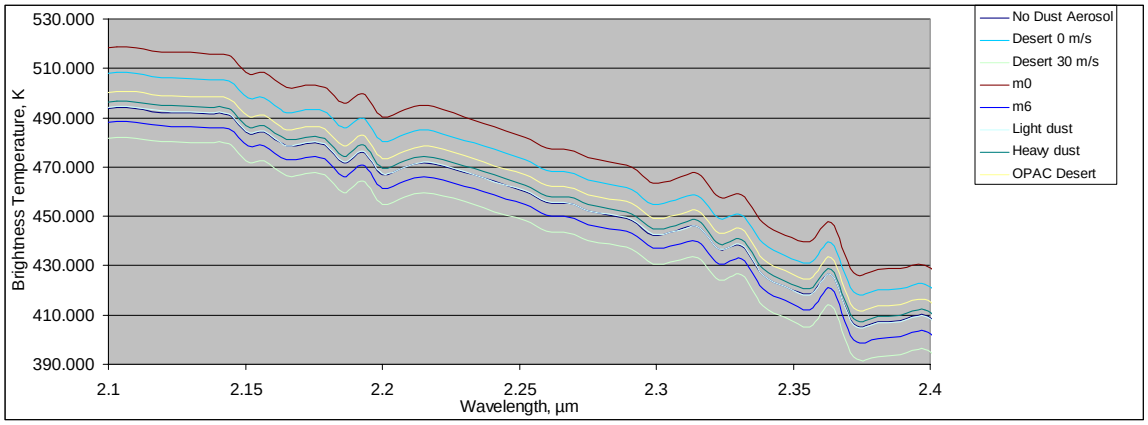

Figure 59. Top-of-the-atmosphere brightness temperature, all cases, spring day, nadir.

Brightness temperatures in the wavelength band between 3.401 and 3.992 µm are fairly flat with a slight decrease in brightness temperature as wavelength increases (see Figure 60). Brightness temperature values for all simulations are similar to the no aerosol simulation. The range of brightness temperature values from every simulation is roughly 5 K at wavelengths below 3.8 µm and only 2 K above 3.8 µm. The largest brightness temperature values come from the OPAC Desert representation. The smallest brightness temperature values result from the Desert 30 m/s dust aerosol representation. The brightness temperature values for each simulation do not cross. The average brightness temperature difference between no aerosol and dust aerosol across this range are small for all simulations.

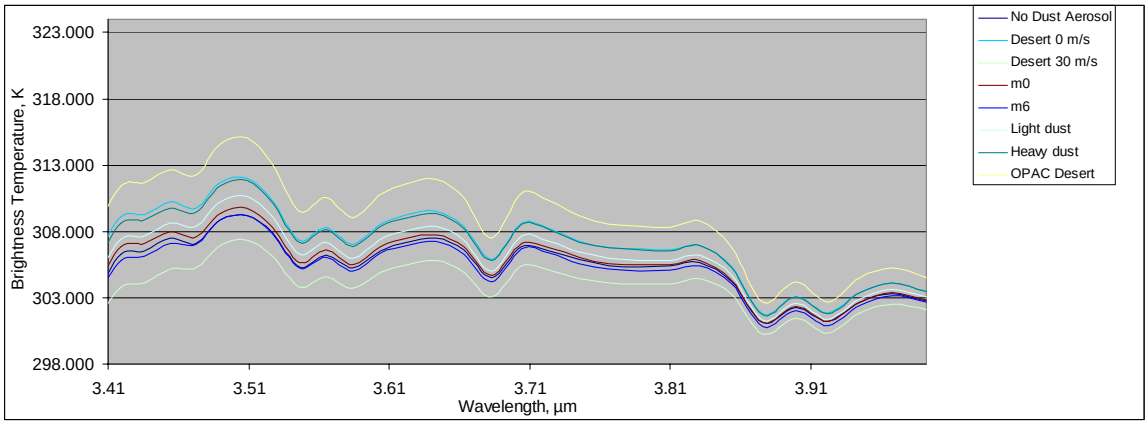

Figure 60. Top-of-the-atmosphere brightness temperature, all cases, spring day, nadir.

Brightness temperatures in the wavelength band between 4.63 and 4.975 µm are variable, with decreasing brightness temperature values through 4.8 µm and increasing values from 4.8 µm wavelengths and higher (see Figure 61). Brightness temperature values for all simulations are very similar to the no aerosol simulation. The range of brightness temperature values from every simulation is roughly 1 K. The largest brightness temperature values come from the no aerosol simulation. The smallest brightness temperature values result from the Desert 30 m/s dust aerosol representation. The brightness temperature values for each simulation do not cross. The average brightness temperature difference between no aerosol and dust aerosol across this range are less than 1 K for all simulations. The Desert 30 m/s dust aerosol results in an average brightness temperature difference from the no aerosol simulation of 0.644 K.

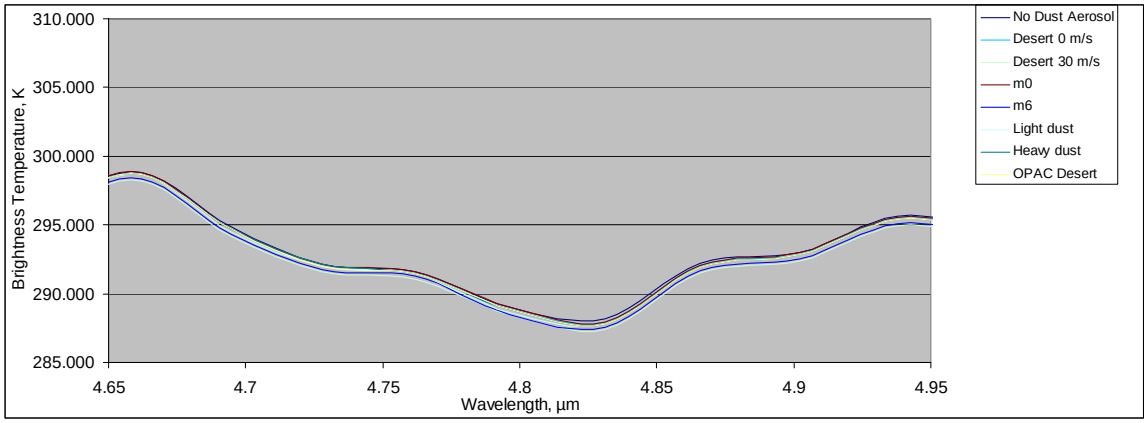

Figure 61. Top-of-the-atmosphere brightness temperature, all cases, spring day, nadir.

The average difference between the no aerosol simulation brightness temperature and the brightness temperatures of various dust aerosols are presented in Figures 62, 63, and Table 11. Of note in this table are the large brightness temperature differences. As wavelength increases, the brightness temperature difference between the no aerosol simulation and any dust aerosol simulation decrease. Another interesting observation is the change in magnitude of the brightness temperature difference with respect to wavelength when comparing the low 0.55 µm optical depth simulations to their high 0.55 µm optical depth counterpart. The m0 simulation produced much higher brightness

temperatures than the no aerosol case below 2.4 µm. The magnitude of the difference is greater than 20 K. At wavelengths longer than 2.4 µm the difference between the m0 simulation brightness temperature and the no aerosol simulation were at most 0.167 K. Contrast this with the m6 simulation - in wavelengths below 2.4 µm, the magnitude of the brightness temperature difference from no aerosol was as much as 5 K. At wavelengths longer the 2.4 µm, the m6 simulation brightness temperature was different from the no aerosol simulation by 0.178 to 0.489 K. The m6 representation is essentially the m0 representation with the addition of a lower concentration, but larger radius mode of dust aerosol. The large disparity between the m0 and m6 representations in terms of average brightness temperature difference when compared with the no aerosol atmosphere must be due to the larger particles. Therefore, the addition of particles of larger radius has a significant impact on top-of-the-atmosphere brightness temperature.

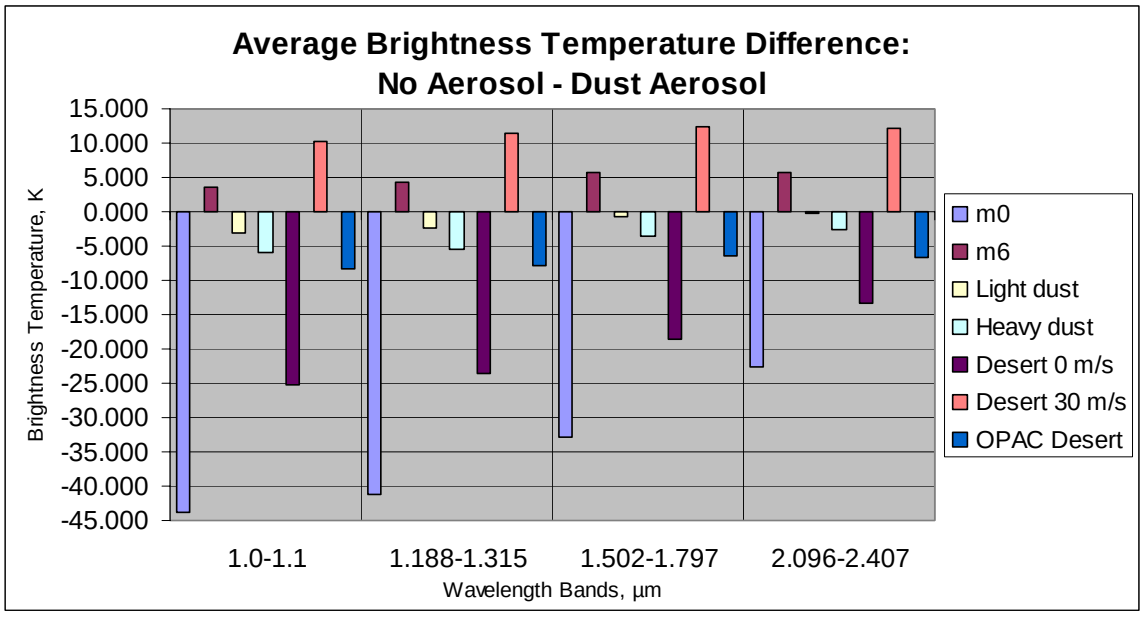

Figure 62. Average brightness temperature difference between no aerosol and dust aerosol, spring day, nadir.

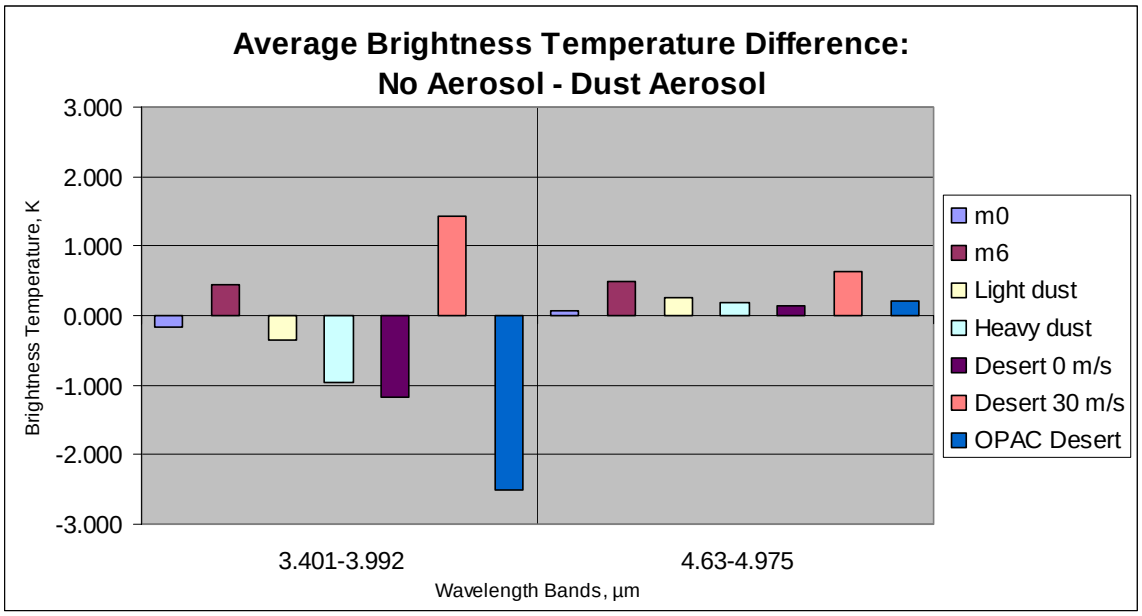

Figure 63. Average brightness temperature difference between no aerosol and dust aerosol, spring day, nadir.

Table 11. Average brightness temperature difference between no aerosol and dust aerosol, spring day, nadir.

	Average Brightness Temperature Difference, K						
Wavelength Band	No Aerosol - Dust Aerosol Representation						
µm	m0	m6	Light dust	Heavy dust	Desert 0 m/s	Desert 30 m/s	OPAC
1.0-1.1	-43.894	3.469	-3.007	-6.045	-25.180	10.302	-8.232
1.188-1.315	-41.273	4.244	-2.404	-5.435	-23.673	11.330	-7.854
1.502-1.797	-32.976	5.631	-0.828	-3.488	-18.578	12.499	-6.503
2.096-2.407	-22.608	5.661	-0.228	-2.531	-13.251	12.236	-6.704
3.401-3.992	-0.167	0.456	-0.340	-0.961	-1.173	1.421	-2.515
4.63-4.975	0.061	0.489	0.262	0.182	0.137	0.644	0.212

F. SPRING DAY 30° ZENITH ANGLE

The spring day 30° zenith angle case was run with the MODTRAN input parameters described in the methodology section. The no dust aerosol simulation results in radiance values presented in Figure 64. Between 1 and 2.6 µm the magnitude of radiance generally decreases according to the Planck function for solar temperature. The values decrease from 3.22×10^{-3} $W \bullet cm^{-2} \bullet ster^{-1} \bullet \mu m^{-1}$ to a minimum of 6.37×10^{-8} $W \bullet cm^{-2} \bullet ster^{-1} \bullet \mu m^{-1}$ in the carbon dioxide absorption band between 2 and 3 µm. The radiance then increases, roughly corresponding to the Planck function

associated with the blackbody temperature of the earth. The minimum radiance of 6.37 x 10^{-8} W•cm^{-2}•$ster^{-1}$•μm^{-1} between 2 and 3 µm increases to a value of 2.07 x 10^{-4} W•cm^{-2}•$ster^{-1}$•μm^{-1} near 5 µm. At wavelengths higher than 3 µm atmospheric absorption bands are represented by lower radiance values. First, the water vapor band is present at wavelengths just greater than 3 µm. Carbon dioxide and nitrous oxide absorption is present between 4 and 5 µm. As expected the spring day off-axis case radiance values are slightly less than the spring day nadir case radiance values.

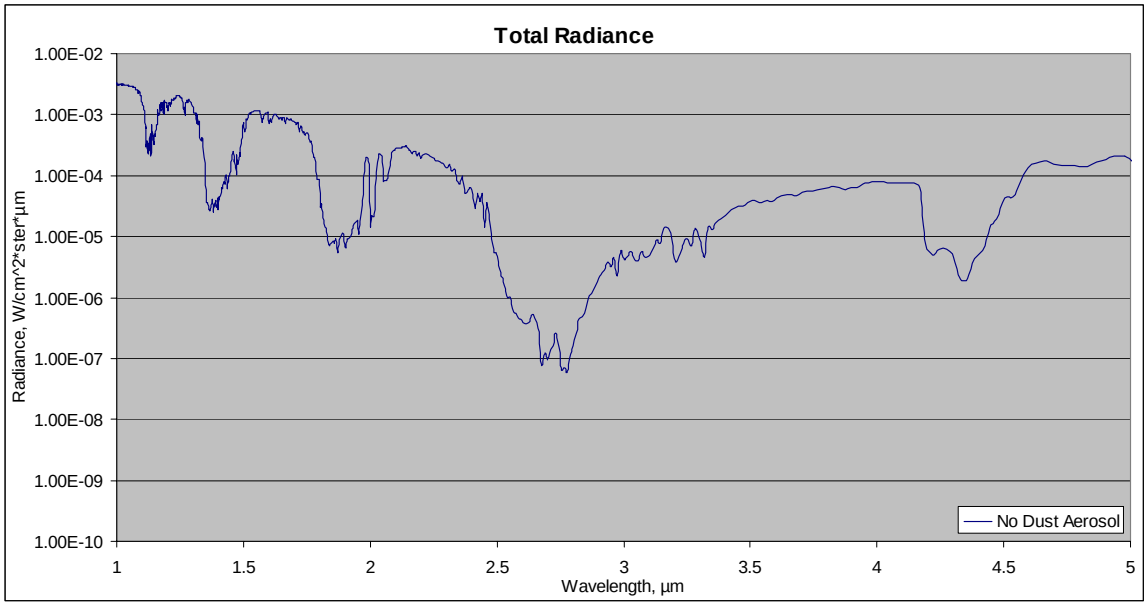

Figure 64. Top-of-the-atmosphere total radiance, no dust aerosol, spring day, 30° zenith angle.

After conversion to brightness temperature as described in the chapter on methodology, the brightness temperatures behave as expected with no dust aerosol present (see Figure 65). Important to note here is the surface temperature of 307.5 K for this case, as the brightness temperature values calculated should be near this value in the atmospheric windows of the wavelength band outside of solar influence. At 1 µm the brightness temperature is 951.344 K. This value is cut nearly in half at 2.033 µm where the brightness temperature is 496.934 K. At 3.003 µm the brightness temperature value is 294.433 K. Once again the sharp decrease in brightness temperature is due to the

surface reflectance model used in the MODTRAN simulations. In the same wavelength span the reflectance changes from 0.7 to just 0.1, therefore much less solar energy is being reflected off of the surface and towards the top-of-the-atmosphere.

The atmospheric absorption bands noted above are revealed as bands of lower brightness temperature, as expected. Surface reflection is very low, but the scattering of radiation by the tropospheric, stratospheric and meteoric background aerosol is present in the simulation. Evidence that this type of scattering is occurring is in the profile of brightness temperatures in the absorption bands. The brightness temperatures show little change across the band, in contrast to the sharp decrease in brightness temperature in the neighboring windows which mirror the surface reflectance.

The windows in the band between 3.4 and 5 μm are quite interesting when viewed from the brightness temperature perspective. This band shows the interaction of solar energy and terrestrial energy. The transmission in this band peaks at roughly 3.5 μm. With this in mind the brightness temperature is expected to be near the 307.5 K surface temperature. The simulations reveal that the brightness temperature is greater than expected at 3.5 μm. The brightness temperatures between 3.4 and 4.1 μm decrease from 309 to 297 K. From 4.5 to 5 μm brightness temperatures vary between 298 and 286 K. Since the brightness temperatures in this band are closer to the surface temperature than transmission would allow, the energy in the simulation must be due to contribution from solar scattering.

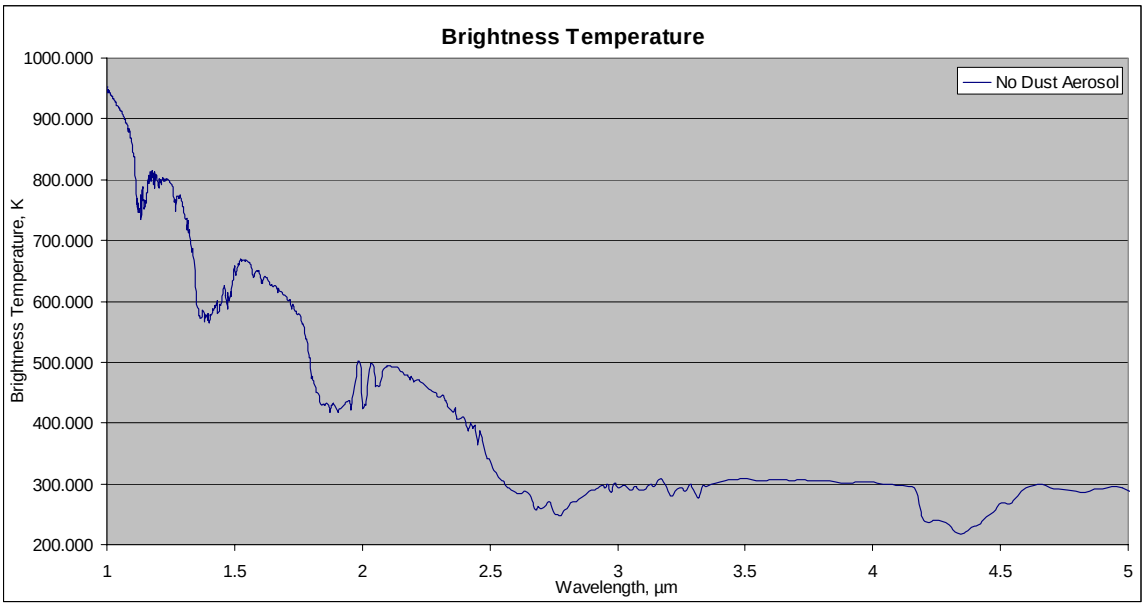

Figure 65. Top-of-the-atmosphere brightness temperature, no dust aerosol, spring day, 30° zenith angle.

As mentioned in the methodology chapter dust aerosols that were non-absorptive were considered as well as absorptive dust aerosols. The difference between the brightness temperatures of the absorptive dust and the non-absorptive dust was significant in all of the atmospheric windows (see Table 12). The differences were larger at shorter wavelengths than at longer wavelengths. This probably relates to the amount of energy involved in these bands, although the wavelength dependence of emitted radiation is also a factor. In addition, the differences were larger for the representations with higher 0.55 µm optical depth (m6 and Desert 30 m/s) than the representations with lower 0.55 µm optical depth (m0 and Desert 0 m/s). The higher 0.55 µm optical depth values result from representations with a larger number of dust aerosol particles per cubic centimeter. Larger dust aerosol particle loading suggests larger extinction by these aerosols. Larger extinction due to dust aerosol causes larger changes to top-of-the-atmosphere brightness temperature. This is why the Desert 30 m/s dust representation exhibits a larger average brightness temperature difference from the no aerosol simulation than the m6 representation. Since the brightness temperature values from both the non-absorptive and absorptive Desert 30 m/s dust representations are larger than the

brightness temperature values from both m6 representations, the difference between the non-absorptive and absorptive Desert 30 m/s dust aerosols are correspondingly larger than the difference between the m6 representations. The exception here is the Heavy dust and Light dust representations. The non-absorptive aerosols minus the absorptive aerosol brightness temperature differences were similar in both the Light dust and Heavy dust aerosol representation despite having different 0.55 μm optical depths. The 0.55 μm optical depths were similar to the other representations with Heavy dust having the higher 0.55 μm optical depth. Brightness temperature differences in this table reveal the importance of accounting for absorption by dust aerosol when calculating radiative transfer between 1 and 5 μm. With that in mind the following examination of brightness temperatures among the different dust representations will focus on the absorptive dust aerosol only.

.

Table 12. Average brightness temperature difference between non-absorptive and absorptive dust, spring day, 30° zenith angle.

	Average Brightness Temperature Difference, K					
Wavelength Band	Non Absorptive - Absorptive Dust Aerosol Representation					
μm	m0	m6	Light dust	Heavy dust	Desert 0 m/s	Desert 30 m/s
1.0-1.1	2.778	11.860	6.852	5.795	-2.757	11.850
1.188-1.315	2.464	12.794	7.435	6.357	-1.968	12.932
1.502-1.797	2.232	13.799	8.249	7.175	-0.028	14.265
2.096-2.407	1.878	14.701	9.148	7.938	2.514	15.236
3.401-3.992	0.304	4.589	3.012	2.442	2.514	5.023
4.63-4.975	0.028	0.178	0.126	0.091	0.140	0.314

Brightness temperatures resulting from the addition of dust aerosols to the simulation across the entire 1 through 5 μm band are found in Figure 66. Since the brightness temperatures range from near 1000 K to below 300 K it is difficult to quantify the difference between the no aerosol simulation and the various dust aerosol simulations. Some spread among the plots between 1 and 3 μm is apparent, but as wavelength increases, the difference between the no aerosol case and the various aerosol simulations decrease. One visible difference is between the no aerosol case and the dust aerosol cases in the absorption bands between 1 and 3 μm. These differences are near 30 K, with the no aerosol simulation having the highest brightness temperature. This is caused by

extinction due to dust aerosol. To better understand the effect of the various dust aerosols on brightness temperature closer examination of narrower wavelength bands is required.

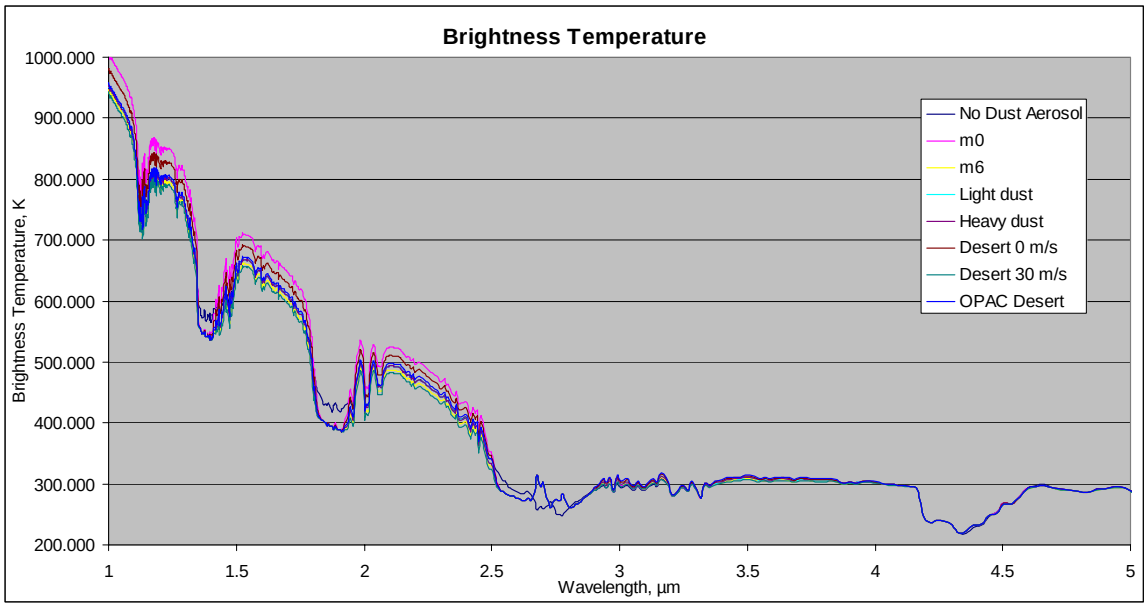

Figure 66. Top-of-the-atmosphere brightness temperature, all cases, spring day, 30° zenith angle.

Wavelength bands were chosen arbitrarily to match up with radiative windows, based on examination of the wavelength range and the variability of the aerosol in the window band. Brightness temperature in the first wavelength band between 1 and 1.1 µm is presented in Figure 67. Brightness temperatures decrease for all simulations similarly to the no aerosol simulation. The range of brightness temperature values from every simulation is very large, over 60 K. The largest brightness temperature values come from the m0 absorptive representation. The smallest brightness temperature values result from the Desert 30 m/s dust aerosol representation. The brightness temperature values for each simulation do not cross, and retain the same difference from the no aerosol simulation throughout this window. In this case the m0 representation is further from the remaining aerosol representations than in the other cases.

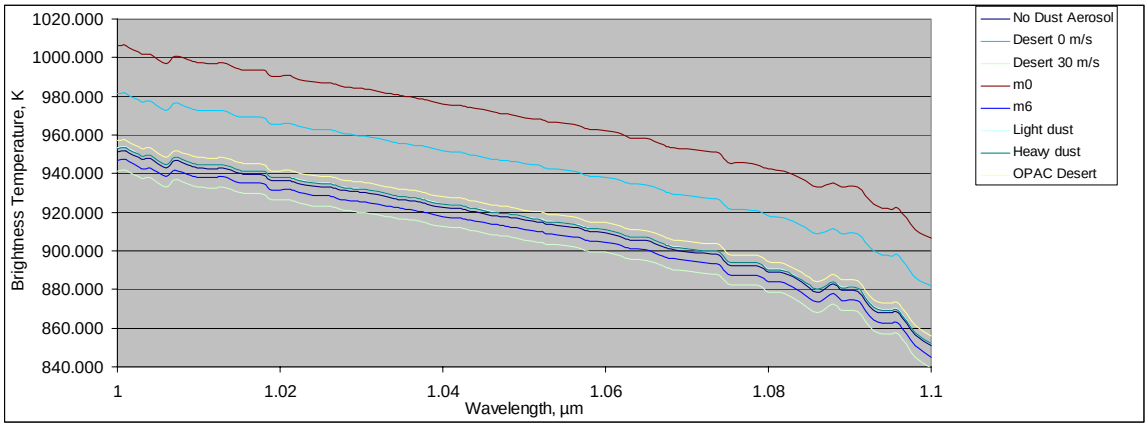

Figure 67. Top-of-the-atmosphere brightness temperature, spring day, 30° zenith angle.

Brightness temperatures in the wavelength band between 1.19 and 1.31 µm are similar to brightness temperature values in the first band examined (see Figure 68). Brightness temperatures decrease for all simulations similarly to the no aerosol simulation. The range of brightness temperature values from every simulation is nearly 60 K. The largest brightness temperature values come from the m0 absorptive representation. The smallest brightness temperature values result from the Desert 30 m/s dust aerosol representation. The brightness temperature values for each simulation do not cross, and retain roughly the same difference from the no aerosol simulation throughout this window.

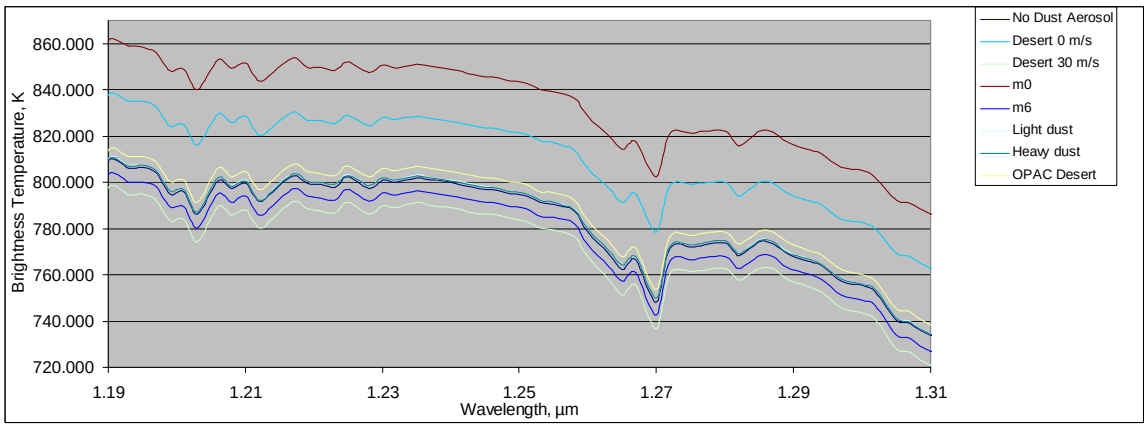

Figure 68. Top-of-the-atmosphere brightness temperature, spring day, 30° zenith angle.

Brightness temperatures in the wavelength band between 1.505 and 1.797 µm follow a similar pattern as in the previous shorter wavelength windows (see Figure 69). Brightness temperatures decrease for all simulations similarly to the no aerosol simulation. The range of brightness temperature values from every simulation is over 50 K. The largest brightness temperature values come from the m0 absorptive representation. The smallest brightness temperature values result from the Desert 30 m/s dust aerosol representation. The brightness temperature values for each simulation do not cross, and retain roughly the same difference from the no aerosol simulation through most of this window. As the wavelength surpasses 1.755 µm the brightness temperatures of all simulations converge.

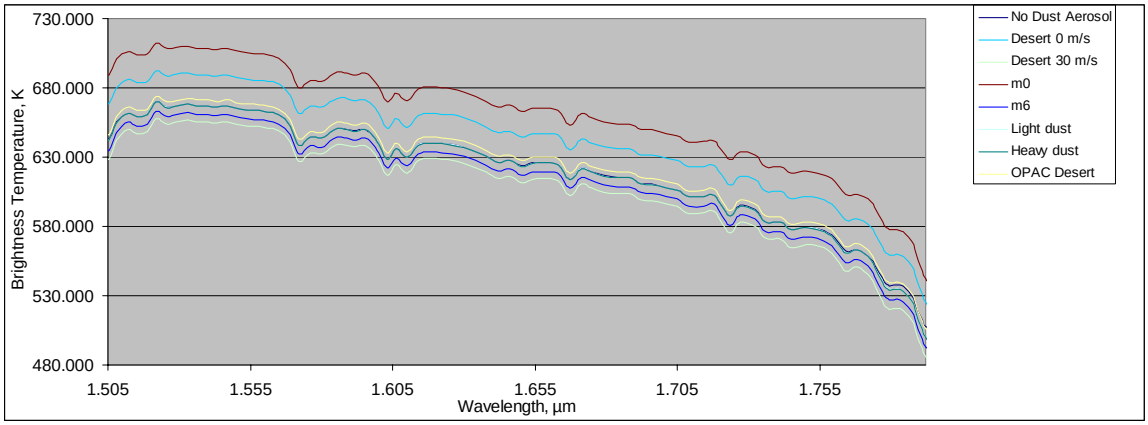

Figure 69. Top-of-the-atmosphere brightness temperature, spring day, 30° zenith angle.

Brightness temperatures in the wavelength band between 2.1 and 2.4 µm follow a similar pattern as in the previous shorter wavelength windows (see Figure 70). Brightness temperatures decrease for all simulations similarly to the no aerosol simulation. The range of brightness temperature values from every simulation has decreased to near 40 K. The largest brightness temperature values come from the m0 absorptive representation. The smallest brightness temperature values result from the Desert 30 m/s dust aerosol representation. The brightness temperature values for each simulation do not cross, and retain roughly the same difference from the no aerosol simulation through most of this window.

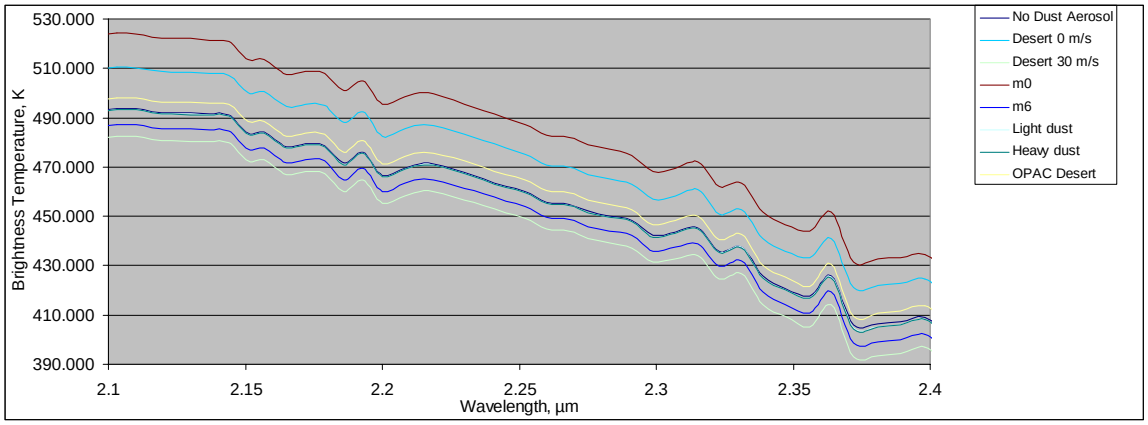

Figure 70. Top-of-the-atmosphere brightness temperature, spring day, 30° zenith angle.

Brightness temperatures in the wavelength band between 3.401 and 3.992 µm are fairly flat with a slight decrease in brightness temperature as wavelength increases (see Figure 71). Brightness temperature values for all simulations are similar to the no aerosol simulation. The range of brightness temperature values from every simulation is roughly 6 K at wavelengths below 3.8 µm and only 2 K above 3.8 µm. The largest brightness temperature values come from the OPAC Desert representation. The smallest brightness temperature values result from the Desert 30 m/s dust aerosol representation. The brightness temperature values for each simulation do not cross. The average brightness temperature difference between no aerosol and dust aerosol across this range are small for all simulations.

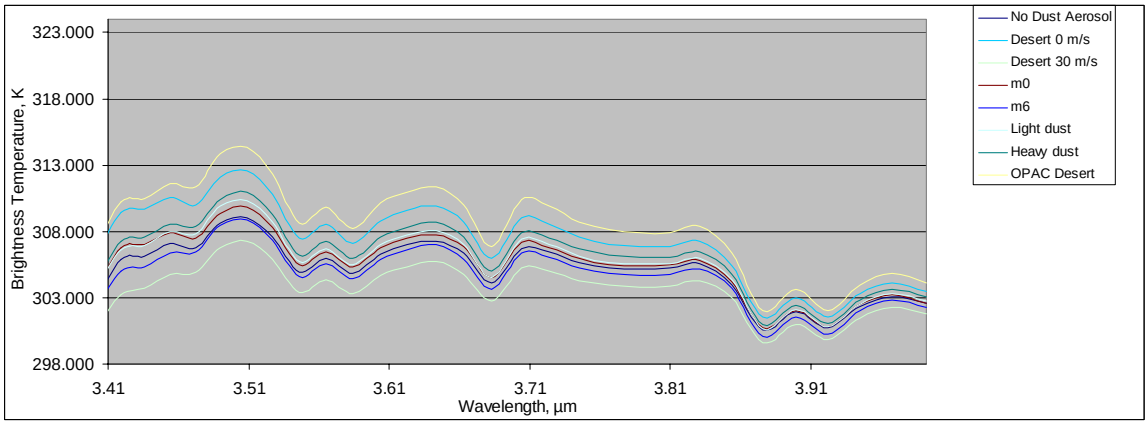

Figure 71. Top-of-the-atmosphere brightness temperature, spring day, 30° zenith angle.

Brightness temperatures in the wavelength band between 4.63 and 4.975 µm are variable, with decreasing brightness temperature values through 4.8 µm and increasing values from 4.8 µm wavelengths and higher (see Figure 72). Brightness temperature values for all simulations are very similar to the no aerosol simulation. The range of brightness temperature values from every simulation is roughly 1 K. The largest brightness temperature values come from the no aerosol simulation. The smallest brightness temperature values result from the Desert 30 m/s dust aerosol representation. The brightness temperature values for each simulation do not cross. The average brightness temperature difference between no aerosol and dust aerosol across this range are less than 1 K for all simulations. The Desert 30 m/s dust aerosol results in an average brightness temperature difference from the no aerosol simulation of 0.758 K.

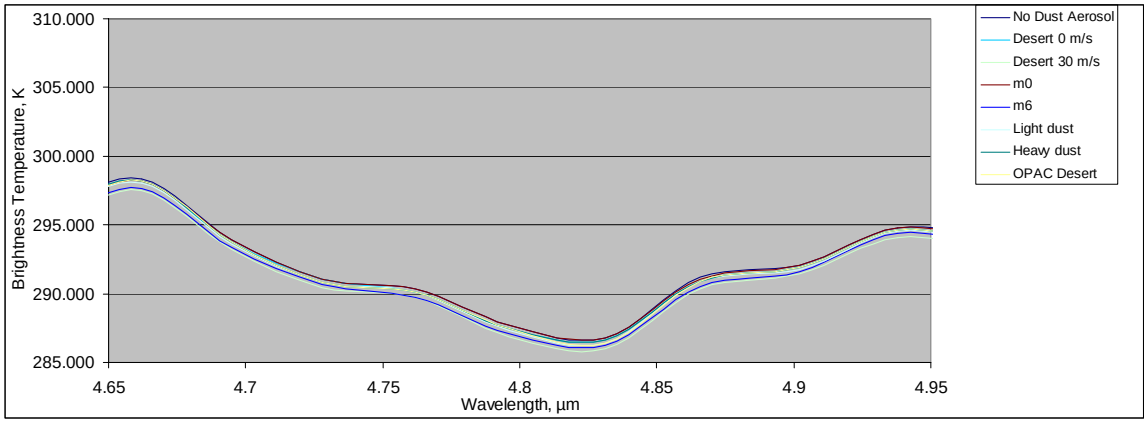

Figure 72. Top-of-the-atmosphere brightness temperature, spring day, 30° zenith angle.

The average difference between the no aerosol simulation brightness temperature and the brightness temperatures of various dust aerosols are presented in Figures 73, 74, and Table 13. Of note in this table are the large brightness temperature differences. As wavelength increases, the brightness temperature difference between the no aerosol simulation and any dust aerosol simulation decrease. Another interesting observation is the change in magnitude of the brightness temperature difference with respect to wavelength when comparing the low 0.55 µm optical depth simulations to their high 0.55 µm optical depth counterpart. The m0 simulation produced much higher brightness

temperatures than the no aerosol case below 2.4 µm. The magnitude of the difference is greater than 25 K. At wavelengths longer than 2.4 µm the difference between the m0 simulation brightness temperature and the no aerosol simulation were at most -0.442 K. Contrast this with the m6 simulation - in wavelengths below 2.4 µm, the magnitude of the brightness temperature difference from no aerosol was as much as 7 K. At wavelengths longer the 2.4 µm, the m6 simulation brightness temperature was different from the no aerosol simulation by 0.307 to 0.571 K. The m6 representation is essentially the m0 representation with the addition of a lower concentration, but larger radius mode of dust aerosol. The large disparity between the m0 and m6 representations in terms of average brightness temperature difference when compared with the no aerosol atmosphere must be due to the larger particles. Therefore, the addition of particles of larger radius has a significant impact on top-of-the-atmosphere brightness temperature.

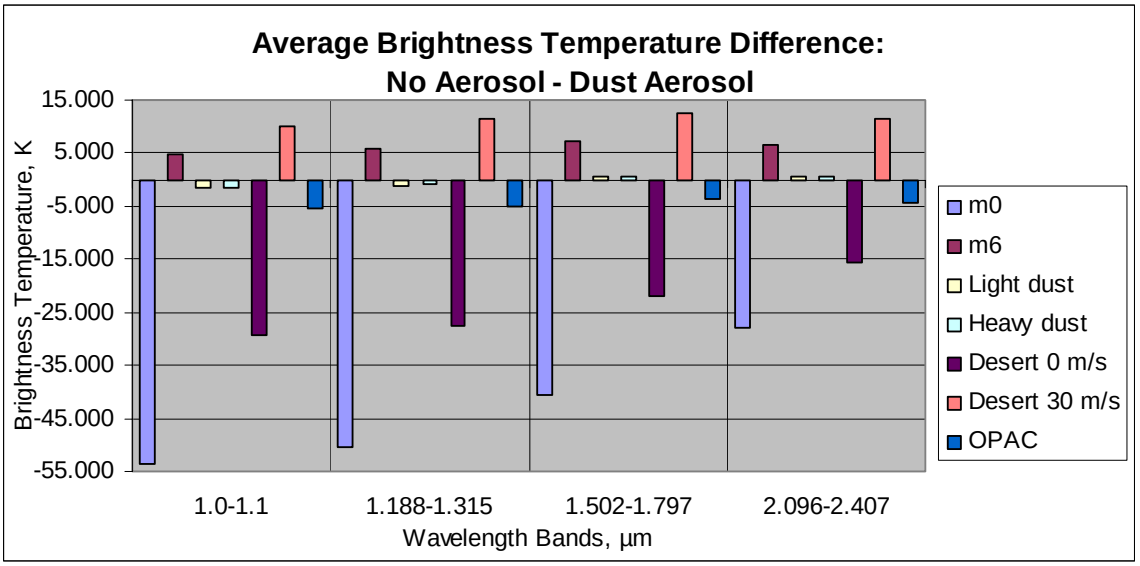

Figure 73. Average brightness temperature difference between no aerosol and dust aerosol, spring day, 30° zenith angle.

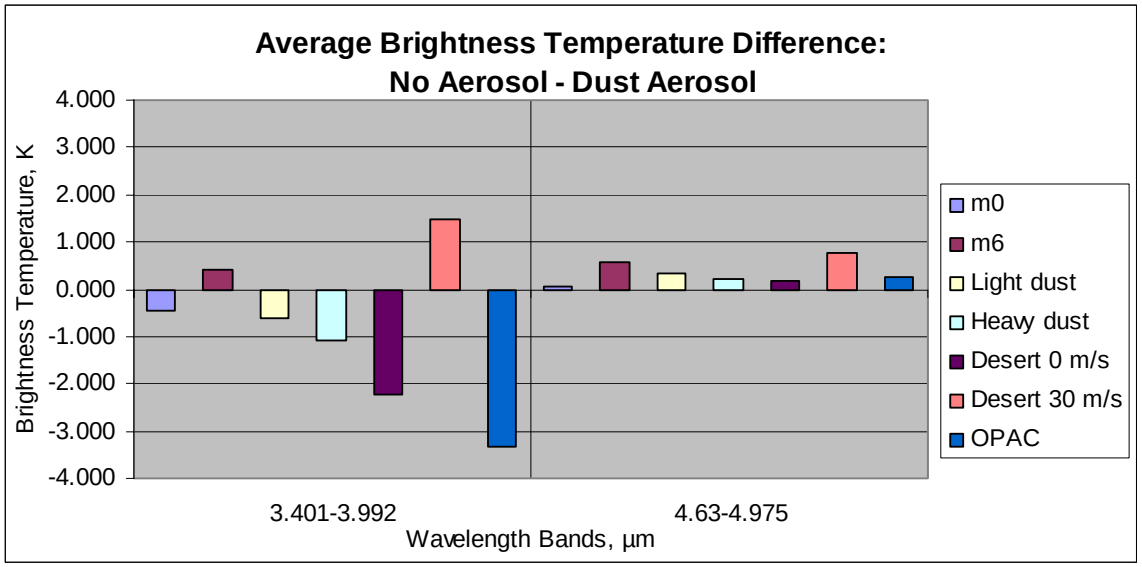

Figure 74. Average brightness temperature difference between no aerosol and dust aerosol, spring day, 30° zenith angle.

Table 13. Average brightness temperature difference between no aerosol and dust aerosol, spring day, 30° zenith angle.

	Average Brightness Temperature Difference, K						
Wavelength Band	No Aerosol - Dust Aerosol Representation						
µm	m0	m6	Light dust	Heavy dust	Desert 0 m/s	Desert 30 m/s	OPAC
1.0-1.1	-53.685	4.877	-1.696	-1.545	-29.371	10.174	-5.389
1.188-1.315	-50.459	5.844	-1.010	-0.905	-27.671	11.365	-4.948
1.502-1.797	-40.487	7.098	0.449	0.536	-21.805	12.444	-3.783
2.096-2.407	-27.866	6.469	0.544	0.621	-15.705	11.418	-4.521
3.401-3.992	-0.442	0.407	-0.610	-1.093	-2.232	1.488	-3.318
4.63-4.975	0.060	0.571	0.329	0.204	0.186	0.758	0.238

G. SPRING NIGHT NADIR

The spring night nadir view case was run with the MODTRAN input parameters described in the methodology section. The no dust aerosol simulation results in radiance values presented in Figure 75. Between 1 and 2.6 µm the magnitude of radiance is small. This energy is solar energy reflected off of the moon and into the scene in the MODTRAN simulation. Radiance increases above 3 µm, roughly corresponding to the Planck function associated with the blackbody temperature of the earth. The minimum radiance of 1.98×10^{-10} W•cm^{-2}•ster^{-1}•µm^{-1} occurs at 1.878 µm, seemingly the beginning of energy from terrestrial emission. Radiance increases to a value of roughly

1.69 x 10^{-4} W•cm^{-2}•$ster^{-1}$•μm^{-1} near 5 µm. Atmospheric absorption is represented by the appropriate absorption bands between 3 and 5 µm. First water vapor absorption is present at wavelengths just greater than 3 µm. Carbon dioxide and nitrous oxide absorption are present between 4 and 5 µm.

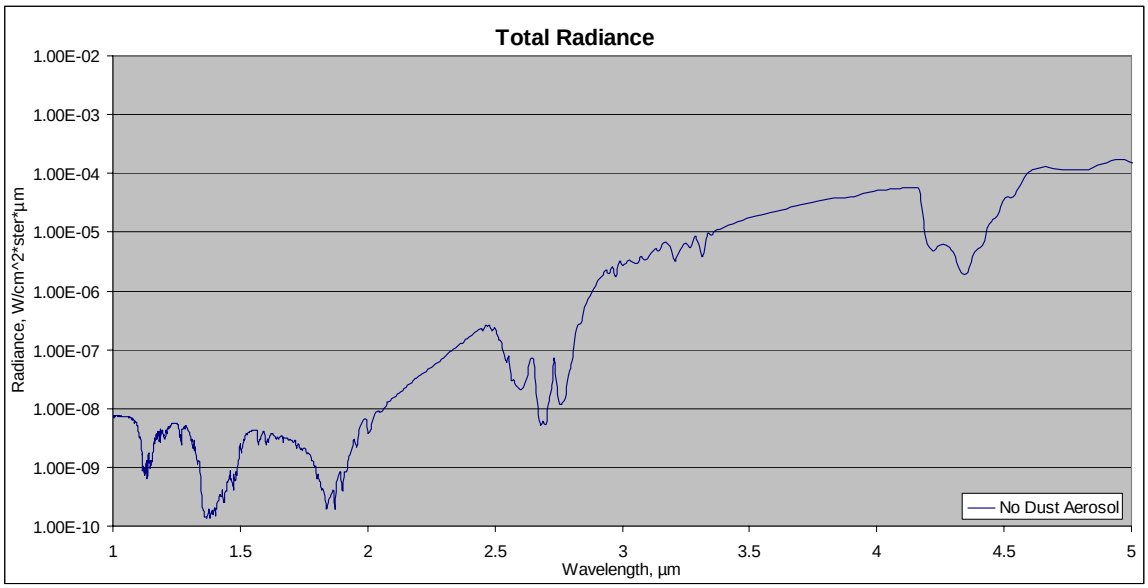

Figure 75. Top-of-the-atmosphere total radiance, no dust aerosol, spring night, nadir.

Brightness temperatures reveal the presence of the lunar energy in the 1 through 3 µm wavelength band (see Figure 76). Important to note here is the surface temperature of 297.3 K for this case, as the brightness temperature values calculated should be near this value in the atmospheric windows of the wavelength band outside of solar influence. At 1 µm the brightness temperature is 512.304 K this is nearly half of the daytime simulation. At 2.014 µm the brightness temperature value decreases to 284.822 K. At 3.003 µm the brightness temperature value is 281.075 K. The decrease in brightness temperature values up to 1.8 µm is due to the surface reflectance model used in the MODTRAN simulations. In the same wavelength span the reflectance changes from 0.7 to just 0.1, therefore much less lunar energy is being reflected off of the surface and towards the top-of-the-atmosphere.

Also interesting to note is the similarity of the 2 and 3 μm brightness temperatures. Since the lunar source inputs much less energy into the calculation, the entire lunar brightness temperature curve shifts further down the chart, and it intersects the terrestrial emission curve at lower wavelengths as a result. In the daytime simulation it seemed that solar energy was influencing the brightness temperature up to 5 μm. This night time simulation reveals the terrestrial energy influencing brightness temperatures at wavelengths as small as 2 μm.

The atmospheric absorption bands below 2 μm are revealed as bands of lower brightness temperature, as expected. Also expected is the fact that the reduction of brightness temperature is smaller in this simulation due to the lower amounts of radiant energy. Surface reflection is very low, but the scattering of radiation by the tropospheric, stratospheric and meteoric background aerosol is present in the simulation. Evidence that this type of scattering is occurring is in the profile of brightness temperatures in the absorption bands. The brightness temperatures show little change across the absorption band, in contrast to the sharp decrease in brightness temperature in the neighboring windows which mirror the surface reflectance.

The absorption bands at wavelengths greater than 2.4 μm are similar to the absorption bands of the daytime simulation in that they represent a decrease from the neighboring atmospheric window of similar magnitude. This points to the relative influence of terrestrial versus solar radiance once again. In this simulation it is clear that terrestrial radiance dominates the brightness temperature to wavelengths as low as 1.9 μm.

Despite the dominance of terrestrial energy to very low wavelengths, the windows in the band between 3.4 and 5 μm are still influenced somewhat by the lunar source. The transmission in this band peaks at roughly 3.5 μm. With this in mind the brightness temperature is expected to be near the 297.3 K surface temperature. The simulations reveal that the brightness temperature is greater than expected at 3.5 μm. The brightness temperatures between 3.4 and 4.1 μm decrease from 290 to 292 K. From 4.5 to 5 μm

brightness temperatures vary between 281 and 290 K. Since the brightness temperatures in this band are closer to the surface temperature than transmission would allow, the energy in the simulation must be due to contribution from lunar scattering.

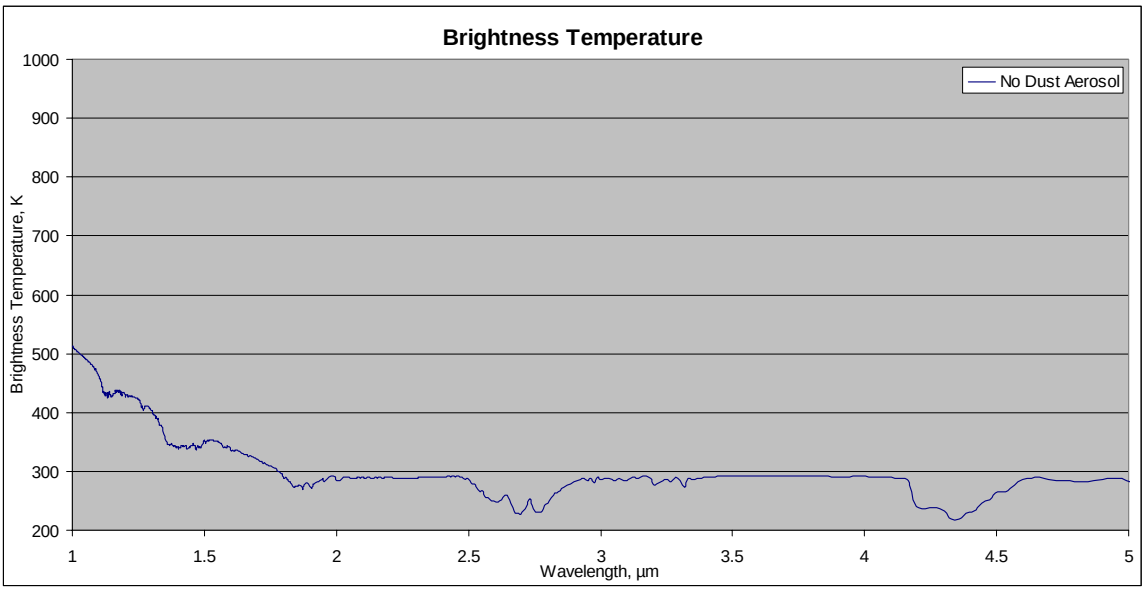

Figure 76. Top-of-the-atmosphere brightness temperature, no dust aerosol, spring night, nadir.

As mentioned in the methodology chapter dust aerosols that were non-absorptive were considered as well as absorptive dust aerosols. The difference between the brightness temperatures of the absorptive dust and the non-absorptive dust was significant in all of the atmospheric windows (see Table 14). The differences were larger at shorter wavelengths than at longer wavelengths. This probably relates to the amount of energy involved in these bands, although the wavelength dependence of emitted radiation is also a factor. In addition, the differences were larger for the representations with higher 0.55 µm optical depth (m6 and Desert 30 m/s) than the representations with lower 0.55 µm optical depth (m0 and Desert 0 m/s). The higher 0.55 µm optical depth values result from representations with a larger number of dust aerosol particles per cubic centimeter. Larger dust aerosol particle loading suggests larger extinction by these aerosols. Larger extinction due to dust aerosol causes larger changes to top-of-the-

atmosphere brightness temperature. This is why the Desert 30 m/s dust representation exhibits a larger average brightness temperature difference from the no aerosol simulation than the m6 representation. Since the brightness temperature values from both the non-absorptive and absorptive Desert 30 m/s dust representations are larger than the brightness temperature values from both m6 representations, the difference between the non-absorptive and absorptive Desert 30 m/s dust aerosols are correspondingly larger than the difference between the m6 representations. The exception here is the Heavy dust and Light dust representations. The non-absorptive aerosols minus the absorptive aerosol brightness temperature differences were similar in both the Light dust and Heavy dust aerosol representation despite having different 0.55 μm optical depths. The 0.55 μm optical depths were similar to the other representations with Heavy dust having the higher 0.55 μm optical depth. Brightness temperature differences in this table reveal the importance of accounting for absorption by dust aerosol when calculating radiative transfer between 1 and 5 μm. With that in mind the following examination of brightness temperatures among the different dust representations will focus on the absorptive dust aerosol only.

Table 14. Average brightness temperature difference between non-absorptive and absorptive dust aerosol, spring night, nadir.

	Average Brightness Temperature Difference, K					
Wavelength Band	Non Absorptive - Absorptive Dust Aerosol Representation					
μm	m0	m6	Light dust	Heavy dust	Desert 0 m/s	Desert 30 m/s
1.0-1.1	0.892	2.978	1.417	1.142	-0.500	4.738
1.188-1.315	0.782	3.342	1.635	1.340	-0.307	5.296
1.502-1.797	0.697	3.430	1.844	1.577	0.218	5.142
2.096-2.407	-0.134	-0.689	-0.475	-0.449	-0.336	-0.821
3.401-3.992	-0.075	-0.555	-0.351	-0.311	-0.241	-0.667
4.63-4.975	0.000	-0.181	-0.108	-0.055	-0.058	-0.211

Brightness temperatures resultant from the addition of several dust aerosols across the entire 1 through 5 μm band are plotted in Figure 77. Since the brightness temperatures range from over 500 K to near 300 K it is difficult to quantify the difference between the no aerosol simulation and the various dust aerosol simulations by examining the plot of the entire wavelength range. Some spread among the plots between

1 and 2 µm is apparent, but as wavelength increases, the difference between the no aerosol case and the various aerosol simulations decrease. One visible difference is between the no aerosol case and the dust aerosol cases in the absorption band at 1.4 µm. The brightness temperature difference here is roughly 20 K, with the no aerosol simulation having the highest brightness temperature. This is caused by extinction due to dust aerosol. To better understand the effect of the various dust aerosols on brightness temperature closer examination of narrower wavelength bands is required.

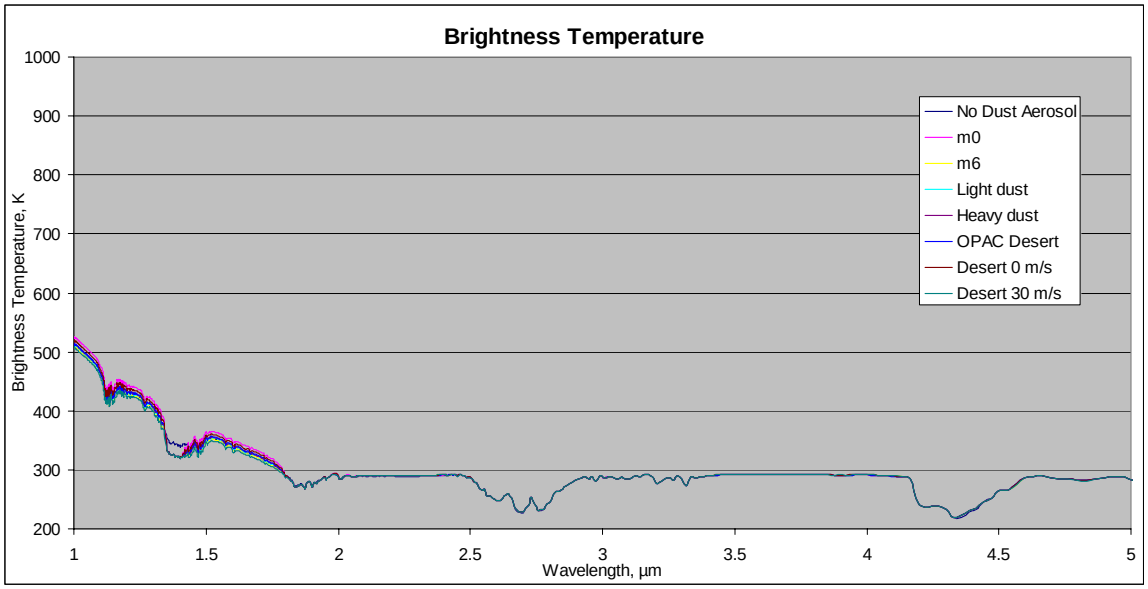

Figure 77. Top-of-the-atmosphere brightness temperature, all cases, spring night, nadir.

Window bands were chosen arbitrarily based on examination of the wavelength range and the variability of the aerosol in the window band. Brightness temperature values in the first band between 1 and 1.1 µmare presented in Figure 78. Brightness temperatures decrease for all simulations similarly to the no aerosol simulation. The range of brightness temperature values from every simulation is smaller than in the daytime simulation roughly 20 K. The largest brightness temperature values come from the m0 dust aerosol representation. The smallest brightness temperature values result

from the Desert 30 m/s dust aerosol representation. The brightness temperature values for each simulation do not cross, and retain the same difference from the no aerosol simulation throughout this window.

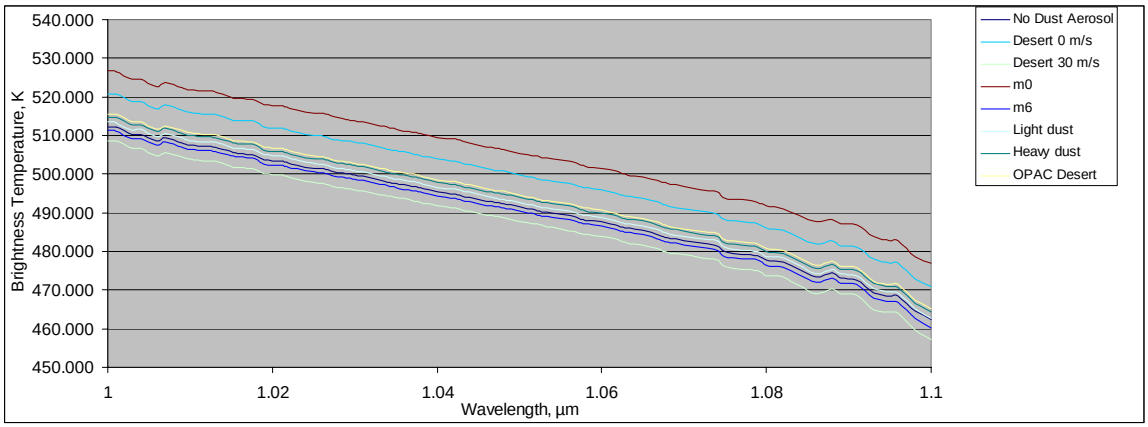

Figure 78. Top-of-the-atmosphere brightness temperature, all cases, spring night, nadir.

Brightness temperatures in the next window band between 1.19 and 1.31 µm, are presented in Figure 79. Brightness temperatures decrease for all simulations similarly to the no aerosol simulation. The range of brightness temperature values from every simulation is larger than in the previously examined band with a range of roughly 20 K. The largest brightness temperature values come from the m0 absorptive representation. The smallest brightness temperature values result from the Desert 30 m/s dust aerosol representation. The brightness temperature values for each simulation do not cross, and retain roughly the same difference from the no aerosol simulation throughout this window.

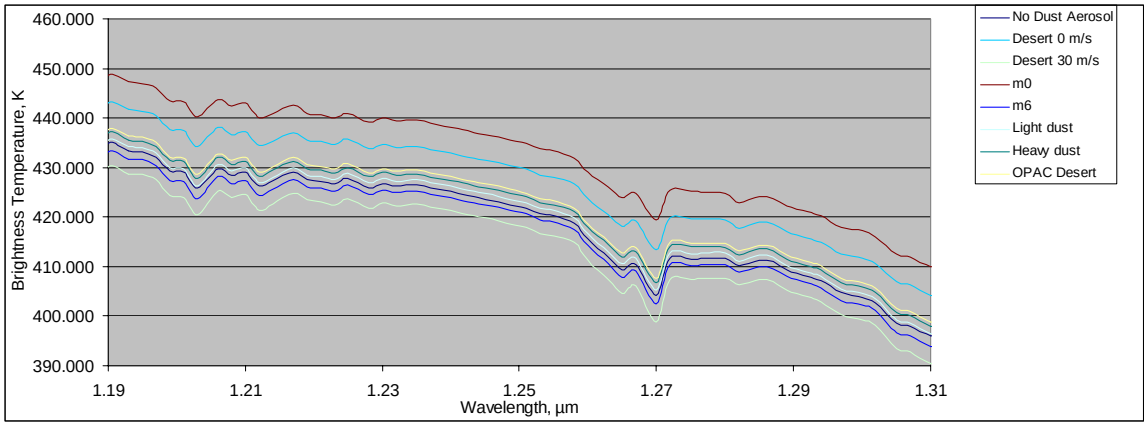

Figure 79. Top-of-the-atmosphere brightness temperature, all cases, spring night, nadir.

Brightness temperatures in the band between 1.505 and 1.797 µm follow a similar pattern as in the previous shorter wavelength windows (see Figure 80). Brightness temperatures decrease for all simulations similarly to the no aerosol simulation. The range of brightness temperature values from every simulation is smaller than the previously examined window with values near 15 K. The largest brightness temperature values come from the m0 absorptive representation. The smallest brightness temperature values result from the Desert 30 m/s dust aerosol representation. The brightness temperature values for each simulation do not cross, and retain roughly the same difference from the no aerosol simulation through most of this window. As the wavelength surpasses 1.755 µm the brightness temperatures of all simulations approach a common value.

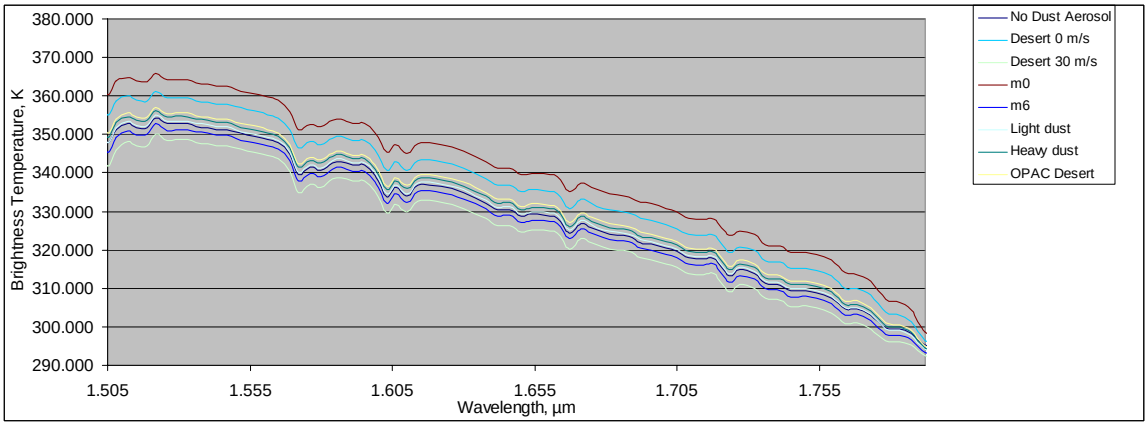

Figure 80. Top-of-the-atmosphere brightness temperature, all cases, spring night, nadir.

Brightness temperatures in the wavelength range between 2.1 and 2.4 µm are quite different from the shorter wavelength windows (see Figure 81). Brightness temperatures are steady for all simulations up to 2.3 µm similarly to the no aerosol simulation. At wavelengths higher than 2.3 µm brightness temperatures from all simulations begin to increase and approach a common value. The range of brightness temperature values from every simulation is much smaller than in the shorter wavelength windows, roughly 1.5 K. The largest brightness temperature values come from the Desert 30 m/s dust aerosol representation. The smallest brightness temperature values result from the no aerosol simulation. The brightness temperature values for each simulation do not cross, and retain roughly the same difference from the no aerosol simulation through most of this window. A final note on this simulation is the grouping of the dust aerosol models at wavelengths shorter than 2.3 µm. The no aerosol simulation is separate from the other dust aerosol representations by roughly 0.75 K. The other representations are grouped roughly within 0.5 K of one another.

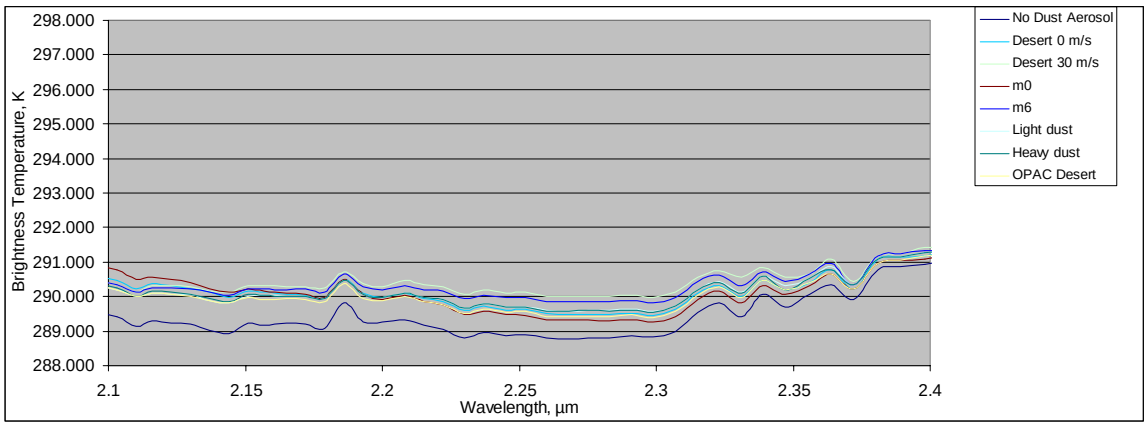

Figure 81. Top-of-the-atmosphere brightness temperature, all cases, spring night, nadir.

Brightness temperatures in the wavelength range between 3.401 and 3.992 µm are somewhat complex (see Figure 82). Below 3.51 µm, all simulations diverge from a common value and increase 2 K. Between 3.51 and 3.81 µm all simulations are steady and range in brightness temperature value by less than 1 K. Above 3.81 µm brightness temperatures converge, drop sharply and then stabilize. The largest brightness

temperature values come from the Desert 30 m/s representation. The smallest brightness temperature values result from the OPAC Desert representation. The brightness temperature values for each simulation begin to cross.

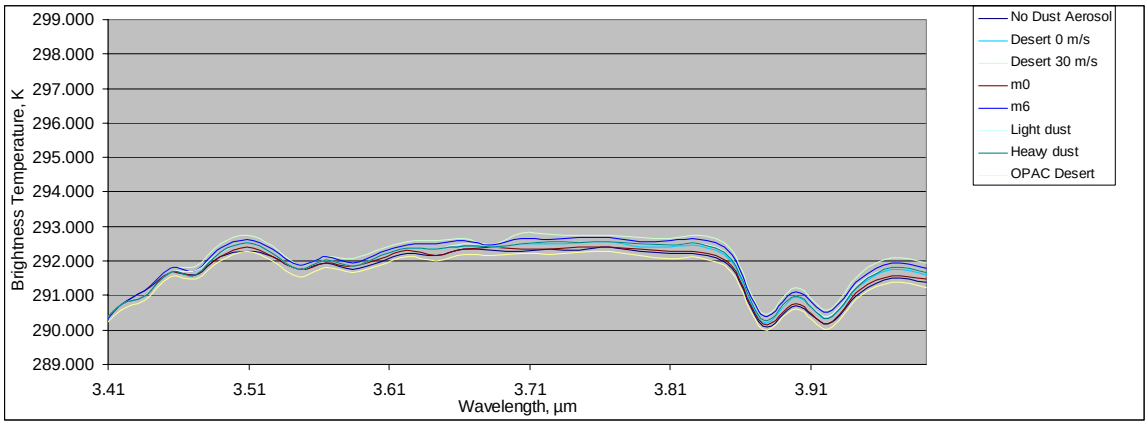

Figure 82. Top-of-the-atmosphere brightness temperature, all cases, spring night, nadir.

Brightness temperatures in the wavelength range between 4.63 and 4.975 µm are variable, with decreasing brightness temperature values through 4.8 µm and increasing values from 4.8 µm wavelengths and higher (see Figure 83). Brightness temperature values for all simulations are very similar to the no aerosol simulation. The range of brightness temperature values from every simulation is less than 0.5 K.

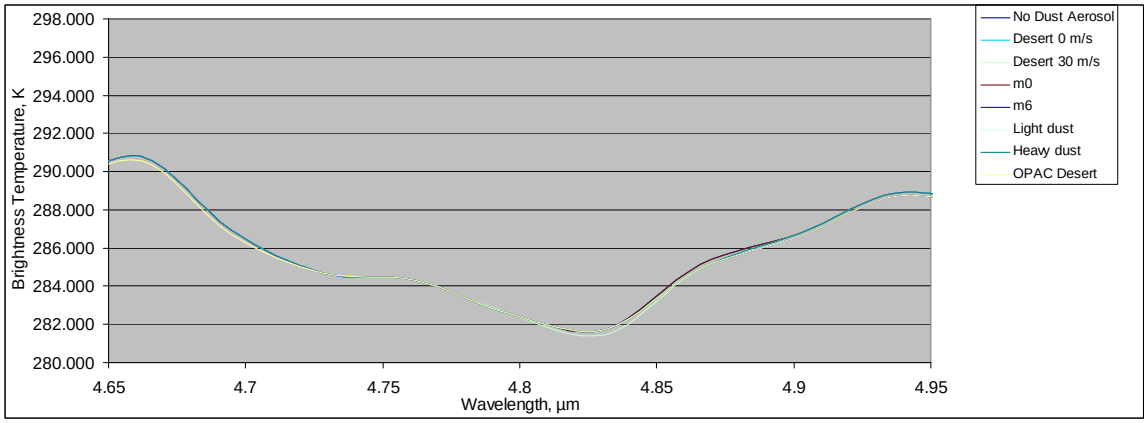

Figure 83. Top-of-the-atmosphere brightness temperature, all cases, spring night, nadir.

The average difference between the no aerosol simulation brightness temperature and the brightness temperatures of various dust aerosols are presented in Figures 84, 85, and Table 15. The magnitudes of values in the table are smaller than exhibited during the daytime case, but there are similarities in behavior. Of note in this table are the relatively large brightness temperature differences. As wavelength increases, the brightness temperature difference between the no aerosol simulation and any dust aerosol simulation decrease. Another interesting observation is the change in magnitude of the brightness temperature difference with respect to wavelength when comparing the low 0.55 μm optical depth simulations to their high 0.55 μm optical depth counterpart. The m0 simulation produced much higher brightness temperatures than the no aerosol case below 1.5 μm. The magnitude of the difference is greater than 10 K. At wavelengths longer than 1.5 μm the difference between the m0 simulation brightness temperature and the no aerosol simulation were at most –0.674 K. Contrast this with the m6 simulation - in wavelengths below 1.5 μm, the magnitude of the brightness temperature difference from no aerosol was as much as 1 K. At wavelengths longer than 1.5 μm, the m6 simulation brightness temperature was different from the no aerosol simulation by -0.066 to -0.893 K. The m6 representation is essentially the m0 representation with the addition of a lower concentration, but larger radius mode of dust aerosol. The large disparity between the m0 and m6 representations in terms of average brightness temperature difference when compared with the no aerosol atmosphere must be due to the larger particles. Therefore, the addition of particles of larger radius has a significant impact on top-of-the-atmosphere brightness temperature.

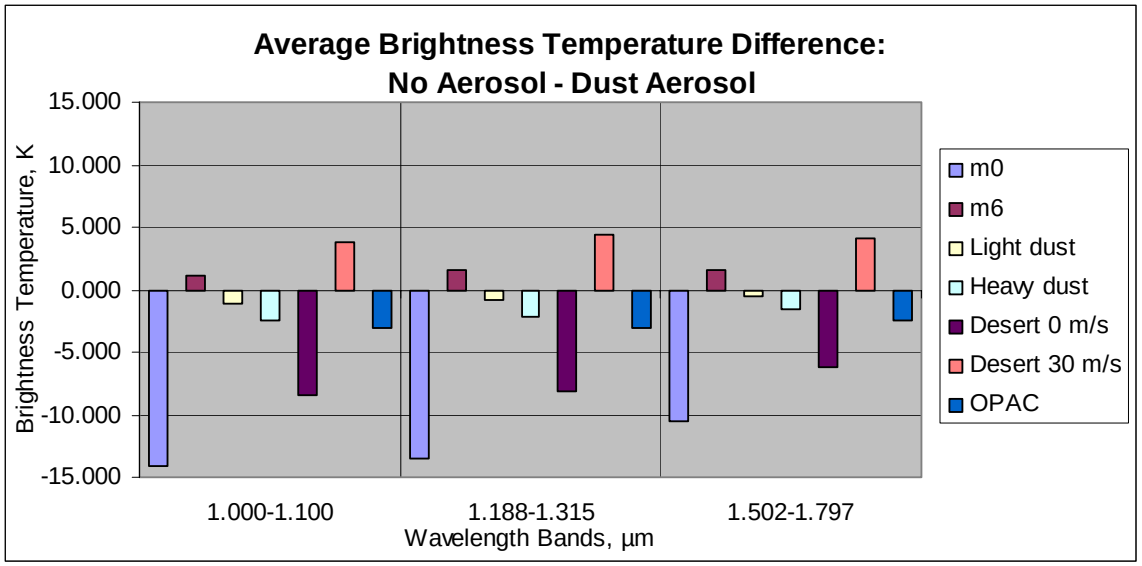

Figure 84. Average brightness temperature difference between no aerosol and dust aerosol, spring night, nadir.

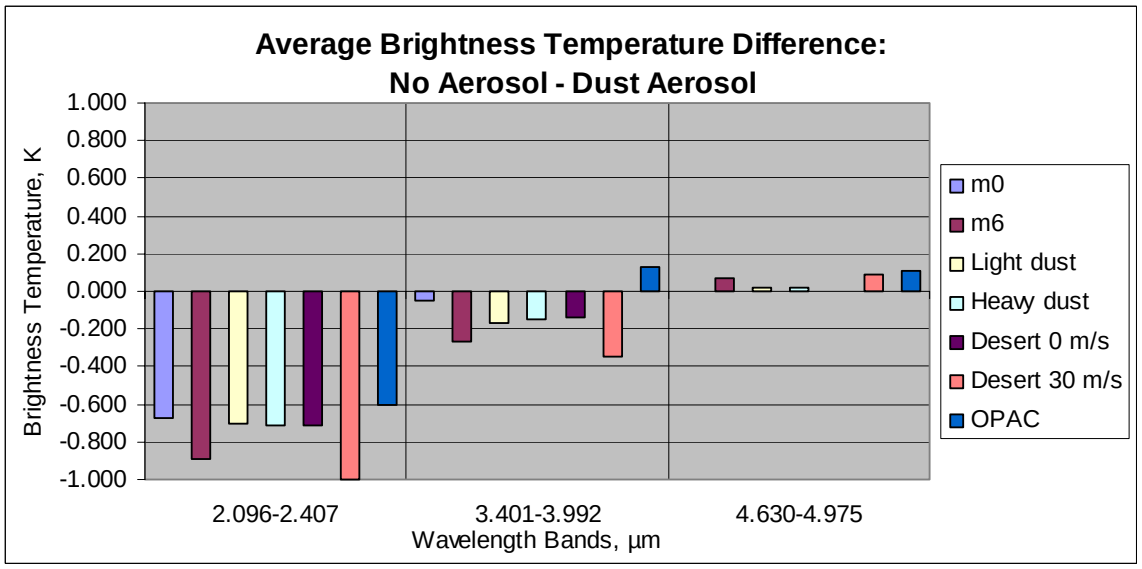

Figure 85. Average brightness temperature difference between no aerosol and dust aerosol, spring night, nadir.

Table 15. Average brightness temperature difference between no aerosol and dust aerosol, spring night, nadir.

	Average Brightness Temperature Difference, K						
Wavelength Band	No Aerosol - Dust Aerosol Representation						
µm	m0	m6	Light dust	Heavy dust	Desert 0 m/s	Desert 30 m/s	OPAC
1.000-1.100	-14.144	1.143	-1.132	-2.434	-8.423	3.824	-3.100
1.188-1.315	-13.543	1.526	-0.887	-2.213	-8.074	4.436	-2.994
1.502-1.797	-10.456	1.604	-0.505	-1.578	-6.131	4.097	-2.466
2.096-2.407	-0.674	-0.893	-0.707	-0.708	-0.713	-0.997	-0.607
3.401-3.992	-0.046	-0.263	-0.165	-0.153	-0.138	-0.344	0.126
4.630-4.975	0.000	0.066	0.018	0.018	0.000	0.087	0.105

H. SPRING NIGHT 30° ZENITH ANGLE

The spring night 30° zenith angle case was run with the MODTRAN input parameters described in the methodology section. The no dust aerosol simulation results in radiance values presented in Figure 86. Between 1 and 2.6 µm the magnitude of radiance is small. This energy is solar energy reflected off of the moon and into the scene in the MODTRAN simulation. Radiance increases above 3 µm, roughly corresponding to the Planck function associated with the blackbody temperature of the earth. The minimum radiance of 1.79 x 10^{-10} W•cm^{-2}•ster^{-1}•µm^{-1} occurs at 1.873 µm, seemingly the beginning of energy from terrestrial emission. Radiance increases to a value of roughly 1.66 x 10^{-4} W•cm^{-2}•ster^{-1}•µm^{-1} near 5 µm. Atmospheric absorption is represented by the appropriate absorption bands between 3 and 5 µm. First, water vapor absorption is present at wavelengths just greater than 3 µm. Carbon dioxide and nitrous oxide absorption are present between 4 and 5 µm.

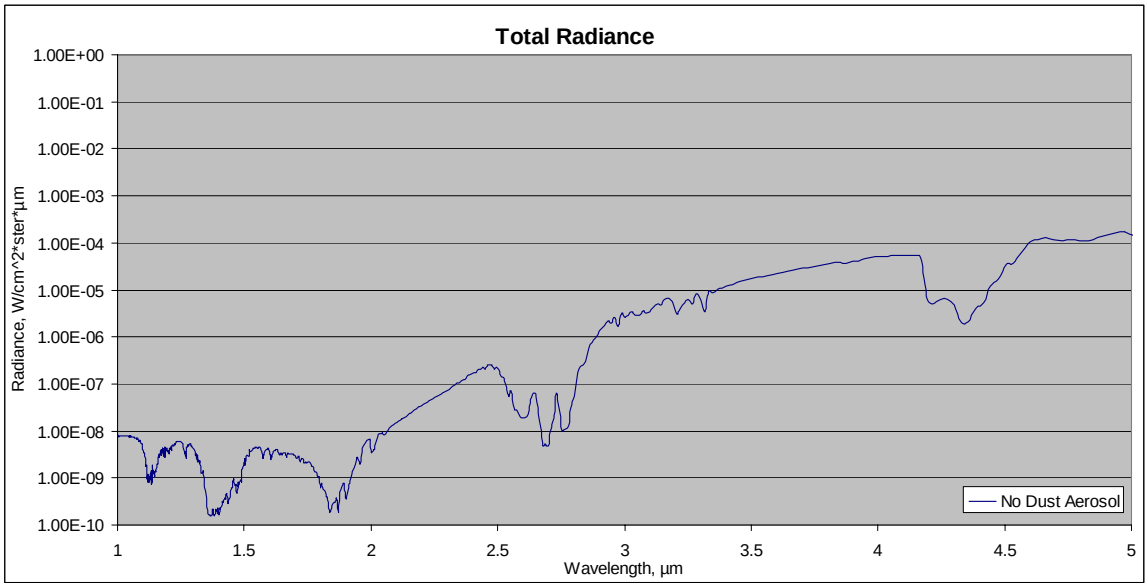

Figure 86. Top-of-the-atmosphere total radiance, no dust aerosol, spring night, 30° zenith angle.

Brightness temperatures reveal the presence of the lunar energy in the 1 through 3 µm wavelength band (see Figure 87). Important to note here is the surface

temperature of 297.3 K for this case, as the brightness temperature values calculated should be near this value in the atmospheric windows of the wavelength band outside of solar influence. At 1 μm the brightness temperature is 513.153 K this is nearly half of the daytime simulation. At 2.008 μm the brightness temperature value decreases to 283.950 K. At 3.003 μm the brightness temperature value is 288.518 K. The decrease in brightness temperature values up to 1.8 μm is due to the surface reflectance model used in the MODTRAN simulations. In the same wavelength span the reflectance changes from 0.7 to just 0.1, therefore much less lunar energy is being reflected off of the surface and towards the top-of-the-atmosphere.

Also interesting to note is the similarity of the 2 and 3 μm brightness temperatures. Since the lunar source inputs much less energy into the calculation, the entire lunar brightness temperature curve shifts further down the chart, and it intersects the terrestrial emission curve at lower wavelengths as a result. In the daytime simulation it seemed that solar energy was influencing the brightness temperature up to 5 μm. This night time simulation reveals the terrestrial energy influencing brightness temperatures at wavelengths as small as 2 μm.

The atmospheric absorption bands below 2 μm are revealed as bands of lower brightness temperature, as expected. Also expected is the fact that the reduction of brightness temperature is smaller in this simulation due to the lower amounts of radiant energy. Surface reflection is very low, but the scattering of radiation by the tropospheric, stratospheric and meteoric background aerosol is present in the simulation. Evidence that this type of scattering is occurring is in the profile of brightness temperatures in the absorption bands. The brightness temperatures show little change across the absorption band, in contrast to the sharp decrease in brightness temperature in the neighboring windows which mirror the surface reflectance.

The absorption bands at wavelengths greater than 2.4 μm are similar to the absorption bands of the daytime simulation in that they represent a decrease from the neighboring atmospheric window of similar magnitude. This points to the relative

influence of terrestrial versus solar radiance once again. In this simulation it is clear that terrestrial emission dominates the brightness temperature to wavelengths as low as 1.9 µm.

Despite the dominance of terrestrial energy to very low wavelengths, the windows in the band between 3.4 and 5 µm are still influenced somewhat by the lunar source. The transmission in this band peaks at roughly 3.5 µm. With this in mind the brightness temperature is expected to be near the 297.3 K surface temperature. The simulations reveal that the brightness temperature is greater than expected at 3.5 µm. The brightness temperatures between 3.4 and 4.1 µm decrease from 292 to 288 K. From 4.5 to 5 µm brightness temperatures vary between 280 and 290 K. Since the brightness temperatures in this band are closer to the surface temperature than transmission would allow, the energy in the simulation must be due to contribution from lunar scattering.

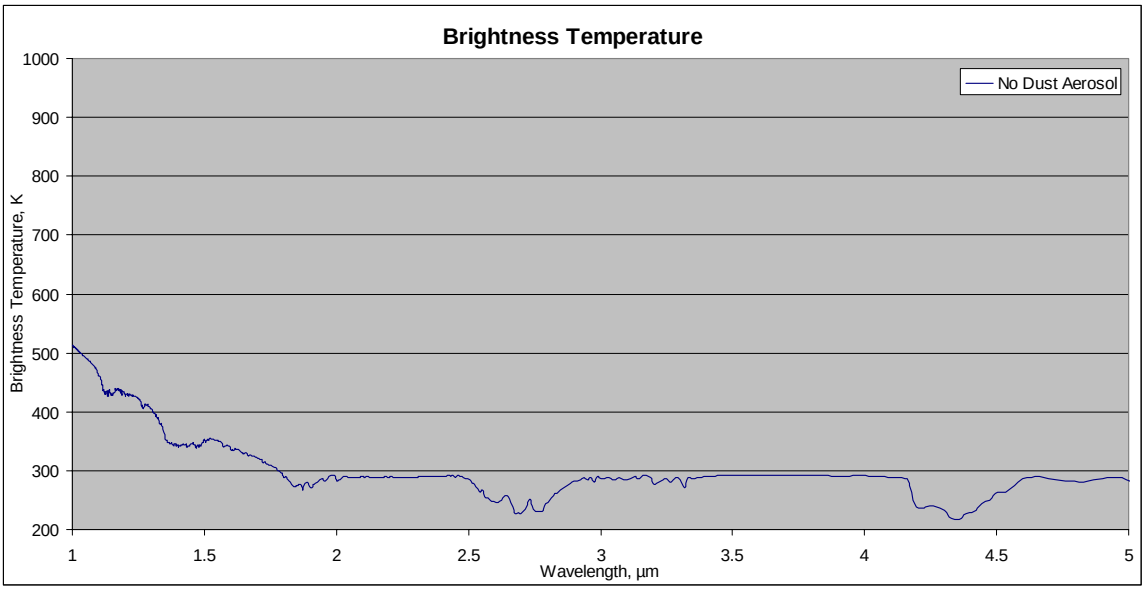

Figure 87. Top-of-the-atmosphere brightness temperature, no dust aerosol, spring night, 30° zenith angle.

As mentioned in the methodology chapter dust aerosols that were non-absorptive were considered as well as absorptive dust aerosols. The difference between the brightness temperatures of the absorptive dust and the non-absorptive dust was

significant in all of the atmospheric windows (see Table 16). The differences were larger at shorter wavelengths than at longer wavelengths. This probably relates to the amount of energy involved in these bands, although the wavelength dependence of emitted radiation is also a factor. In addition, the differences were larger for the representations with higher 0.55 μm optical depth (m6 and Desert 30 m/s) than the representations with lower 0.55 μm optical depth (m0 and Desert 0 m/s). The higher 0.55 μm optical depth values result from representations with a larger number of dust aerosol particles per cubic centimeter. Larger dust aerosol particle loading suggests larger extinction by these aerosols. Larger extinction due to dust aerosol causes larger changes to top-of-the-atmosphere brightness temperature. This is why the Desert 30 m/s dust representation exhibits a larger average brightness temperature difference from the no aerosol simulation than the m6 representation. Since the brightness temperature values from both the non-absorptive and absorptive Desert 30 m/s dust representations are larger than the brightness temperature values from both m6 representations, the difference between the non-absorptive and absorptive Desert 30 m/s dust aerosols are correspondingly larger than the difference between the m6 representations. The exception here is the Heavy dust and Light dust representations. The non-absorptive aerosols minus the absorptive aerosol brightness temperature differences were similar in both the Light dust and Heavy dust aerosol representation despite having different 0.55 μm optical depths. The 0.55 μm optical depths were similar to the other representations with Heavy dust having the higher 0.55 μm optical depth. Brightness temperature differences in this table reveal the importance of accounting for absorption by dust aerosol when calculating radiative transfer between 1 and 5 μm. With that in mind the following examination of brightness temperatures among the different dust representations will focus on the absorptive dust aerosol only.

Table 16. Average brightness temperature difference between non-absorptive dust aerosol and absorptive dust aerosol, spring night 30° zenith angle.

	Average Brightness Temperature Difference, K					
Wavelength Band	Non Absorptive - Absorptive Dust Aerosol Representation					
μm	m0	m6	Light dust	Heavy dust	Desert 0 m/s	Desert 30 m/s
1.0-1.1	1.073	4.033	1.650	0.841	0.266	9.408
1.188-1.315	0.959	4.312	1.875	1.066	0.475	9.869
1.502-1.797	0.697	3.430	1.844	1.577	0.218	5.142
2.096-2.407	-0.114	-0.582	-0.414	-0.389	-0.280	-0.624
3.401-3.992	-0.073	-0.593	-0.391	-0.338	-0.255	-0.716
4.63-4.975	0.000	-0.216	-0.104	-0.082	-0.113	-0.282

Brightness temperatures resultant from the addition of several dust aerosols across the entire 1 through 5 μm band are plotted in Figure 88. Since the brightness temperatures range from over 500 K to near 300 K it is difficult to quantify the difference between the no aerosol simulation and the various dust aerosol simulations by examining the plot of the entire wavelength range. Some spread among the plots between 1 and 2 μm is apparent, but as wavelength increases, the difference between the no aerosol case and the various aerosol simulations decrease. One visible difference is between the no aerosol case and the dust aerosol cases in the absorption band at 1.4 μm. The brightness temperature difference here is roughly 10 K, with the no aerosol simulation having the highest brightness temperature. This is caused by extinction due to dust aerosol. To better understand the effect of the various dust aerosols on brightness temperature closer examination of narrower wavelength bands is required.

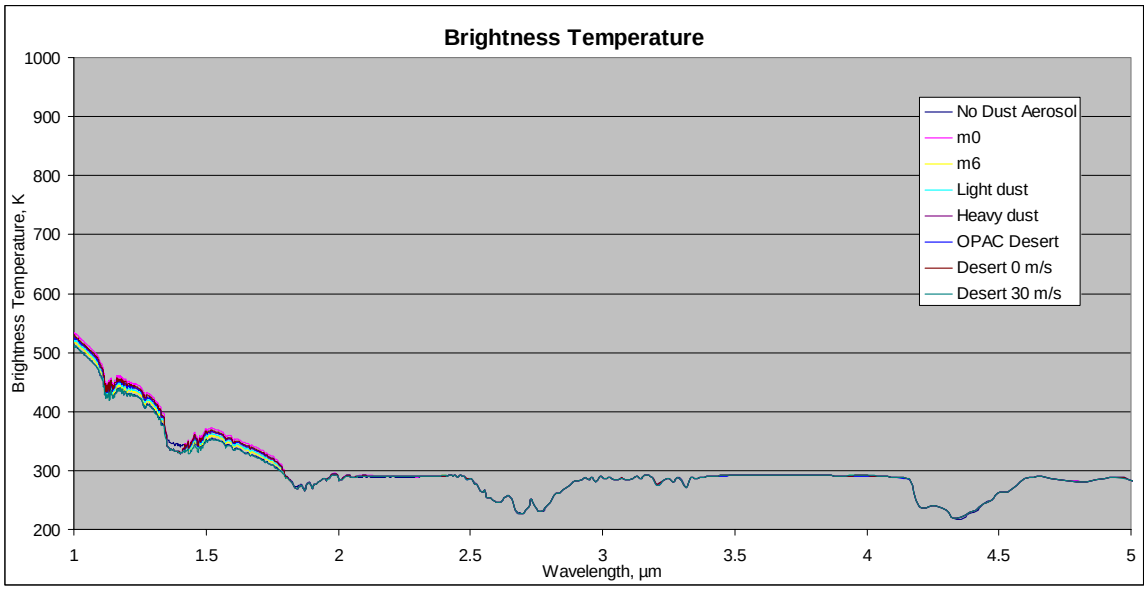

Figure 88. Top-of-the-atmosphere brightness temperature, all cases, spring night, 30° zenith angle.

Window bands were chosen arbitrarily based on examination of the wavelength range and the variability of the aerosol in the window band. Brightness temperatures in the first band between 1 and 1.1 µm are presented in Figure 89. Brightness temperatures decrease for all simulations similarly to the no aerosol simulation. The range of brightness temperature values from every simulation is smaller than in the daytime simulation roughly 20 K. The largest brightness temperature values come from the m0 dust aerosol representation. The smallest brightness temperature values result from the no dust aerosol simulation. The brightness temperature values for each simulation do not cross, and retain the same difference from the no aerosol simulation throughout this window.

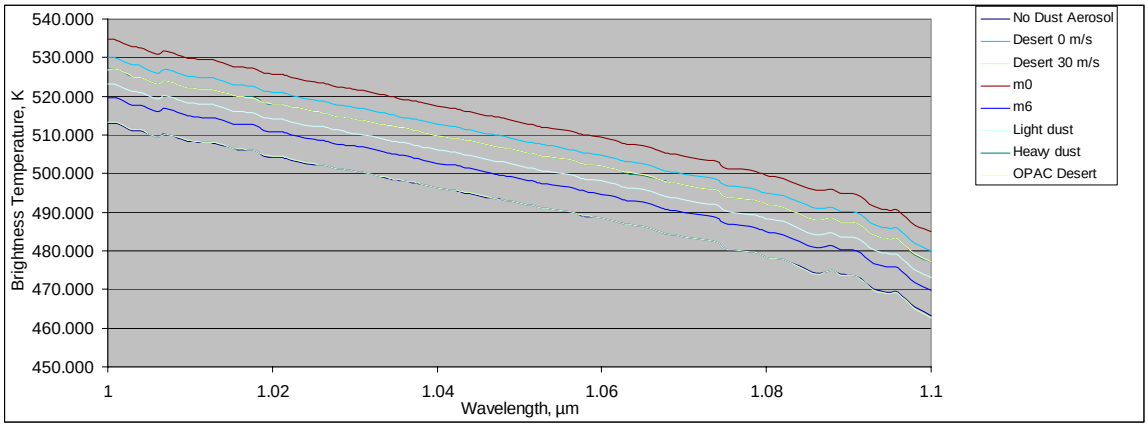

Figure 89. Top-of-the-atmosphere brightness temperature, all cases, spring night, 30° zenith angle.

Brightness temperatures in the next window band between 1.19 and 1.31 µm are presented in Figure 90. Brightness temperatures decrease for all simulations similarly to the no aerosol simulation. The range of brightness temperature values from every simulation is larger than in the previously examined band with a range of roughly 30 K. The largest brightness temperature values come from the m0 absorptive representation. The smallest brightness temperature values result from the MODTRAN Desert 30 m/s dust aerosol representation. The brightness temperature values for each simulation do not cross, and retain roughly the same difference from the no aerosol simulation throughout this window.

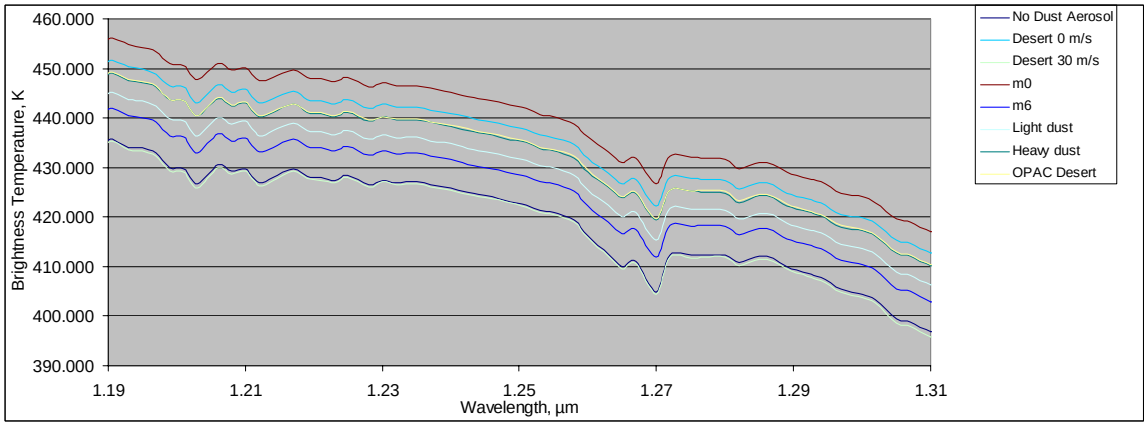

Figure 90. Top-of-the-atmosphere brightness temperature, all cases, spring night, 30° zenith angle.

Brightness temperatures in the band between 1.505 and 1.797 µm follow a similar pattern as in the previous shorter wavelength windows (see Figure 91). Brightness temperatures decrease for all simulations similarly to the no aerosol simulation. The range of brightness temperature values from every simulation is smaller than the previously examined window with values near 15 K. The largest brightness temperature values come from the m0 absorptive representation. The smallest brightness temperature values result from the MODTRAN Desert 30 m/s dust aerosol representation. The brightness temperature values for each simulation do not cross, and retain roughly the same difference from the no aerosol simulation through most of this window. As the wavelength surpasses 1.755 µm the brightness temperatures of all simulations approach a common value.

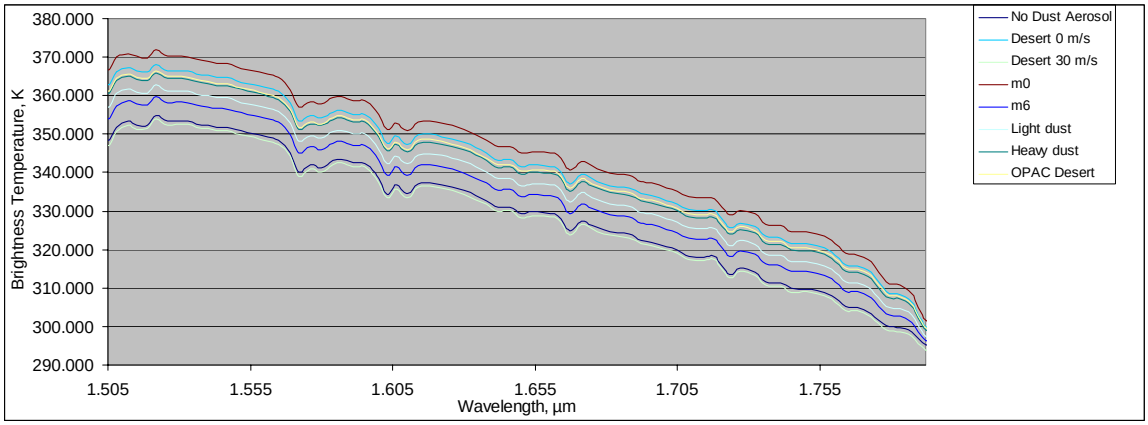

Figure 91. Top-of-the-atmosphere brightness temperature, all cases, spring night, 30° zenith angle.

Brightness temperatures in the wavelength range between 2.1 and 2.4 µm are quite different from the shorter wavelength windows (see Figure 92). Brightness temperatures are steady for all simulations up to 2.3 µm similarly to the no aerosol simulation. At wavelengths higher than 2.3 µm brightness temperatures from all simulations begin to increase and approach a common value. The range of brightness temperature values from every simulation is much smaller than in the shorter wavelength windows, roughly 1.5 K until 2.3 µm, at which point all simulations converge and

slightly increase. The largest brightness temperature values come from the m0 dust aerosol representation below 2.2 µm. The largest brightness temperature values come from the Desert 30 m/s dust aerosol representation above 2.2 µm. The smallest brightness temperature values result from the no aerosol simulation. The brightness temperature values for each simulation cross. A final note on this simulation is the grouping of the dust aerosol models at wavelengths shorter than 2.3 µm. The no aerosol simulation is separated from the other dust aerosol representations by roughly 0.75 K. The remaining models are grouped roughly within 0.5 K of each other.

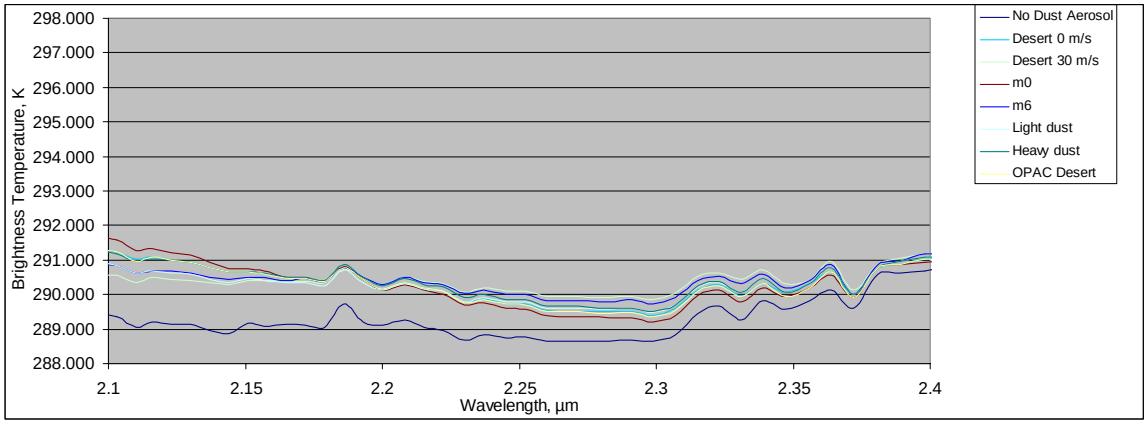

Figure 92. Top-of-the-atmosphere brightness temperature, all cases, spring night, 30° zenith angle.

Brightness temperatures in the wavelength range between 3.401 and 3.992 µm are somewhat complex (see Figure 93). Below 3.51 µm, all simulations diverge from a common value and increase 2 K. Between 3.51 and 3.81 µm all simulations are steady and range in brightness temperature value roughly 0.75 K. Above 3.81 µm brightness temperatures converge, drop sharply and then stabilize. The largest brightness temperature values come from the Desert 30 m/s representation. The smallest brightness temperature values result from the OPAC Desert representation. The brightness temperature values for each simulation cross one another.

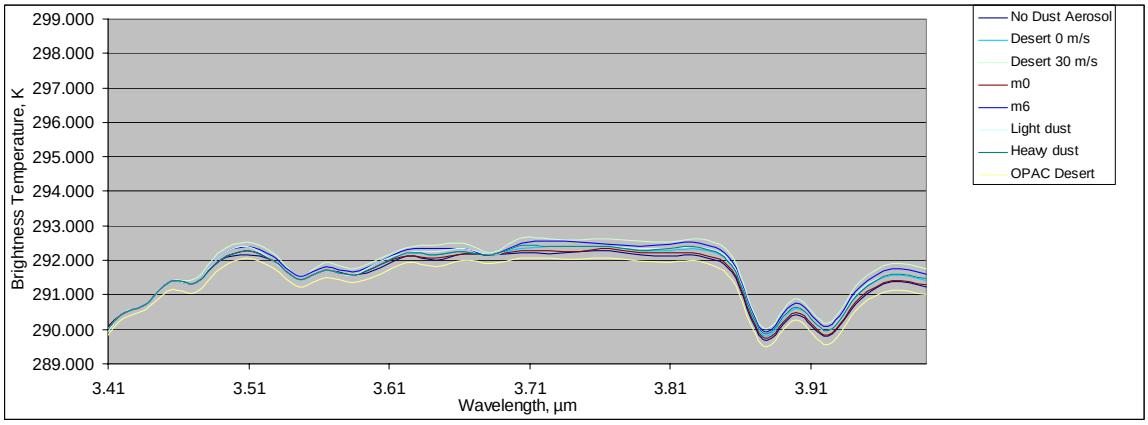

Figure 93. Top-of-the-atmosphere brightness temperature, all cases, spring night, 30° zenith angle.

Brightness temperatures in the wavelength range between 4.63 and 4.975 µm are variable with decreasing brightness temperature values through 4.8 µm and increasing values from 4.8 µm wavelengths and higher (see Figure 94). Brightness temperature values for all simulations are very similar to the no aerosol simulation. The range of brightness temperature values from every simulation is less than 0.25 K.

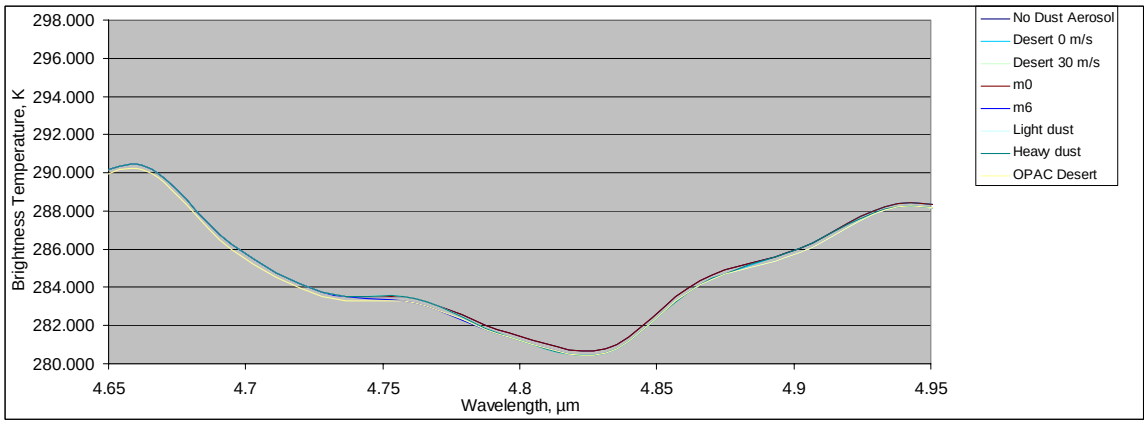

Figure 94. Top-of-the-atmosphere brightness temperature, all cases, spring night, 30° zenith angle.

The average difference between the no aerosol simulation brightness temperature and the brightness temperatures of various dust aerosols are presented in Figures 95, 96,

and Table 17. The magnitudes of values in the table are smaller than exhibited during the daytime case, but there are similarities in behavior. Of note in this table are the relatively large brightness temperature differences. As wavelength increases, the brightness temperature difference between the no aerosol simulation and any dust aerosol simulation decrease. Another interesting observation is the change in magnitude of the brightness temperature difference with respect to wavelength when comparing the low 0.55 μm optical depth simulations to their high 0.55 μm optical depth counterpart. The m0 simulation produced much higher brightness temperatures than the no aerosol case below 1.5 μm. The magnitude of the difference is greater than 15 K. At wavelengths longer than 1.5 μm the difference between the m0 simulation brightness temperature and the no aerosol simulation were at most 1.021 K. Contrast this with the m6 simulation - in wavelengths below 1.5 μm, the magnitude of the brightness temperature difference from no aerosol was greater than 4 K. At wavelengths longer than 1.5 μm, the m6 simulation brightness temperature was different from the no aerosol simulation by -0.132 to -1.113 K. The m6 representation is essentially the m0 representation with the addition of a lower concentration, but larger radius mode of dust aerosol. The large disparity between the m0 and m6 representations in terms of average brightness temperature difference when compared with the no aerosol atmosphere must be due to the larger particles. Therefore, the addition of particles of larger radius has a significant impact on top-of-the-atmosphere brightness temperature.

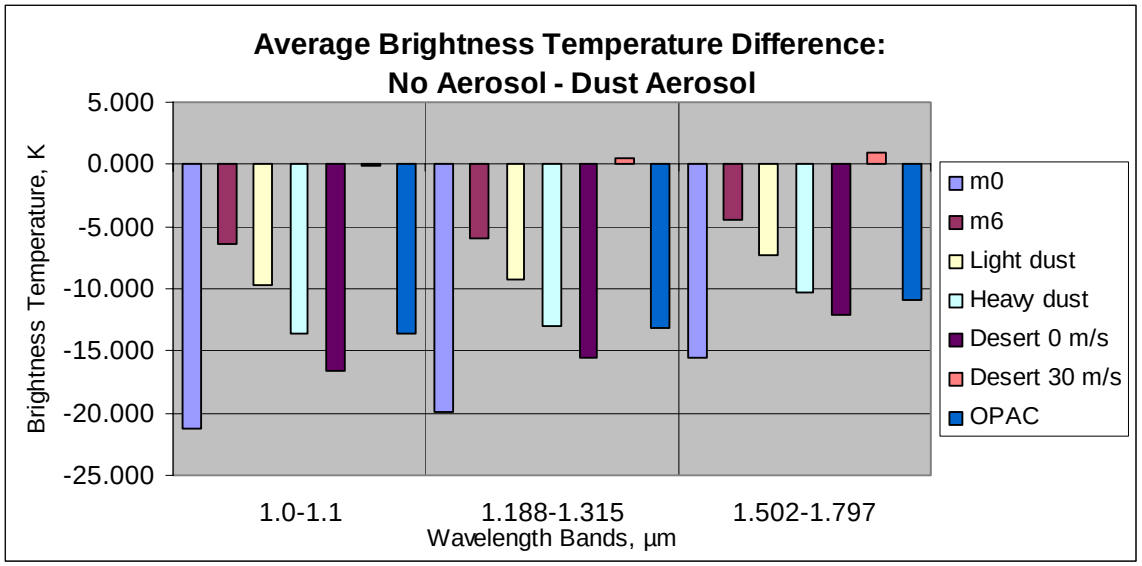

Figure 95. Average brightness temperature between no aerosol and dust aerosol, spring night, 30° zenith angle.

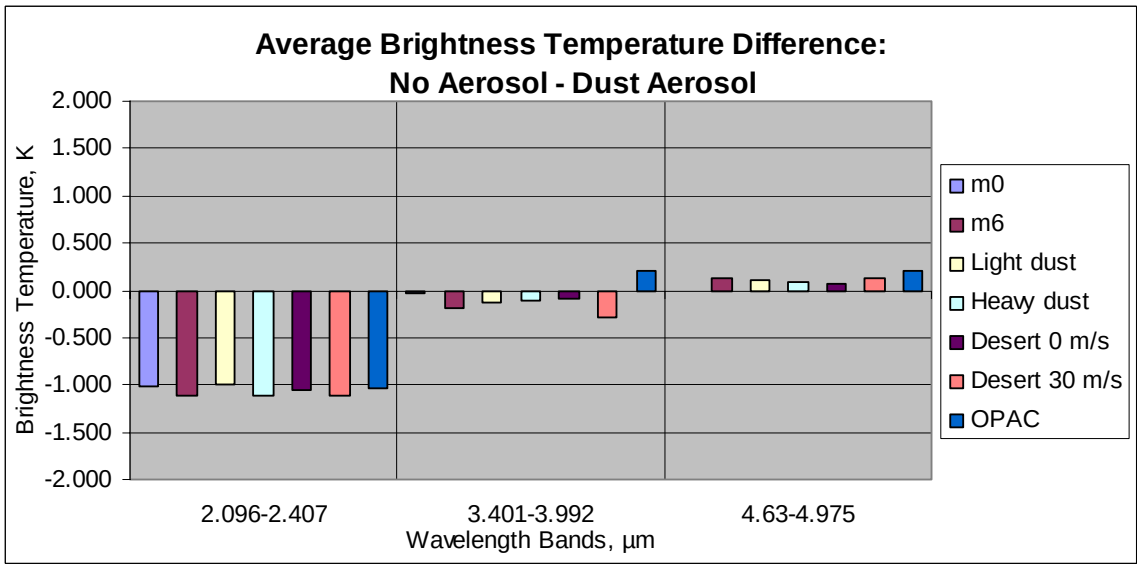

Figure 96. Average brightness temperature between no aerosol and dust aerosol, spring night, 30° zenith angle.

Table 17. Average brightness temperature difference between no aerosol and dust aerosol, spring night, 30° zenith angle.

	Average Brightness Temperature Difference, K						
Wavelength Band	No Aerosol - Dust Aerosol Representation						
µm	m0	m6	Light dust	Heavy dust	Desert 0 m/s	Desert 30 m/s	OPAC
1.0-1.1	-21.178	-6.448	-9.772	-13.625	-16.527	-0.026	-13.636
1.188-1.315	-19.929	-6.006	-9.284	-12.969	-15.609	0.557	-13.186
1.502-1.797	-15.504	-4.501	-7.240	-10.229	-12.117	0.954	-10.844
2.096-2.407	-1.021	-1.113	-0.987	-1.107	-1.046	-1.110	-1.025
3.401-3.992	-0.036	-0.195	-0.126	-0.104	-0.090	-0.286	0.204
4.63-4.975	0.000	0.132	0.111	0.093	0.062	0.126	0.214

I. DUST AEROSOL COMPLEXITY

In each of the results chapters, the reasoning for choosing an absorptive dust aerosol representation over a non-absorptive dust aerosol representation was presented. In order to compare the m0 and m6 dust aerosol representations to the other available aerosols, the index of refraction was set at the 0.55, 3, 4, and 5 μm for every dust aerosol representation. This is an approximation and it is more realistic to vary index of refraction with the varying modes of the dust aerosol size distribution. Longtin notes:

> Specifically, an atmosphere containing a desert aerosol is an inhomogeneous and "dirty" medium and, therefore, using a single value for the index of refraction a each wavelength is not the best way to approach the problem. It would be better to treat the aerosol as a heterogeneous mixture of different types of particles (Longtin et. al., 1988)

The following paragraphs compare the simplified index of refraction applied by wavelength approach and the index of refraction applied by component. In Table 18, the non-absorptive Desert 30 m/s dust aerosol minus the absorptive Desert 30 m/s dust aerosol is presented in the center column. This study concludes that this difference is enough to require absorption to be accounted for when representing dust aerosol. The third column in the table is the difference between the absorptive Desert 30 m/s dust aerosol and the Desert 30 m/s representation in MODTRAN. These average differences are also significant and should not be ignored. The most accurate dust aerosol representation should also include differing components, with different properties for each mode.

Table 18. Average brightness temperature difference between absorptive Desert 30 m/s dust aerosol and Desert 30 m/s from MODTRAN dust aerosol.

Wavelength Band	Desert 30 m/s Average Brightness Temperature Difference, K	
μm	Non Absorptive - Absorptive	Absorptive -MODTRAN
1.0-1.1	11.900	9.317
1.188-1.315	12.817	8.429
1.502-1.797	14.134	5.109
2.096-2.407	15.299	0.751
3.401-3.992	3.412	2.677
4.63-4.975	0.219	3.512

THIS PAGE INTENTIONALLY LEFT BLANK

VI. CONCLUSIONS

A. CONCLUSIONS

Radiative transfer in the wavelength range between 1 -5 μm is characterized by this study. Brightness temperatures values were presented from radiative transfer calculations including no aerosol situations and several situations where varying dust aerosol types were present. Brightness temperature differences were very large day and night, particularly in wavelengths up to 3 μm. For wavelengths above 3 μm, the impact of dust aerosol is reduced, but, still affects uncertainty in remotely sensed measurements. These results indicate that any remote sensing requiring high degrees of accuracy between 1 -5 μm wavelengths must take into account dust aerosol contamination.

Dust aerosol can be represented by several different representations as along as absorption is considered. In this study dust aerosol indices of refraction were applied to the m0 and m6 representations. This change in electromagnetic properties allowed the m0 and m6 representations to be comparable to other more complex dust aerosol representations. The fact that the existing NPS algorithm aerosol models can represent dust if changed to reflect the absorptive properties of dust allows potential use of the NPS algorithm as a measure of dust optical depth and potentially a source of input for PAIS.

Several dust models are available for use by PAIS. Every dust aerosol used in the simulations produced values of radiance and brightness temperature that were similar in behavior to the no aerosol case. This means that they are all probably realistic representations of dust aerosol. This study produced a range of possible values from dust contamination, but it also reveals that a range of dust inputs exists for PAIS to draw from. Currently a single dust representation that varies by wind speed is used to capture all possible dust aerosol conditions. This may not represent all possible dust aerosol conditions. If PAIS was to choose several representative dust aerosols from the seven dust aerosol representations used here, based on some outside information like NAAPS data or an observation, it would be more likely to capture the real atmospheric dust aerosol. If the PAIS process then simulated radiative transfer through each of the dust

aerosol representations it is more likely that the actual atmospheric radiative transfer solution would be found. In addition the uncertainty of radiative transfer under dust aerosol conditions that may never be precisely defined would be gained.

B. FURTHER STUDY

Dust aerosol is placed in the lowest 2 km of atmosphere in this study. Additional study about the vertical distribution of the various dust aerosol representations would be important to improving the PAIS process. In fact some work has been done coupling NAAPS output with MODTRAN radiative transfer characterization (Lucyk, 2007). This is important to clear up the ambiguous nature of the impact of the dust aerosol emission on the top-of-the-atmosphere brightness temperature.

This study characterized aerosols at 0.55, 3, 4, and 5 μm. This simplification makes the fidelity of the output between these wavelengths questionable. Confidence in the results below 2 μm is lower than in the longer wavelength results, because of the spectral distance between 0.55 and 3 μm. Confidence in the results of this study at wavelengths from 2 through 5 μm is high, but could be improved. If the aerosol were to be characterized at higher spectral resolution this question would be moot.

Further study into the impact of size distribution on radiative transfer would be valuable. The precise reasons behind the different dust representations causing different radiative transfer results were not found in this study. If a study were conducted that varied the radius and number density of a given distribution while other parameters were held constant the impact of size distribution could be quantified.

Retrievals of aerosol properties from remote sensors should be examined in order to provide PAIS with observed data to aid in accurate representation of dust aerosol conditions. Ideally, the retrieval would yield dust aerosol type, size distribution/mass concentration and electromagnetic properties. If this is not obtainable, then retrieval of any of the noted parameters above could be coupled with conceptual models of the other parameters to ensure the most representative dust aerosol is provided by PAIS.

An ensemble approach to dust aerosol radiative transfer impact should be studied. If some dust aerosol representation was chosen as the most representative of the actual conditions, radiative transfer calculations could be made with several variations of the dust representation to provide information about the statistical variability/uncertainty in the result. For example, if the dust aerosol representation m0 is chosen, instead of simply modeling radiative transfer through the m0 dust once the system, radiative transfer could be modeled several times. Each time the properties of m0, such as index of refraction or size distribution, would be changed slightly. Once radiative transfer calculations had been made from each of these perturbations a range of impacts to radiative transfer by the atmospheric dust could be presented.

THIS PAGE INTENTIONALLY LEFT BLANK

LIST OF REFERENCES

Ackerman, S. A., 1989: Using the radiative temperature difference at 3.7 and 11 μm to track dust outbreaks. Remote Sens. Environ. 27, 129-133.

Bergman, J., C. Bird, and H. Tryon, 1996: Atmospheric Slant Path Analysis Model quick reference users handbook. Air Force Combat Climatology Center Users Handbook AFCCC-UH-96-002, 21 pp.

Berk, A., G. P., Anderson, P. K. Acharya, J. H. Chetwynd, L. S. Bernstein, E. P. Shettle, M. W. Matthew, and S. M. Adler-Golden, 1999: MODTRAN 4 User's Manual. Air Force Research Laboratory, p. 98. Air Force Research Laboratory: Hanscom Air Force Base, MA, 1999.

Brown, B. B., 1997: Remote measurement of aerosol optical properties using the NOAA POES AVHRR and GOES imager during TARFOX. M.S. thesis, Department of Meteorology, Naval Postgraduate School, 84 pp.

Collins, D. R., H. H. Jonsson, J. H. Seinfeld, R. C. Flagan, S. Gasso, D. Hegg, P. B. Russell, B. Schmid, J. M. Livingston, E. Ostrom, K. J. Noone, L. M. Russell, and J. P. Putuad, 2000: In situ aerosol size distributions and clear column radiative closure during ACE-2. Tellus, 52B, 498-525.

D'Almeida, G. A., P. Koepke, and E. P. Shettle, 1991: Atmospheric Aerosols Global Climatology and Radiative Characteristics. A. Deepak, 561 pp.

Durkee, P. A., K. E. Nielsen, P. J. Smith, P. B. Russell, B. Schmid, J. M. Livingston, B. N. Holben, C. Tomasi, V. Vitale, D. Collins, R. C. Flagan, J. H. Seinfeld, K. J. Noone, E. Ostrom, S. Gasso, D. Hegg, L. M. Russell, T. S. Bates, and P. K. Quinn, 2000: Regional aerosol optical depth characteristics from satellite observations: ACE-1, TARFOX and ACE-2 results. Tellus, 52B, 484-497.

Fischer, K., 1975: Mass absorption indices of various types of natural aerosol particles in the infrared. Applied Optics, 14, 2851-2856.

Johnson, D.,1996: Atmospheric Slant Path Analysis Model held output users handbook. Air Force Combat Climatology Center Users Handbook AFCCC-UH-96-003, 21, p. 76.

Jennings, S. G., R. G. Pinnick, and H. J. Auvermann, 1978: Effects of particulate complex refractive index and particle size distribution variations on atmospheric extinction and absorption for visible through middle IR wavelengths. Applied Optics, 17, 3922-3928.

Kidder, S. Q., and T. H. Vonder Harr, 1995: Satellite Meteorology, an Introduction. Academic Press, 466 pp.

Laven, P., cited December 2006: The optics of a water drop Mie scattering and the Debye series. [Available online at http://www.philiplaven.com/index1.html].

Lenoble, J., 1985: Radiative Transfer in Scattering and Absorbing Atmospheres: Standard Computational Procedures. A. Deepak, 300 pp.

Liou, K. N., 1992: Radiation and Cloud processes in the Atmosphere. Oxford University Press, 487 pp.

Longtin, D.R., E. P. Shettle, J. R. Hummel, and J. D. Pryce, 1988: A wind dependent desert aerosol model: radiative properties. Air Force Geophysics Laboratory Tech. Rep. AFGL-TR-88-0112, p. 114. Air Force Geophysics Laboratory:Hanscom Air Force Base, MA, 1988.

Lucyk, P., 2007: Vertical variation of dust and its impact on the top-of-the-atmosphere brightness temperature in the midwave infrared. M.S. thesis, Department of Meteorology, Naval Postgraduate School, 84 pp.

Patterson, E. M., 1981: Optics of crystal aerosols. J. Geophys. Res., 86, 3236-3246.

Phillips, J. A., 1991: Improved Point Analysis Model users guide. Air Force Global Weather Central Tech. Note AFGWC-TN-91-001, p. 214.

Seinfeld, J. H., and S. N. Pandis, 1998: Atmospheric Chemistry and Physics: From Air Pollution to Climate Change. John Wiley and Sons, 1326 pp.

Shirkey, R. C., and D. H. Tofsted, 2006: High resolution electro-optical aerosol phase function database, PFNDAT2006. Army Research Laboratory Tech. Rep. ARL-TR-3877, 60 pp.

Twomey, S., 1977: Atmospheric Aerosols. Elsevier/North Holland, 302 pp.

INITIAL DISTRIBUTION LIST

1. Defense Technical Information Center
   Ft. Belvoir, Virginia

2. Dudley Knox Library
   Naval Postgraduate School
   Monterey, California

3. Air Force Weather Technical Library
   AFCCC/DOO
   Asheville, North Carolina

4. Major Dean Carter
   AFCCC/DON
   Asheville, North Carolina

5. Professor Philip A. Durkee, Meteorology Department Chairman
   Naval Postgraduate School
   Monterey, California

6. Kurt Nielsen, MR/NE
   Naval Postgraduate School
   Monterey, California